Guidelines for Authors

This periodical is a publication of the Academic Publishing and Translation Directorate of Qassim University. Its purpose is to provide an opportunity for scholars to publish their original research.

Manuscripts will be published in on of the following platforms:

i) **Article:** It should be original and has a significant contribution to the field in which the research was conducted.
ii) **Review Article:** A critical synthesis of the current literature in a particular field, or a synthesis of the literature in a particular field during an explicit period of time.
iii) **Brief Article (Technical Notes):** A short article (note) having the same characteristics as an article.
iv) **Innovation and Invention Reports**
v) **Forum:** Letters to the Editor, comments and responses, preliminary results or findings, and miscellany.
vi) **Book Reviews**

The Editorial Board will consider manuscripts in the following fields:

- Electrical Engineering
- Civil Engineering
- Mechanical Engineering
- Chemical Engineering
- Computer Engineering
- Mining and Petroleum Engineering
- Computer Science
- Information Technology
- Information Systems
- Basic Engineering and Computer Sciences

A manuscript should be submitted in English, and, if accepted for publication, it should not be published elsewhere without the written permission of the Editor-in-Chief.

General Instructions

1. **Submission of manuscripts for publication:** Papers must be presented in final page format (not more than 20 pages, A4 size), along with a compact disk (CD) containing the contribution executed on a PC using MS Word or any updated version of it. Manuscripts should be typed using Times New Roman, 12 points font, and one and half space. Pages are to be numbered consecutively and are to include all illustrative material, such as tables and figures, in their appropriate places in the text. If the author does not follow these guidelines, the paper is likely to be rejected or delayed.
2. **Abstracts:** Manuscripts for articles, review articles, and brief articles require both Arabic and English abstracts, using not more than 200 words..
3. **Keywords:** Each article must have keywords before both abstracts (English and Arabic) and they should not exceed 10 words.
4. **Tables and other illustrations:** Tables, figures, charts, graphs and plates should be planned to fit the Journal's page size (A4 incl. running heads). Line drawings are to be presented on high quality tracing paper using black India ink. Copies are not permitted for use as originals. Line quality is required to be uniform, distinct, and in proportion to the illustration. Photographs may be submitted on glossy print paper, in either black and white, or color, or made by using Adobe Photoshop. Tables and other illustrative material must include headings or titles, and captions for figures.

5. **Abbreviations:** The names of periodicals should be abbreviated in accordance with *The World List of Scientific Periodicals.* e.g., *et al., J. of Food Sci.*
For weights and measurements, and where appropriate, abbreviations rather than words are to be used, e.g., cm, mm, m, km, cc, ml, g, kg, min, %, etc., Fig.
Latin abbreviations such as: *op. cit., loc. cit., ibid.,* are to be in italic (if they are used).
6.**References:** References are mentioned numerically [between brackets] in the text and a list of references are provided at the end of the manuscript as follows:
a- Journals: [number] followed by the last name of the author (authors), First name or abbreviation, "paper title" , journal title , volume and issue numbers, (the year of publications between parentheses) , and page numbers.
Example: Sawyer, D. A. "Pounding of Rainwater on Flexible Roof Systems," Proceedings ASCE, Journal of the Structural Division, Vol. 93, No. 1, (1967), pp.127-147.
b- Books: Book references must include author, book title, the publisher's location, and publisher, and the year of publication.
Example: Feld, J., and Carper, K., Construction failure, 2nd Ed., New York, Wiley, 1997.
7. **Content Note or Footnote:** A content note or footnote is a note from the author to the reader providing clarifying information. A content note is indicated in the text by using a half-space superscript number (e.g. … books[3] are …). Content notes are to be sequentially numbered throughout the text. A reference may be cited in a content note by the use of the standard (Author, Date) style in the same way they are used in the text.
Content notes are to be presented below a solid half-line separating them from the text of the page in which the footnote is mentioned (in single column). Use the same half-space superscript number assigned in the content note(s) in the text to precede the content note itself.
8. **Proofs:** No changes, additions or deletions will be allowed in the pageproof stage.
9. **Opinions:** Manuscripts submitted to the Journal for publication contain the author's conclusions and opinions and, if published, do not constitute a conclusion or opinion of the Editorial Board.
10. **Offprints:** Two copies of the journal and twenty reprints of the accepted papers will be sent to the authors.
11. **Correspondence:** All correspondence may be addressed to:

E-mail: quecjour@qec.edu.sa

12. **Frequency:** …Two issues per year…….

Subscription and Exchange:

E-mail: quecjour@qec.edu.sa

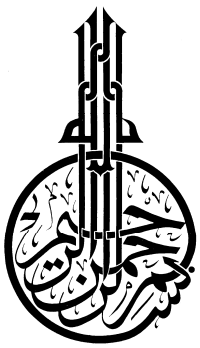

In The Name of ALLAH,
Most Gracious, Most Merciful

Qassim University Scientific Publications
(Refereed Journal)

Volume (4) – NO.(1)

Journal of
Engineering and Computer Sciences

January 2011 – Muharram 1432H

Scientific Publications & translation

EDITORIAL BOARD

Deposif: 1429/2023

Journal of Engineering and Computer Sciences,
Qassim University, Vol. 4, No. 1, PP 1-105, for English (January 2011/Moharram 1432H.)

Contents

Page

Journal of Engineering and Computer Sciences
Qassim University, Vol. 4, No. 1, pp. 1-19 (January 2011/Moharram 1432H)

Behaviour of an Earth Dam Using Finite Element Modelling with Different Soil Constitutive Models: Case Study of El Hma Dam, Ben Arous, Tunisia

Khaled Kheder[1], Zouhair M'rabet [2], Abdallah Jrad [3], and Ridha El Ouni [4]

[1] *Geography Department, College of Arabic Language and Social Sciences*
Al Quassim University – Saudi Arabia
khaledkheder@ymail.com
[2] *Consultant, Geo-Risk Consulting*
New York – USA
zouhair.mrabet@yahoo.com
[3] *Office National d'Assainissement, Département de Génie Civil*
Tunis – Tunisie
jrad.Abdallah@yahoo.com
[4] *Institut National Agronomique de Tunis, Département de Géotechnique des barrages*
Tunis – Tunisie
AlOuni.Ridha@yahoo.com

(Received 12/10/2009; accepted for publication 10/10/2010)

Abstract. The present paper deals with the analysis of the behaviour of an earth dam at the end of construction, during the first filling of the reservoir and at long term by using Finite Element Method. In this analysis, El Hma dam, which located in Tunisia, has been selected as a case study. Three constitutive laws including elastic, Mohr-Coulomb and Drucker-Prager, were assumed to present the material characteristics of the dam and its foundation. Attention will be given to the study of predicted deformation, stresses and pore pressure distributions. The interpretations of the predicted results lead to evaluate the dam behaviour.

Keywords: earth dam, Finite Element Modelling, Constitutive models.

1. Introduction

Prediction of the deformations of an earth dam has a significant effect on its performance and safety. Significant movements and settlements of the crest and the body of the dam can occur during various stages of the construction of the dam, at the end of construction, the first filling of the reservoir and during the operation of the dam.

The first filling of the reservoir is the most important stage in the earth dam construction because the effect of wetting. Increasing of water level in reservoir involves the deacrease in geotechnical property values and the Young modulus of the material in the submerged sections of the structure. Once the filling of the reservoir is completed, the dam undergoes long-term deformations [1]. The weight of the embankment and the pressure of the reservoir water involve the fill material to settle resulting in a vertical movement of the structure. The reservoir water pressure also causes permanent horizontal deformation perpendicular to the longitudinal axis of embankment. However large permanent deformations could occur due to reservoir drawdown [2].

On the hand, in embankment dams the progress of filling of the reservoir will develop a considerable pore pressure within the core of the dam. The increasing of water level in the reservoir may double the pore pressure in the core due to seeping the water within the dam which may lead to excess pore pressure in the core ending to hydraulic fracturing of the dam.

Today, the finite element method has become established as a useful tool to model the deformation of earth dams. The concept of the finite element method, which is used to analyze expected displacements, strains, stresses and pore water pressures in the structure associated with different loading and boundary conditions, is extensively described by Zienkiewicz [3]. To perform the finite element analysis of the dam, the selection of the material model is essential [4]. Recently, efforts has been devoted toward the development of more sophisticated and refined constitutive models, which resemble the behaviour of real engineering materials more closely [5]. More constitutive models associated with various degrees of sophistication and complexity, have been reported in the literature [6]. A new generation of programs and codes can now be run comfortably on a personal computer.

In this paper, emphasis is given on practical applications of the finite element method to analyze the deformation of an earth dam. El Hma dam, which located in Tunisia, has been selected as case of study. The presented results are limited to only one cross-section in the middle of the dam. Three constitutive models including Elastic, Mohr Coulomb and Drucker-Prager, were assumed to present the construction material characteristics of the dam and its foundation, have been considered.

Finite element analyses were conducted using widely used commercial finite element software package ABAQUS [7], which is developed by Hibbitt, Karlsson and Sorensen, Inc. It is a general-purpose commercial finite element software, capable of performing linear and non-linear analyses. Moreover, it has many built-in material models for many types of analyses in its material library.

However the most critical problem in predicting deformations of earth dams by using finite element modelling is to obtain characteristics of the fill materials. The difficulty in determining material characteristics is the main cause of uncertainty in modeling of deformations. Results of properly monitoring schemes may be used to enhance the predicted model. Due to the uncertainty of the model parameters [8], the monitored deformations of El Hma dam should be performed to improve the model [9]. The monitoring of the deformation of the dam will be discussed in another communication.

2. Material Models

The material models used for the analyses are plasticity models and the elasticity model. These material models are available in the ABAQUS [7] materials library and they can be used with the plane strain continuum type elements.

3. Elasticity Model

The elasticity model, either linear elastic or porous elastic model, demonstrates the ability of the constitutive law to simulate the non-linearity behavior of materials due to revertible strains. In this model the linear relationship between stress and strain is the simplest link implying a constant proportionality between general stress increments and strain increments [10]. The full link between stresses and strains can be written as a compliance relationship:

$$\sigma_{ij} = D_{ijkl} . \varepsilon_{kl}$$

This expression describes Hooke's Law of elasticity. If isotropic marerial behaviour is independent of the direction of the solicitation; only two independent constants subsist in the last expression:

$$\sigma_{ij} = \lambda . (\sum_{k} \varepsilon_{kk}) . \delta_{ij} + 2\mu\varepsilon_{ij}$$

Where: λ and μ are lamé's constants, and δ_{ij} is the kronecker tensor. The elasticity model has been implemented numerically in ABAQUS 6.4 [7].

4. Drucker Prager Elasto-Plasticity Model

The use of Drucker Prager criterion for soil modelling has been extensively reported and fully described in literature ([11]). Within this framework, the Drucker-Prager yield criterion under plane strain conditions which have been considered to model the embankment-foundation system materials.

Drucker-Prager criterion has been successfully adopted in analysis of geomaterials [5]. It is considered as a generalization of the von Mises criterion for cohesionless soil, taking into account the first invariant of stress tensor J_1 and the second invariant of deviatoric stress tensor J_2. In principal stress space, the criterion is given as:

$$F(\sigma_{ij}) = \sqrt{J_2(\sigma_{ij})} + \alpha J_1(\sigma_{ij}) - k \leq 0$$

J_1 represents the trace of stress tensor $(J_1 = \sigma_1 + \sigma_2 + \sigma_3)$, α and k are material parameters related to the soil friction angle and the cohesion and σ_1, σ_2 and σ_3 being the principal stresses of a stress tensor.

$$J_2 = \frac{1}{6}\left[(\sigma_1 - \sigma_2)^2 + (\sigma_2 - \sigma_3)^2 + (\sigma_3 - \sigma_1)^2\right]$$

In the principal stress space $(\sigma_1, \sigma_2, \sigma_3)$, the failure mechanism is represented by a cylindrical cone-shape surface and having as axis (hydrostatic axis) a straight line of equation:

$$\sigma_1 = \sigma_2 = \sigma_3 .$$

- If α = 0 the Drucker-Prager criterion can be reduced to von Mises type criterion. Therefore, the cylindrical cone shape surface becomes a cylinder.
- If α > 0, the plastic strain is associated with an increasing of volume, i.e. dilatancy
- Under plane strain conditions, displacements perpendicular to the cross section are assumed to be zero, the yielding criterion matches Mohr Coulomb criterion

The plastic potential, which controls the soil dilatancy, is defined as:

$$G(\sigma_{ij}) = \sqrt{J_2(\sigma_{ij})} + \beta J_1(\sigma_{ij}) + \text{Constant}$$

Where, β is a parameter of behaviour law.

If the associative flow rule is adopted, parameters α and β are equal. The Drucker-Prager model can be reduced to Von Mises type criterion by letting α = β = 0.

The associated elasticity is the Hooke's linear elasticity. The Drucker-Prager criterion embraces in total 5 parameters: E, v, k, α, β.

The expression of the criterion leads to the following remark: in compression and for the case of sand, friction angles are limited to small values. However, many experimental results prove the contrary. It is obvious that the Drucker-Prager criterion does not adapted to the modelling of sands.

Generally, a correspondence can be established between parameters α, β and k of the Drucker- Prager envelope and φ, ψ and c of the Mohr-Coulomb envelope. For axis metrical triaxial conditions, $(\sigma_2 = \sigma_3)$, the correspondence between both criteria leads to the following relationships (Chen W.-F and A. F. Saleeb, (1982)) :

$$\alpha = \frac{2\sin\varphi}{\sqrt{3}(3-\sin\varphi)}$$

$$\beta = \frac{2\sin\psi}{\sqrt{3}(3-\sin\psi)}$$

$$k = \frac{6c\cos\varphi}{\sqrt{3}(3-\sin\varphi)}$$

Under plane strain conditions, ($\varepsilon_2 = 0$, for example), the hypothesis of the associative flow rule and the correspondence between criteria leads to the following relationships [10]:

$$\alpha = \frac{tg\varphi}{\sqrt{9+12tg^2\varphi}}$$

$$\beta = \frac{tg\varphi}{\sqrt{9+12tg^2\varphi}}$$

$$k = \frac{3c}{\sqrt{9+12tg^2\varphi}}$$

5. Mohr-Coulomb Model

The Mohr Coulomb yield criterion has a long history of usage in classical soil shear strength characteristics in terms of the Mohr-Coulomb cohesion c and friction ϕ. This criterion is used for cohesionless soil and for cohesive soil at long term [12]. Tresca criterion, which is considered as a particular case of Mohr- Coulomb criterion, is used for cohesive soil at short term.

The Mohr-Coulomb criterion is composed of two straight lines in the Mohr (τ, σ) plane where τ and σ are the shear and normal stresses on the failure plane. The mathematical expression of these two straight lines can be expressed as:

$$F(\sigma_{ij}) = \sigma_1 - \sigma_3 - (\sigma_1 + \sigma_3)\sin\varphi - 2c\cos\varphi \le 0$$

They are inclined of an angle ϕ regarding the normal stress axes. With σ_1 and σ_3 being the maximum and minimum principal stresses, respectively

$(\sigma_1 \le \sigma_2 \le \sigma_3)$ and c and ϕ are the angle of friction and the cohesion of the soil materials, respectively.

Mohr-Coulomb model can be reduced to Tresca type criterion by letting $\varphi = 0$. In principal stress space $(\sigma_1, \sigma_2, \sigma_3)$, the criteria presented defined by the function F is a pyramid associated with hexagonal cross-section and having as axis a straight line of equation:

$$\sigma_1 = \sigma_2 = \sigma_3$$

When $\varphi = 0$, this pyramid transforms into a circular cylinder.

The plastic potential can be expressed in terms of minimum and maximum principal stresses as:

$$G(\sigma_{ij}) = \sigma_1 - \sigma_3 + (\sigma_1 + \sigma_3)\sin\psi + \text{constant}$$

Where, ψ is the dilatancy angle. For $\psi = \varphi$ this is corresponds to the associative flow rule. Mohr-Coulomb model involves five parameters, namely Young's modulus, E, Poisson's ratio, ν, the cohesion, *c*, the friction angle, ϕ, and the dilatancy angle, ψ.

The Drucker-Prager model does not suffer from the non-smooth corner regions that generally affect Mohr-Coulomb-type soil models. A number of investigators prefer Drucker-Prager plasticity model due to the relative smoothness of the yield surface, the corresponding lack of sharp corners, the ability to model ductile tensile failure, and the coupling between shear failure compressive plasticity.

In addition, it is more realistic in that the Drucker-Prager model predicts a saturation of soil strength with increasing effective confining stresses. However, the classical Mohr-Coulomb model unrealistically predicts no saturation of shear strength with increasing effective normal confining stresses [4].

6. Boundary Conditions of a Free Surface Flow through Earth Dam

As the water flows, the soil in the dam undergoes volume changes in response to changes in total stress. Volume changes can generate pore-water pressures and alter the transient flow regime within the embankment dam [13]. The solution to these problems requires that soil behaviour be analyzed by incorporating the effects of the transient flow of the pore-fluid through the voids, and therefore requires that a two phase continuum formulation be available for porous media [14].

A procedure was incorporated in the ABAQUS computer program for performing finite element analysis on the behaviour of a dam including water seepage. ABAQUS has been coded based on a procedure that couples stress equilibrium (mechanical behaviour) and water flow (hydraulic behaviour) using the Theory of Consolidation for soil layers. Generally, flow of water through both saturated and unsaturated soil follows Darcy's law [13]. However, boundary conditions associated with the complexity of domains are not specified or

prescribed, for example free-surface boundary. Therefore, the resolution of the flow equation is sometimes not straightforward. A water flow associated with free surface is characterized by a free surface limiting water flow to its top boundary. The seepage through an embankment dam is an example of unconfined flow bounded at the upper surface by a phreatic surface. The relative position of the free surface is an internal variation of the element to which hydraulic and mechanical properties depend on positions of saturated or unsaturated zones, respectively.

7. El Hma Earth Dam

El Hma dam is an embankment dam built across El Hma River located at Morneg town in the district of Ben Arous, Tunisia. The dam controls a hill slope reservoir of about 123 km^2 and receives an annual average discharge of about 7.8 Mm^3. Its maximum operating capacity amounts to 12 Mm^3.

The main objectives of the realization of El Hma dam are to:

- Recharge the Morneg aquifer at the downstream side of the dam;
- Minimize damage caused by flooding and preserve the discharge of high flood seasons (flood control);
- Meet the requirements of irrigation supply to Morneg region, Tunisia (over 760 hectares of land).

The embankment consists of a thick impervious core, impervious blanket, upstream shoulder and downstream shoulder. The construction materials used for the embankment are:

- The core consists of brown compacted clay, protected upstream and downstream by granular filters. These filters protect the core dam and are considered as transition zones between the core and upstream and downstream shoulders.
- Upstream shoulder consists of mixed material (clay, brown silt and materials taken from necessary excavations of conglomerates of unified structure and from the spillway)
- Downstream shoulder consists of cobbly and clayey gravels, and is considered as permeable. A berm width of about 7 m is located at downstream slope, which may provide additional stability to both the embankment and the foundation. The berm is covered with a 0.50 m thick rock fill layer lying on a transition layer having a thickness of about 0.25 m.
- Impervious blanket of about 1.50 m thick exists over all the downstream shoulder in order to protect the foundation against the risk of potential piping.

Average slopes of the dam are made of 1V: 3 H and 1V: 3.5 H upstream and downstream faces respectively. Figure (1) shows an example of a general schematic cross-section of El Hma dam. In table (1), the main dimensions of the Al Hma dam are summarized.

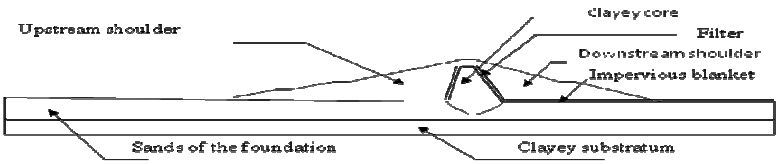

Fig. (1). General schematic cross-section of El Hma dam ([15]).

Table (1). El Hma dam geometry [13].

Dam length (m)	1200
Embankment height from the ground level (m)	26
Embankment width at its base (m)	196
Crest width (m)	6
Core width at the top/bottom (m)	4/5

The reservoir and the foundation area are infilled with sediments of Quaternary age. A sandy shallow soil layers are overlying an impervious clayey substratum. The thickness of the sandy layer is varying between 13 m at the upstream side and 7 m at downstream side, and mainly consists of sand and cobbles associated with clayey interbedded layers. The clayey substratum has an approximate thickness of about 9 m at the upstream side to about 13 m at the downstream side.

8. Finite Element Analyses

Figure (2) shows the finite element idealization considered for the embankment-foundation system. The embankment and foundation soils have been discretized into four nodded-quadrilateral elements. A total of 395 elements and 596 nodes were used. ABAQUS automatically meshes the geometry according to the given element size.

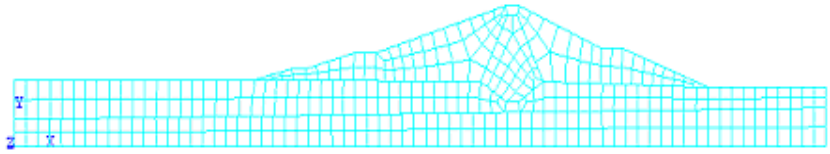

Fig. (2). Two-dimensional finite element mesh proposed for embankment-foundation system.

Zero vertical and horizontal displacements are specified at the substratum contact. However, the foundation is free to move in the vertical direction and fixed in horizontal direction at the left and right sides. However, the coupled hydro-mechanical model will be limited to the embankment including few elements of the upstream shoulder and the core, and the dam foundation.

In the horizontal direction, the model site was extended from the dam surfaces to about 101.5 meters and 50 meters from left and right sides, respectively.

Then the total width of the foundation is about 345.42 meters. The dam foundation was modelled to the depth of 21 meters below the ground level.

At the end of construction of the dam a significant pore pressure development is expected either in the embankment or foundation during construction of the embankment [12]. The embankment is constructed in layers with soils at or above their optimum moisture content that undergo internal consolidation because of the weight of the overlying layers. Embankment layers may become saturated during construction as a result of consolidation of the layers: there is drainage of the water from the soil during construction resulting in the development of significant pore pressures. The end of construction behavior modelling is analyzed in dry condition. The shear strength parameters are considered as based on geomechanical classification and laboratory tests, odometer and triaxial cells, performed on a dry material [16]. Geotechnical parameters of the embankment and foundation materials used for the modelling are summarized in table (2).

Table (2). Geotechnical parameters.

Parameter	Embankment soil			Filter	Foundation soil	
	Core	Upstream shoulder	Downstream shoulder		Sand and cobbles with clayey interbedded layers	Clayey substratum
C(kPa)	72	50	0	0	0	70
ϕ (°)	21	23	48	36	46	19
E(MPa)	17.5	19	80	40	75	17
ν	0.32	0.3	0.25	0.27	0.23	0.33
ψ (°)	21	23	48	36	46	19
E	0.578	0.525	0.42	0.47	0.44	0.59
K(m/s)	10^{-9}	10^{-8}	10^{-3}	10^{-6}	2.10^{-3}	10^{-8}

In table (2), ϕ is the soil friction angle, c is the cohesion, E is the Young's modulus, ν is the Poisson's ratio, ψ is the dilatancy angle, e is the void index, and k is the permeability.

The analysis during the reservoir filling is performed considering two effects associated with pressure of water and wetting. The buoyancy forces that correspond to the water level of the reservoir are also accounted for. These forces are evaluated in the conditions corresponding to the minimum and maximum water levels in the reservoir. Then the difference between them was gradually applied to the slope during a time span coinciding with the average time required by filling. During the filling of the reservoir, the values of geotechnical parameters decrease through the embankment as well as the Young modulus because of the wetting effect [15].

The long-term analysis is performed, under assumptions neither variations associated to the periodic variations of the level of the reservoir nor seismic loading, are accounted for. The maximum storage reservoir level is considered that is maintained long enough to produce a steady-state seepage condition. In the long-term behavior analysis all materials are considered fully drained (effective)

associated with wet material conditions. The values of geotechnical parameters and elastic parameters (Young modulus and Poison's ratio) of the construction materials decrease [15].

Subsequently and due to the change of the embankment volume on the dam foundation, several analyses need to be performed in order to predict the material behaviours at the embankment-foundation interface.

9. Prediction of Settlement

The finite element analysis is performed to predict the vertical displacement of El Hma dam at the end of construction, during first impounding and at long term. Results of analyses illustrating the evolution of settlements at the embankment-foundation interface for the elastic, Drucker-Prager [20] and for Mohr-Coulomb criteria at the end of construction, during first reservoir filling and at long term have been plotted in figures (3 to 5).

A comparison between different criteria used at the embankment-foundation interface for the three different states: end of construction, during first impounding and at long term have been depicted in figures (6 to 8).

At the end of construction of the dam, the calculated settlement underneath the crest, more precisely at the embankment-foundation interface, reached approximately 0.56 m for the elastic model, 0.70 m for Drucker-Prager criterion and 1.04 m for Mohr-Coulomb criterion. After impounding, the calculated settlement under the crest, especially at the embankment-foundation interface, increases to reach approximately 0.70 m for the elastic model, 0.80 m for Drucker-Prager criterion and 1.70 m for Mohr-Coulomb criterion. At long term, these calculated settlements continue to increase and reach approximately 0.80 m for the elastic model, 1.30 m for Drucker-Prager criterion and 2.00 m for Mohr-Coulomb criterion.

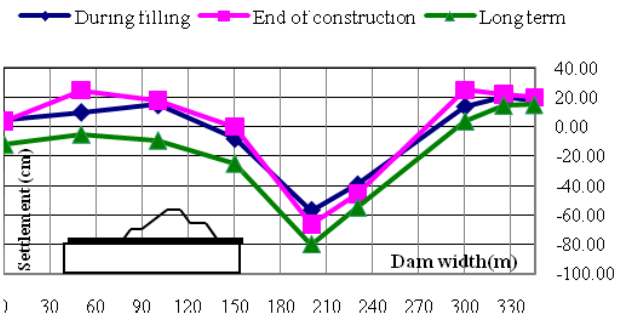

Fig. (3). Settlement at the interface embankment-foundation-Elastic model

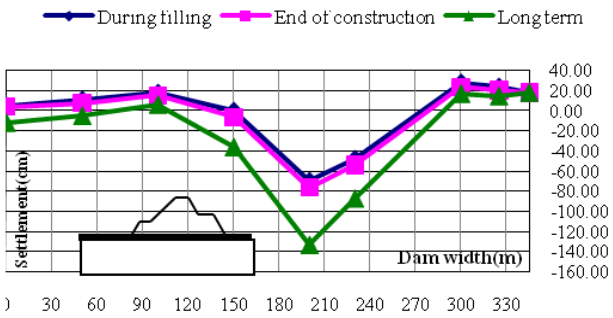

Fig. (4). Settlement at the interface embankment-foundation- Drucker-Prager model

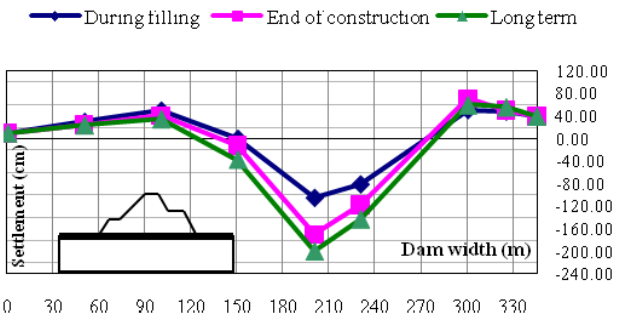

Fig. (5). Settlement at the interface embankment-foundation- Mohr-Coulomb model

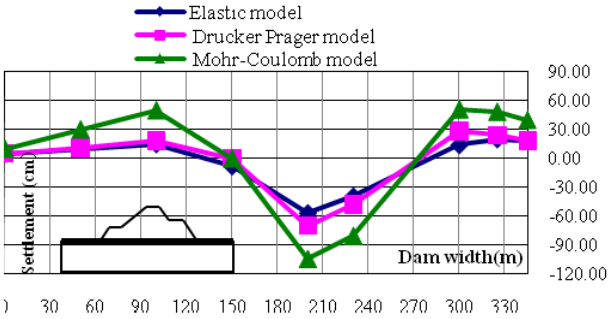

Fig. (6). Settlement at the interface embankment-foundation at end of construction - comparison between different criteria.

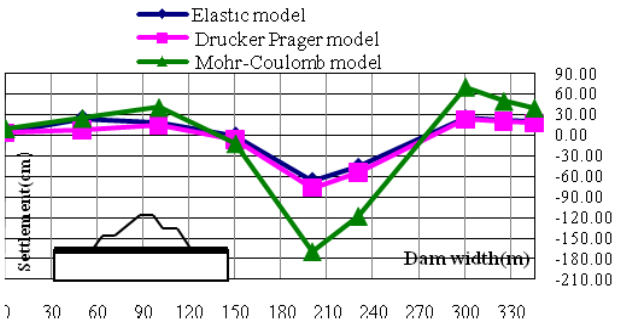

Fig. (7). Settlement at the interface embankment-foundation during filling-comparison between different criteria.

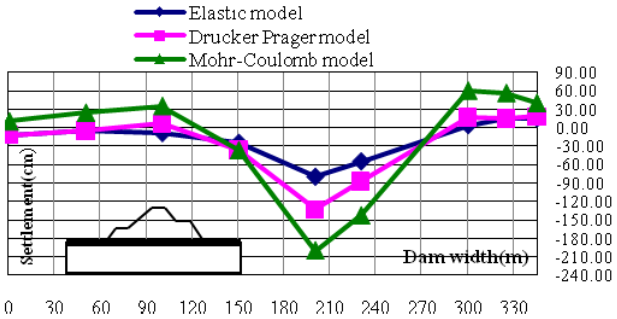

Fig. (8). Settlement at the interface embankment-foundation at long term -comparison between different criteria.

At the end of construction, these calculated settlements under the embankment are associated with significant swellings at the upstream and downstream toes of the dam. Then, these swellings decrease, due to soil consolidation, and reach small values at long term for all three criteria at the upstream toe level of the structure.

The decreasing of vertical displacement at the upstream toe of the dam is caused by the effects of pressure of water and effect of wetting. Similar observation can be demonstrated for the downstream toe of the dam that at long term the soil swelling stabilizes. However these displacements remain more significant compared to those occurred at the upstream toe of the dam.

The magnitude of settlements is due to the following combination:

- the consolidation corresponding to an increasing of effective stresses

- modifications of effective stresses due to variations of volumetric weight of foundation and embankment soils and variations of pore pressures associated with settlements
- the development of significant lateral strains.

10. Prediction of Horizontal Displacements

Distributions of horizontal displacements within the dam depend strongly on the consolidation state under the embankment. Horizontal displacement predictions of the dam and the downstream berm for three criteria; elastic, Drucker-Prager and for Mohr-Coulomb at the end of construction, during first reservoir impounding and at long term have been plotted in figures (9 to 11). When plotting displacement versus the height, the heterogeneity of materials across the dam from the berm level to foundation layers has been considered.

As can be seen from the figures, these displacements reach their maximum values beneath the downstream berm of the dam body. Additionally, the slope changes once new material is crossed. At long term, horizontal displacements increase over the time to reach their maximum values about 0.62 m for Mohr-Coulomb criterion, about 0.45 m for Drucker-Prager criterion and about 0.32 m for elastic criterion.

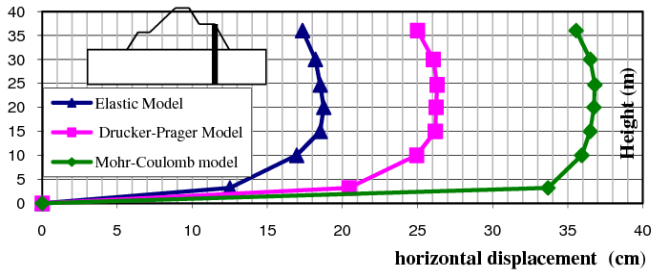

Fig. (9). Horizontal displacement of the downstream shoulder at the end of construction.

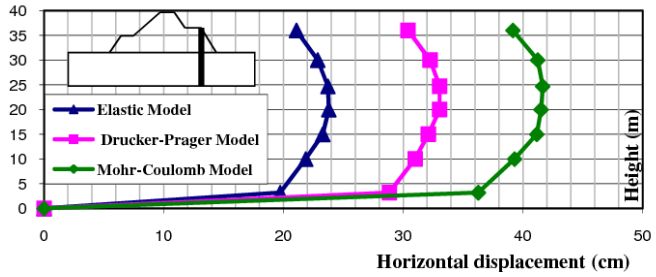

Fig. (10). Horizontal displacement of the downstream shoulder during filling.

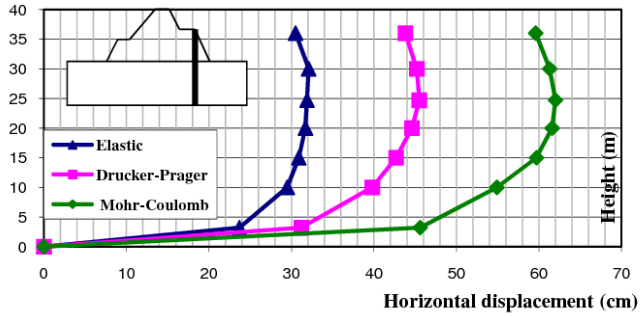

Fig. (11). Horizontal displacement of the downstream shoulder at long term.

11. Prediction of Stress State and Pore Pressure

ABAQUS is also used to conduct effective stress analysis. First, the nodal pore pressures are evaluated through a finite element seepage calculation adopting the same mesh used also for the stress analyses. Then, the nodal forces equivalent, in the finite element sense, to the calculated pore pressures are determined and introduced as external loads in the stress analysis.

The development of pore pressure in the central zone of the core is quite large comparing with that in the other two sides of the clayey core. Moreover, as can be seen that the pore pressure increases under the upstream and downstream toes of the dam for Mohr-Coulomb criterion, while under the crest of the dam the maximum pore pressure is developed for elastic and Drucker-Prager criteria.

Superposed stress diagrams for different criteria at long term have been plotted in figures (13 to 14). The maximum stress under the crest of the dam is a tensile stress for three criteria. Adversely, in the upstream and downstream toes of the dam the stresses are not higher. However, it should be noted, therefore, that in Figure (13), the estimated stress from 2D modelling of about 2.5 MPa under the middle of the dam is not realistic. The estimated stress from the three-dimensional model is of about 9.50 MPa. More investigation, mainly the results from automated monitoring surveys, should be conducted in order to verify and to enhance the Finite Element model.

Obviously, in figure 14 the behaviour of the dam at long term is totally compressive in term of effective stresses. This gives a realistic idea of the dam behaviour. The concentration of compressive effective stresses under the crest reaches about 2.4 MPa for the elastic criterion, about 2.5 MPa for the Mohr-Coulomb criterion and about 3.6 MPa for the Druger-Prager criterion.

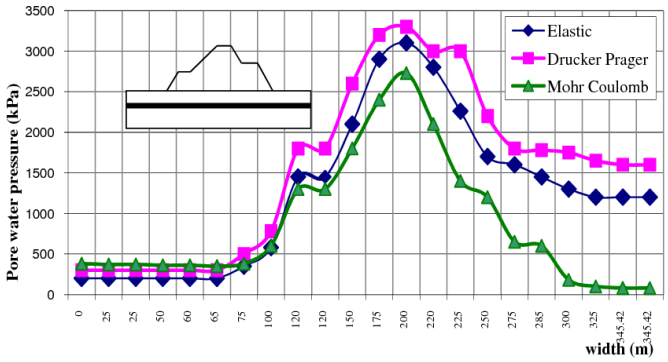

Fig. (12). Pore water pressure in the middle of the foundation at long term.

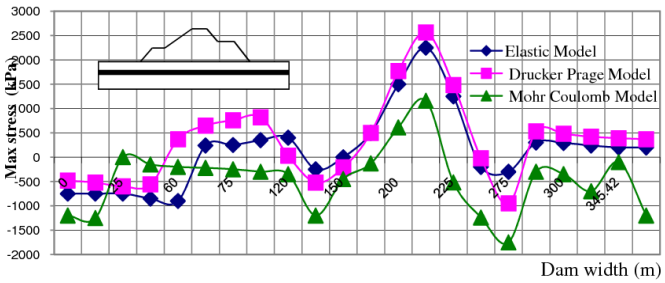

Fig. (13). Maximum stress in the principal plane at the middle of the dam foundation using different behavior models at long term.

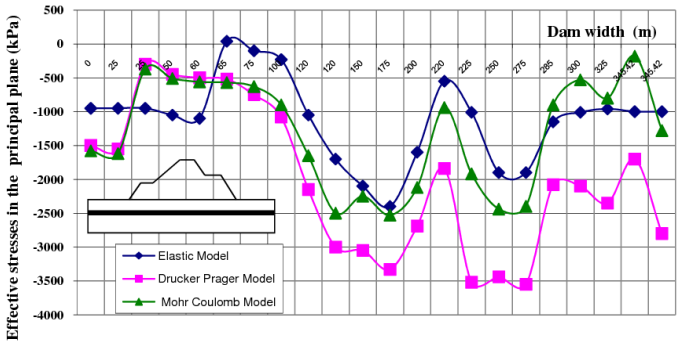

Fig. (14). Effective stress calculated in the principal plane at the middle of the dam foundation by different behaviour models at long term.

12. Conclusion and Recommendations

The results of two-dimensional numerical modelling with ABAQUS software and its constituent models led to results highlighting the potential benefits of using this approach to predict the behaviour of El Hma earth dam**.**

El Hma embankment dam was used as a case study to apply and compare different constitutive models. The behaviour criteria that will be judged the more suitable is the one that gives the closer deformation values to the observed deformation. However, more elaborated constitutive model should be used in attempting to reach a more realistic final state of stress.

However, he most critical problem encountered in modeling the deformations is obtain in-situ characteristics of construction soil material, which is the main source of uncertainty in modeling the deformations. The selection of material model in order to predict the behaviour of earth structure is most important when dealing with finite element modelling.

The long-term prediction of settlement of the El Hma earth dam, a simple creep model should be introduced in order to predict long-term time-dependent fill materials behaviour and the evaluation of model parameters. For future analysis a concepts from viscoplasticity and constitutive model that describes the soil creep behaviour should be incorporated.

Further research must be devoted to the development of integrated monitoring systems to increase the reliability of El Hma dam. The mathematical modeling of deformations by using finite element method should be integrated in the design and analysis of monitoring surveys. The location of the sensors or the observed targets must include points where maximum deformations are expected. As depicted in Figure 13, the estimated stress from 2D modelling of about 2.5 MPa under the middle of the dam is not realistic. The automated monitoring surveys should be conducted in the middle of the dam in order to verify and to enhance the Finite Element model.

13. Acknowledgments

The authors extend their gratitude to the Direction of Large Hydraulic Structure of the Ministry of Agriculture, Tunisia, who provides support and required documents concerning El Hma dam.

14. References

[1] Peignaud, "*Observation pendant et après la construction du remblai. Chapitre IX (Remblai et fondation sur sols compressibles*". Ouvrage collectif publié sous la direction de JP Magnan E.P.C, (1984).

[2] Tedd P., Charles J.A., Holton I. A., and Robertshaw A. C.,. "Deformation of embankment dams due to changes in reservoir level", *Proceedings of 13th International Conference on Soil Mechanics and Foundation Engineering*, New Delhi, Vol. 3, (1994), pp. 951-954,.

[3] Zienkiewicz, O. C. "*The Finite Element Method in Engineering Science*", McGraw-Hill, London, (1971).

[4] Kondner, R.L, "Hyperbolic stress-strain response: cohesive soils", *Journal of the Soil Mechanics and Foundation Division, ASCE*, 89 (SM1), (1963), pp. 115-143.
[5] Duncan, J.M. and C.Y. Chang, "Nonlinear analysis of stress and strain in soils". *Journal Soil Mech. and Found. Div., ASCE*, 96(SM5), (1970), pp. 1629-1653.
[6] Duncan, J.M., "State of the art: limit equilibrium and finite-element analysis of slopes". *ASCE Journal of Geotechnical. Engineering*, 122 (7), (1996), pp. 577-596.
[7] Habbitt, "*Finite Element Software Package*", Karlsson and Sorrenson Inc. (2003) ABAQUS.
[8] Mrabet, Z., El Ouni, Kheder, K. "Probabilistic modelling and reliability analysis of earth structures in geotechnical engineering". *First Euro Mediterranean in Advances on Geomaterials and Structures, Hammamet*, 3-5 May Tunisia, (2006).
[9] Londe P., "*Le role des instruments de mesure dans les fondations des grands ouvrages*". Annales ITBTP. Sols et fondations n°168, (1979).
[10] Chen W. F and A. F. Saleeb, "*Constitutive Equations for Engineering Materials*", Vol. 1. Elasticity and Modelling, Wiley, New York, (1982).
[11] Desai, C. S. "Theory and Application of the Finite Element Method in Geotechnical Engineering". In Application of the Finite Element Method in Geotechnical Engineering, *A Symposium, C. S. Desai (ed.), U.S. Army Engineer Waterways Experiment Station, Vicksburg, Miss.*, (1972), pp. 3-90.
[12] Binquet J., "*Comportement de construction des remblais argileux des barrages de Bir M'cherge, L Mornaguia, Sidi Salem et BouHertma (Tunisie)*". Journées, barrage en argile", EDF-Chambéry, (1986).
[13] Jafarzadeh, F. and R. Shafipour, "Seepage Analysis of an earth dam considering three-dimensional effects of valley shape and material inhomogeneities", *12th Panamerican Conference of Soil Mechanic and Geotechnical Engineering*, Cambridge, Massachusetts, U.S.A., (2003).
[14] Mrabet, Z. & Giles, D., "Uncertainties in the stationary seepage modelling". *Fifth International Conference on Hydroinformatics*, Cardiff, UK, 1-5 July, 2002, Vol. 2, (2002), pp 205-212.
[15] Jrad, A., "*Modelisation du comportement d'un barrage en terre*". Master thesis. National School of Engineering of Tunis, (2004).
[16] El Ouni, "Application des lois de comportement des sols à la modélisation de barrage lebna": *Colloque international sur le risque en Génie civil*, Hammamet, (2004), pp 19-24.
[17] El Ouni, Ennabli et Ben Abdallah, "*Le comportement en cours de construction des remblais argileux des barrages : Sidi Salem, Bouhertma et Lebna*", (1990).
[18] El Ouni, "*Comportement des l'argiles compactées - Application au barrage lebna*". Thèse de doctorat INPG. Grenoble, (1990).

[19] El Ouni, "*Les lois de comportement des sols et leurs applications à la modélisation de deux barrages en terre*". Thèse de doctorat FUSAG Belgique, (2000).
[20] Drucker, D.C. and W. Prager, "Soil Mechanics and Plastic Analysis or Limit Design". *Quarterly of Applied Mathematics*, Vol. 10, (1952), pp. 157-165.
[21] Bazant, Z.P. and R.J. Krizek, "Endochronic Constitutive Law for Liquefaction of Sand" *ASCE Journal of Engineering Mechanics*, Vol. 102, No. EM2, (1976), pp. 225-238.
[22] Bordes J.-L., "*Auscultation des barrages en terre : Appareils, mise en place et suivi*". Session de formation continue. ENPC et EHTP – Raba, (1984).
[23] Chrzanowski A., Szostak-Chrzanowski A., Massiéra M., Whittaker C.,"Monitoring and Numerical Modelling of Deformations of Large Dams – a Case Study", *Journal of Technical Sciences, Publisher University of Warmia and Mazury*, Olsztyn, (2002), pp. 47-60.
[24] Kheder K., "*Méthodologie d'études de la stabilité des carrières souterraines complexes exploitées par chambres et piliers abandonnés*". Thèse de Doctorat de l'Institut National Polytechnique de Lorraine. Laboratoire de Mécanique des Terrains de l'Ecole des Mines de Nancy, (1996).
[25] Krouma N, "*Modélisation du comportement Mécanique des sols*". Master thesis. National School of Engineering of Tunis, (2004).

السلوك الميكانيكي لسد أرضي باستعمال طريقة المحاكاة العناصر المحدودة مع إدراج قوانين مختلفة لسلوك التربة المستعملة : منطقة الدراسة سد الحمى بن عروس تونس

خالد محمد خضر[١] زهير مرابط[٢] عبد الله جراد[٣] رضا العوني[٤]

[١] *أستاذ مساعد قسم الهندسة المدنية بكلية الهندسة بجامعة الخرج khaledkheder@ymail.com*

[٢] *مستشار هندسي بمكتب الدراسات الهندسية جيو ريسك للإستشارات, نيويورك الولايات المتحدة الأمريكية zouhair.mrabet@yahoo.com*

[٣] *مهندس أول بالديوان الوطني للتطهير قسم الهندسة المدنية تونس jrad.Abdallah@yahoo.com*

[٤] *أستاذ مشارك بقسم الهندسة الجيوتقنية للسدود بالمعهد الوطني الفلاحي بتونس AlOuni.Ridha@yahoo.com*

(قدم للنشر في ٢٠٠٩/١٠/١٢م ؛ وقبل للنشر في ٢٠١٠/١٠/١٠م)

ملخص البحث. هذا البحث يهتم بدراسة السلوك الميكانيكي لسد أرضي في نهاية البناء, عند أول ملء الخزان بالمياه, و بالأخذ بعين الاعتبار عامل الوقت على المدى الطويل من الاستغلال بالمحاكاة بطريقة العناصر المحدودة (Finite Elements Method). في هذا البحث تم التطرق إلي سد الحمى بتونس والذي تم اختياره كمثال دراسي. من أجل فهم سلوكه تم الاعتماد علي ثلاثة قوانين رياضية أساسية لمحاكاة خصائص المواد المستعملة في البناء جسم السد وقاعدته وهي على التوالي : قانون المرونة (Elastic Law), الإلستوبلاستيكي مور- كولونب ودراكر- براقر (Mohr-Coulomb and Drucker-Prager Elasto-Plastic Laws). في هذا الإطار تم الاهتمام بدراسة تقييم التشوهات والجهد والضغط المائي داخل السد وكذلك تحليل النتائج المتوقعة والتي تمكن من تقدير السلوك الشامل لهذا السد.

Journal of Engineering and Computer Sciences
Qassim University, Vol. 4, No. 1, pp. 21-40 (January 2011/Moharram 1432H)

Optimal Design of a Fuzzy Logic Stabilizer For A Superconducting Generator in a Multi-Machine System Using Particle Swarm Optimozation

R. A. F. Saleh

Electrical Engineering Dept., College of Engineering,
Qassim University, Qassim, Saudi Arabia
ragaeys@yahoo.com

(Received 14/7/2009; accepted for publication 10/7/2010)

Abstract. This paper presents and describes an approach for the optimal design of a fuzzy logic stabilizer to enhance the stability of a superconducting generator (SCG) in a multi-machine system. The input signals to the proposed fuzzy stabilizer are the SCG speed deviation and acceleration. In this approach, unsymmetrical nonlinear membership functions are used, while number of stabilizer parameters to be properly designed is 15, including scaling factors for input and output variables along with widths and centers of fuzzy sets of input variables. Particle swarm optimization (PSO) technique is employed to search for optimal settings of the fuzzy stabilizer parameters. Simulation results show that the proposed, PSO-tuned fuzzy stabilizer provides good damping to SCG in a multi-machine environment when operating in conjunction with conventional stabilizers on other machines.

Keywords: Fuzzy logic stabilizer, Superconducting generator, Multi-machine system, Particle swarm optimization

1. Introduction

The application of superconductors to electric power apparatus is considered a key technology for the current century. The electric power demand has been steadily increased worldwide. This tendency will continue in the future, and therefore the capacities of the power transmission systems have to increase. Large power systems require developing a more efficient and stabilizing technology for large amounts of power transmission. One promising method is to introduce the superconducting generator (SCG), which has a very low synchronous reactance [1]. Superconducting generators have also many other potential advantages compared with the conventional generators such as higher efficiency and smaller size and weight. The advantages of SCG have drawn more interest in industrial countries since 1970's, such as in Japan where many R&D projects on SCGs were conducted at utility companies, power plant manufacturers and other organization toward 200-MW class pilot machine [2-6]. Despite these advantages, SCG field winding has an extremely large time constant. The excitation system is therefore not able to change quickly the field current to meet the grid requirements under transient conditions. Inevitably, the only control means feasible to enhance SCG stability following power system faults is the fast-acting governors on the steam supplies to the turbine.

Transient stability is one of the most important issues that should be investigated in power system planning, operation, and expansion. It is mainly concerned with maintaining generator synchronization following a sudden and major disturbance or an abrupt change in load or generation power. The importance of this issue increases when considering a superconducting generator in a multi-machine system. In the past, a number of investigations have been conducted to study and improve the behaviour of a superconducting generator in a multi-machine system [7-8], The results reported in [7] show that the incorporation of a SCG in a multi-machine system increases its stability reserve, but slightly reduces the overall damping of the system. However, a good improvement in the performance and stability limits can be achieved by using a conventional lead stabilizer in the governor loop of the SCG [8]. Alternative stabilizers based on adaptive control techniques have been proposed [9-11]. However, the on-line parameter identification is still questionable especially during fault periods. Recently, fuzzy logic control has emerged as one of the most fruitful research areas, and many applications for enhancing power system stability have been reported in literature [12-13]. A recent literature survey on the work done on the fuzzy logic controller and the approaches made to enhance its effectiveness are given in the introduction of Ref. [14]. The fuzzy logic stabilizer is essentially a multi-parameter controller, whose performance depends on the shape of membership functions, rule base and scaling factors. However, the design of a fuzzy stabilizer with satisfactory performance is a rather difficult problem. To overcome this problem, genetic algorithm (GA) was proposed as an efficient technique for the optimal design of power system stabilizers [15-16]. More recently, a new heuristic search method called *particle swarm optimization* (PSO) has been introduced [17-18]. PSO is characterized as a simple concept, easy to implement, and computationally efficient.

Theses features make PSO technique able to accomplish the same goal as GA optimization in a new and faster way. A number of very recent successful applications of PSO on various power system problems have been reported in literature [19-21]. Nevertheless, a new optimization method called "*Biogeography-Based Optimization*" (BBO) has been recently introduced [22]. BBO has common features with GA and PSO, but also it has different characteristics that distinguish it from other population-based optimization techniques. However, BBC method still has a long way to go to prove its validity as an efficient, global search technique. The objective of this paper is to enhance the stability of a SCG in a multi-machine system using fuzzy governor controller optimally designed by the PSO technique.

2. System under Study

The multi-machine system under consideration is shown in Fig. (1). It is a twelve-bus four-machine power system. The machine at bus 3 is a superconducting generator, while the other three machines are conventional generators. The four generating units are connected to four load areas as shown in the figure. Based on Park's d-q axis representation, each conventional machine is modelled by seven non-linear differential equations [23]. The order of SCG model is increased to nine to accommodate the double-screened rotor. Transmission lines are modeled using the π-method, and the loads are represented by constant impedances. Each conventional generator is equipped with a typical excitation system and a conventional power system stabilizer (PSS) having the transfer function $G_s(1+0.15s)/(1+0.015s)$ [24], where G_s is a gain. The block diagram of the excitation system is shown in Fig. (2). In this study, the mechanical input to each conventional generator is assumed constant. Meanwhile, a detailed representation for the prime mover of the SCG is used, because it is the main concern of this study. The SCG is driven by a three-stage steam turbine with reheat. The turbine is controlled by fast acting electro-hydraulic governors fitted to the main and interceptor valves, which are working in unison. Mathematical models for SCG, turbine and governors, along with the system parameters are given in the Appendix.

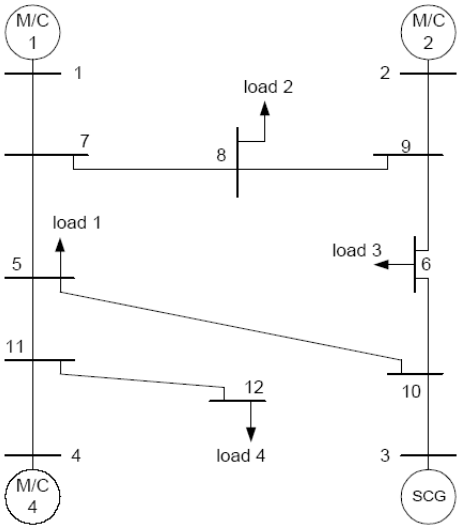

Fig. (1). Four-machine power system

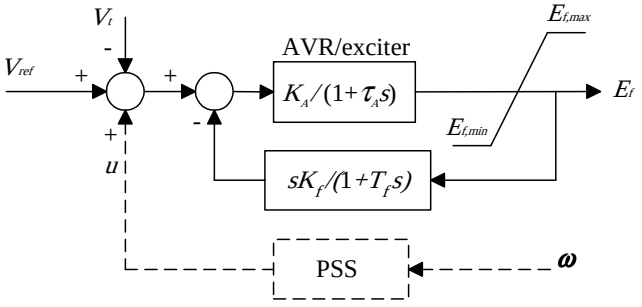

Fig. (2). Excitation system block diagram

3. Particle Swarm Optimization

Particle swarm optimization (PSO) models the behavior and cooperation aspects of individual members within a social system. In this model, the system is populated with individual particles, referred to as "swarm", representing possible solutions to the problem considered. Particles fly around in a multidimensional search space. During flight, each particle adjusts its position according to its own experience, and experience of neighbouring particles, making use of the best position encountered by itself and its neighbours. In PSO algorithm, each solution is represented as a particle in a swarm, having a position and velocity. Each position coordinate represents a

parameter value. Thus, for an n-dimensional optimization, each particle has a position in n-dimensional space that represents a solution [18]. The PSO starts with generation of initial swarm particles, assigning a random position and a random velocity for each particle. Then, PSO algorithm evaluates each particle's fitness using a predefined fitness (objective) function. The position with the highest fitness value in the entire run is referred to as "global best position" (g_{best}). Meanwhile, each particle keeps track of its highest fitness value. The location of this value is called "personal best position" (p_{best}). The algorithm then proceeds by updating the velocity of each particle using its current velocity and its distance from g_{best} and p_{best} according to the following equation:

$$v_i^k = w^k v_i^{k-1} + c_1 r_1 (p_{best,i} - x_i^{k-1}) + c_2 r_2 (g_{best,i} - x_i^{k-1}) \quad (1)$$

i = 1, 2, 3, ……..m

v_i^k is the velocity of particle i at iteration k

x_i^k is the position of particle i at iteration k

r_1, r_2 are uniformly distributed random numbers in the range [0, 1]

c_1, c_2 are positive constants

w^k is the inertia weight at iteration k

m is the number of particles in a swarm

As originally developed, large inertia weight is recommended at initial stages of the search process to enhance the global exploration, while lower values of the inertia weight are preferred at final stages to improve local exploration. The inertia weight can be decreased either linearly over search iterations or in a non-linear form as follows [18]:

$$w^k = \alpha w^{k-1} \quad (2)$$

Where α is a decrement constant. Another important parameter of PSO procedure is the maximum velocity (V_{max}) of a particle in any given dimension. This parameter determines the resolution with which the search space is explored. After updating the velocities, the position of each particle is modified according to the following equation:

$$x_i^k = x_i^{k-1} + v_i^k \quad (3)$$

The algorithm proceeds by updating the best position of each particle according to its new position; the global best position is then updated as well. This procedure is repeated until a specified termination condition is met.

4. Fuzzy Logic Stabilizer

In this section, the determination of an efficient control signal, *u*, based on fuzzy logic is described. This signal is then introduced into the governor side of the SCG turbine as shown in Fig. (3).

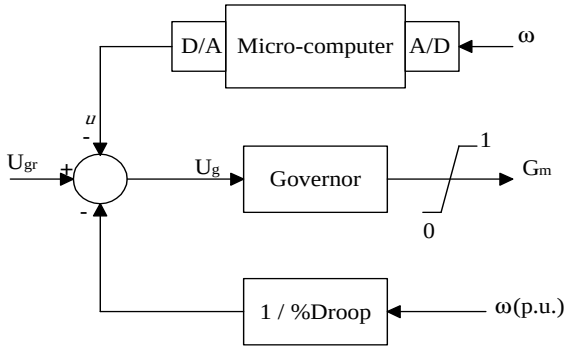

Fig. (3). The governor control system

Speed deviation, ω, and its derivative, $\dot{\omega}$, are chosen as input variables. Actual speed is the only signal to be measured. Then ω signal is determined, and $\dot{\omega}$ signal is computed as:

$$\dot{\omega}(k) = [\omega(k) - \omega(k-1)] / T_s \tag{4}$$

where T_s is the sampling interval. Two scaling factors, K_A and K_B, are used to map ω and $\dot{\omega}$, respectively into their predefined universes of discourse, which are divided into seven overlapping fuzzy sets; named positive large "PL", positive medium "PM", positive small "PS", zero "ZE", negative small "NS', negative medium "NM", and negative large "NL". A non-linear (nearly bell-shaped) membership function is assigned for each fuzzy set such that if a crisp input "x" belongs to a set of range [a-b], width "d" and center "c", then its degree of membership μ_x, in this set is defined by the following function:

$$\mu_x = \begin{cases} (2(x-a)/d)^2 & \text{if } a \le x \le c \\ (2(b-x)/d)^2 & \text{if } c \le x \le b \\ 0 & \text{else} \end{cases} \tag{5}$$

Table (1) shows the fuzzy rules that are assigned for the SCG system. Each entry in Table (1) represents a control rule, which takes the form: "IF ω is A, AND $\dot{\omega}$ is B, THEN *u* is C", where A, B, and C are fuzzy sets as defined by relation (5).

These fuzzy rules are individually applied on the fuzzified inputs, resulting in an output fuzzy set, for each rule, clipped to a degree defined as:

$$\mu_c(u_i) = \min(\mu_A(\omega), \mu_B(\dot{\omega})) \tag{6}$$

The aggregated fuzzy outputs are converted into a single crisp value using the "weighted average" defuzzification method, which gives the output control signal as:

$$u = K_u \frac{\sum_{i=1}^{m} \mu_c(u_i).u_i}{\sum_{i=1}^{m} \mu_c(u_i)} \tag{7}$$

where K_u is a scaling factor, m is the number of rules giving contribution to the fuzzy output at the sampling instant considered, and u_i is the center value of the fuzzy set in consequent i. According to the structure of fuzzy logic stabilizer described above, the number of fuzzy sets, to which an input value belongs at a time, depends on how much overlap between adjacent fuzzy sets is.

Table (1). Fuzzy logic control rules for SCG system

ω \ $d\omega/dt$	**NL**	**NM**	**NS**	**ZE**	**PS**	**PM**	**PL**
NL	NS	PS	PM	PM	PM	PL	PL
NM	NS	NS	PS	PS	PM	PM	PL
NS	NM	NS	NS	PS	PS	PM	PM
ZE	NM	NM	NS	ZE	PS	PM	PM
PS	NM	NM	NS	NS	PS	PM	PM
PM	NL	NM	NS	NS	PS	PS	PS
PL	NL	NL	NM	NM	NS	NS	PS

5. PSO-Based Stabilizer Parameters Selection

The tuning parameters of the fuzzy stabilizer are K_A, K_B and K_u. Additional twelve adjustable parameters (six for ω fuzzy sets, and six for $\dot{\omega}$ sets) are introduced to enhance the effectiveness of the proposed fuzzy stabilizer. Namely, d_1, d_2, d_3 and d_4, which stand for widths of fuzzy sets (LP, MP, SP, ZE) of ω, and C_2 and C_3 which stand for centers of fuzzy sets (MP, SP) respectively. Similarly, d'_1, d'_2, d'_3, d'_4, C'_2 and $C'3$ are assigned for $\dot{\omega}$ fuzzy sets. Therefore, we have now fifteen parameters (K_A, K_B, K_u, d_1, d_2, d_3, d_4, C_2, C_3, d'_1, d'_2 , d'_3, d'_4, C'_2, C'_3) to be optimally chosen. This task is achieved using PSO technique. First, a quadratic performance index is defined as:

$$J = (\sum_{k=1}^{N} [\omega(k)]^2)^{0.5} \quad (8)$$

where $\omega(k)$ is the deviations of the SCG speed from the steady state value. The problem of designing a fuzzy logic stabilizer is then transformed into an optimization problem, where PSO is utilized off-line to select the stabilizer parameters. The proposed stabilizer was designed at the loads and operating points of case #1 shown in Table (5). However, like many recursive and stochastic methods, PSO itself has a number of parameters to be properly specified. The main PSO parameters are the initial inertia weight, w^0, and the maximum allowable velocity, V_{max}. The initial inertia weight is set at 1, and V_{max} at 12.5% of the search space of each variable. The swarm size of PSO is chosen to be 60 particles. Other parameters are set as decrement constant α=0.98, and $c_1 = c_2 = 2$.

6. Simulation Results

In this study, the SCG exciter voltage and the mechanical input to all conventional generators were kept constant during transients. The optimization process was carried out in response to a three-phase to ground fault of 200-ms duration at bus 5 at the end of line 5-10. Variation of the performance index J with the number of iterations is shown in Fig. (4), which indicates that J converges to 20.2 after 120 iterations. The performance index J was recalculated when the conventional stabilizer is installed with the SCG instead of the fuzzy stabilizer. In this case, it was found J =21.1, which is less than that with the proposed fuzzy stabilizer. The optimal fuzzy stabilizer parameters selected by PSO are K_A=0.584, K_B=0.358, K_u=1.616. The optimized fuzzy sets for ω and $\dot{\omega}$ have taken the shapes shown in Fig. (5).

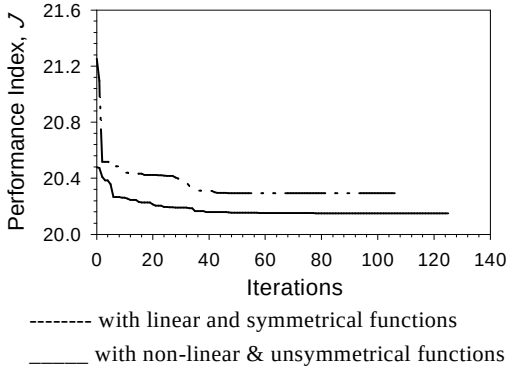

Fig. (4). Convergence of performance index with different designs

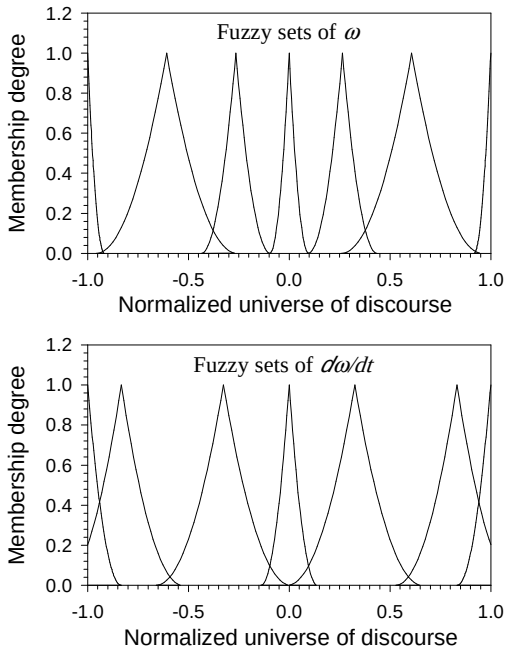

Fig. (5). Optimized fuzzy sets of ω and $d\omega/dt$

Since there is no infinite-bus, machine 4 was taken as a reference unit. The rotor angles of the other machines are shown with respect to that of the reference unit. The multi-machine system performance was obtained at three situations. First, when the four generators are not equipped with stabilizers. Second, when each conventional generator is equipped with a conventional PSS, while the SCG is stabilized via a governor lead stabilizer [8]. Third, as in second, but the governor lead stabilizer is replaced with the governor fuzzy stabilizer designed above. The SCG performance is shown in Fig. (6), Fig. (7), and Fig. (8). These figures also show the performance of other machines in the system. Fig. (9) shows the system response to the same fault, but with loads and operating points given under case #2 in Table (5) in the Appendix. The simulation results show that the incorporation of the proposed PSO-based fuzzy stabilizer in the governor loop of the SCG leads to a significant improvement in the SCG performance and an appreciable increase in damping of the rotor oscillations with a reduction in the rotor first swing. This can clearly be noticed from Figs. (6a), (6c) and Fig. (7). Fig. (10) shows that the fuzzy stabilizer damps well the SCG oscillations when it swings against the other machines in the system. This gives an indication that the proposed stabilizer is able to damp multimode oscillations in the system under study.

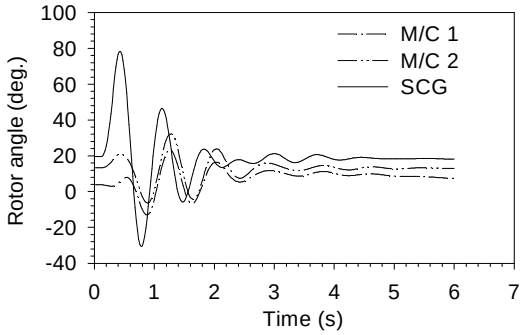

Fig. (6-a). System response to SC at operating point #1, all machines without stabilizer

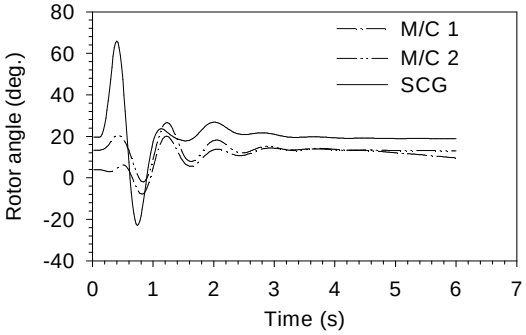

Fig. (6-b). System response to SC at operating point #1, conventional machines with PSS and SCG with lead stabilizer

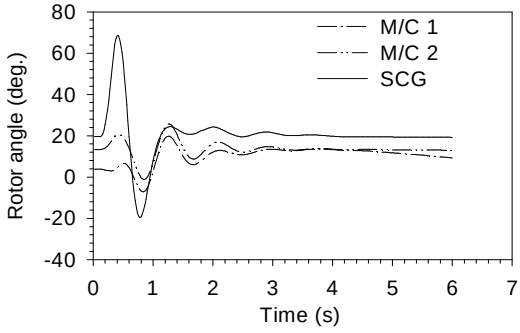

Fig. (6-c). System response to SC at operating point #1, conventional machines with PSS and SCG with fuzzy logic stabilizer

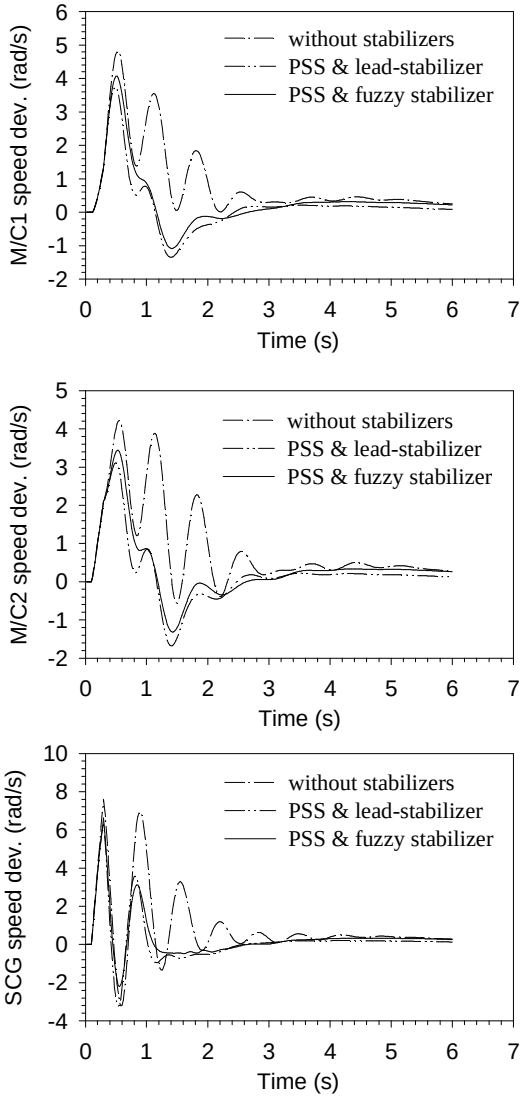

Fig. (7). System response to SC for 200 ms at operating point #1

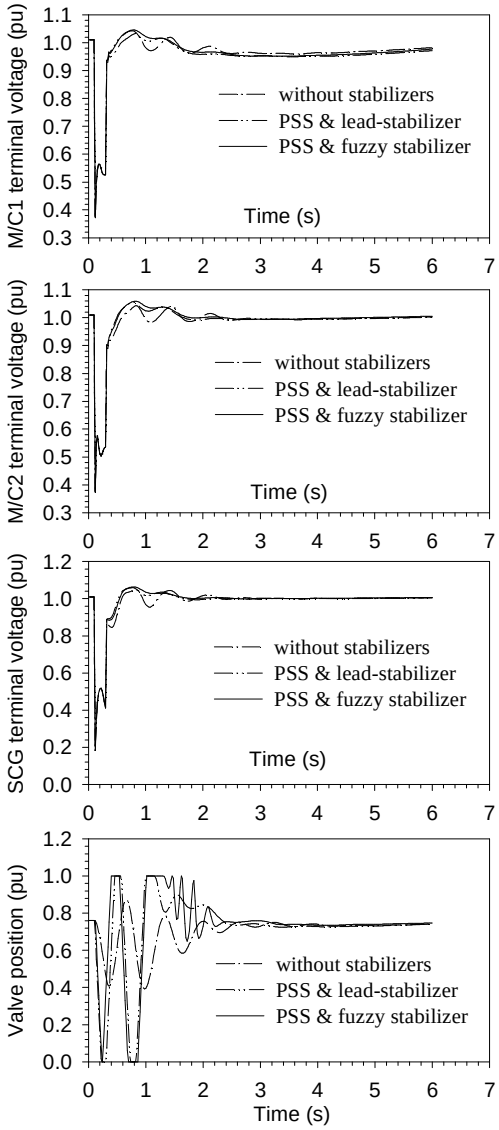

Fig. (8). System response to SC for 200 ms at operating point #1

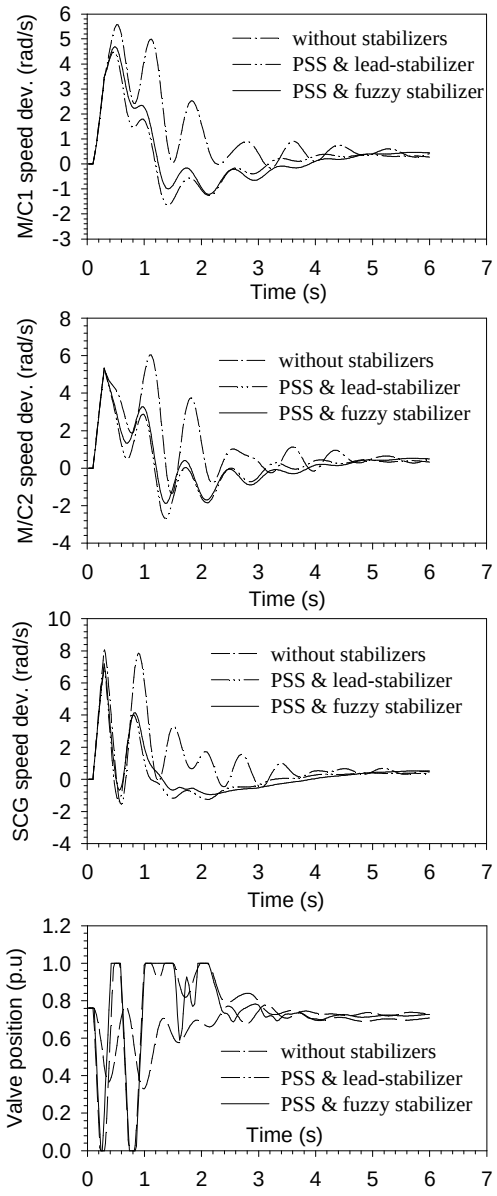

Fig. (9). System response to SC for 200 ms at operating point #2

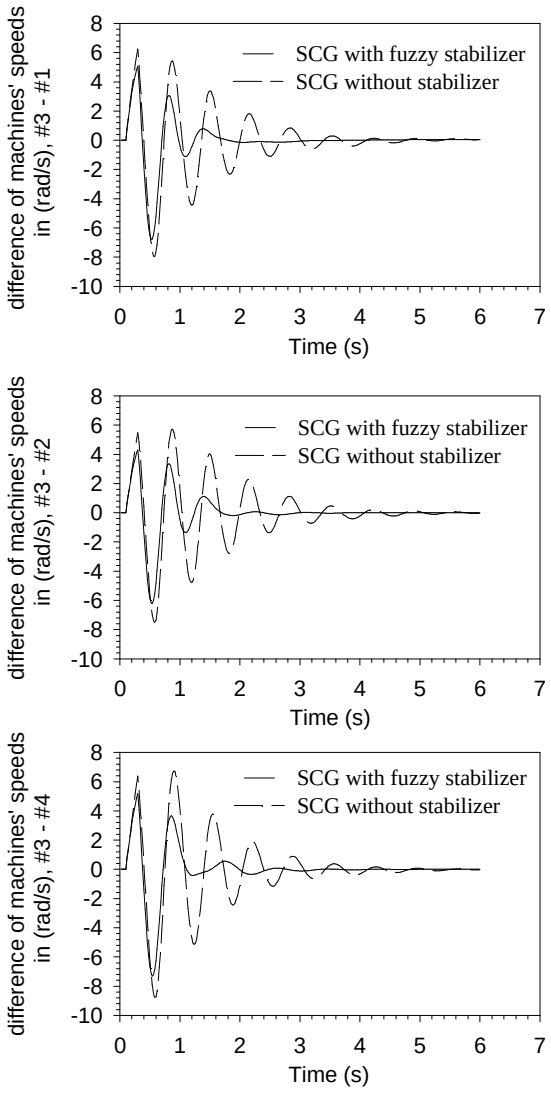

Fig. (10). System response to SC for 200 ms at operating point #1

7. Conclusion

This paper has proposed an approach for the design of a fuzzy logic stabilizer for transient performance improvement of a superconducting generator (SCG) operating in a multi-machine system. A set of fuzzy decision rules relating the SCG status, in terms of its speed deviation and acceleration, to the control action required was assigned based on previous experience with controller design. A performance index was defined, and then PSO technique was used to optimize a set of unknown stabilizer parameters at the specified loads. The results of non-linear simulation study show the effectiveness of the proposed PSO-tuned fuzzy stabilizer in damping the rotor oscillations and therefore enhancing the SCG stability.

8. References

[1] Nitta, T., Shirai, Y., Kawauchi, T., Okada, T., and Ogawa, Y., "Transient stability limit issues at three-phase short-circuit in parallel running of both a superconducting generator and a conventional one", *Electrical Engineering in Japan*, Vol. 115, No. 6, (1995), pp. 62-70.

[2] Ueda, K., Shiobara, R., Takahashi, M., and Ageta, T., "Measurement and analysis of 70 MW superconducting generator constants", *IEEE Trans. on Applied Superconductivity*, Vol.9, No.2, (1999), pp.1193-1196.

[3] Tsukiji, H., Hoshino, T., and Muta, I., "Output power limit of 200 MW class brushless super-conducting generator excited with magnetic flux pump" *IEEE Trans. on Applied Superconductivity*, Vol.11, No.1, (2001), pp.2335-2338.

[4] Amm, K., "100 MVA HTS Generator Development Update", *DOE HTS Wire Workshop*, Jan 19th, (2005).

[5] Maki, M., "Design study of high-temperature superconducting generators for wind power systems", 2008, *Journal of Physics*: *Conf. Ser*. 97 012155 (6pp)

[6] Goddard, K. F., Lukasik, B. and Sykulski, J. K. "Alternative Designs of High-Temperature Superconducting Synchronous Generators", *IEEE Trans. on Applied Superconductivity*, Vol. 19, No.6, (2010), pp. 3805-3811.

[7] Rahim, Y.H.A., Osheba, S.M., Alyan, M.A.A.S., and Al-Ohaly, A.A., "Stability of a multi-machine system incorporating a superconducting generator", *IEEE trans. on EC*, Vol. 3, No.3, (1988), pp.458-464.

[8] Osheba, S.M., Alyan, M.A.A.S., and Rahim, Y.H.A., "Comparison of transient performance of superconducting and conventional generators in a multi-machine system", *IEE Proc., Pt. C*, Vol. 135, No.5, (1988), pp. 389-395.

[9] Wu, Q.H., and Hogg, B.W., "Adaptive controller for a turbogenerator system", *IEE Proc., Pt. D*, Vol.135, (1988), pp. 35-42.

[10] Lim, C.M. and Hiyama, T., "Self tuning control scheme for stability enhancement of multi-machine power systems", *IEE Proc., Pt .C*, Vol.137, No.4, (1990), pp. 269-275.

[11] Chen, G.P., Malik, O.P., Hope, G.S., Qin, Y.H. and Xu, G.Y., "An adaptive power system stabilizer based on the self optimizing pole shifting control strategy", *IEEE Trans. on EC*, Vol.8, No.4, (1993), pp.639-645.

[12] Hiyama, T., “Robustness of fuzzy logic power system stabilizers applied to multi-machine power system”, *IEEE Trans. on EC*, Vol. 9, No. 3, (1994), pp.451-459.
[13] El-Metwally, K.A., Hancock, G.C., and Malik, O.P., “Implementation of a fuzzy logic PSS using a micro-controller and experimental test results”, *IEEE Trans. on EC*, Vol.11, No.1, (1996), pp.91-96.
[14] Mohaghegh, S., Venayagamoorthy, G., and Harely, R., "Fully evolvable optimal neurofuzzy controller using adaptive critic designs," *IEEE Trans. on Fuzzy Systems*, Vol.16, No. 6, (2008), pp. 1450-1461.
[15] Wen J.Y, Cheng, S.J., and Malik, O.P., “A synchronous generator fuzzy excitation controller optimally designed with a genetic algorithm”, *IEEE Trans. on Power Systems*, Vol.13, No.3, (1998), pp. 884-889.
[16] Saleh, R.A.F., and Bolton, H.R., “Genetic algorithm-aided design of a fuzzy logic stabilizer for a superconducting generator”, *IEEE Trans. on Power Systems*, Vol. 15, No.4, (2000), pp.1329-1335.
[17] Kennedy, J., and Eberhart, R., “Particle swarm optimization”, *Proc. of IEEE Int. Conf. on Neural Networks*, Vol. IV, (1995), pp.1942-1948.
[18] Eberhart, R., and Shi, Y., “Particle swarm optimization: developments, applications and resources”, *Proc. of the 2001 Congress on Evolutionary Computation*, Vol. 1, (2001), pp.81-86.
[19] Abido, M.A., “Optimal design of power system stabilizers using particle swarm optimization”, *IEEE Trans. on EC*, Vol. 17, No. 3, (2002), pp. 406-413.
[20] Park, J.B., Lee, K.S., Lee, K.Y., “A particle swarm optimization for economic dispatch with non-smooth cost functions”, *IEEE Trans. on Power Systems*, Vol. 20, No.1, (2005), pp.34-41.
[21] Abou El-Ela, A.A., Fetouh, T., Bisher, M.A., and Saleh, R.A.F., "Power systems operation using particle swarm optimization technique", *Electric Power Systems Research* 78, (2008), pp. 1906-1913.
[22] Simon, D., “Biogeography-Based Optimization,” *IEEE Transactions on Evolutionary Computation*, Vol. 12, No. 6, (2008), pp. 702-713.
[23] Hogg, B.W., “Representation and control of turbo-generators in electric power systems”, Chapter 5 in ‘*Modeling of dynamical systems’*, V.2, Peter Peregrinus Ltd., (1981).
[24] Anderson, P.M., and Fouad, A.A., “*Power systems control and stability*", 2nd edition, IEEE Press, New York, (1994).
[25] Saleh, R.A.F., “Stability improvement of a fully superconducting generator by fuzzy logic control”, *Journal of Engineering and Computer Sciences* , Qassim University, Vol. 1, No. 1, (2008), pp.19-28.
[26] Pullman, R.T., and Hogg, B.W., "Integrated control system for a turbo-generator", *International Journal of Control*, Vol. 29, (1979), pp. 505-521.

9. Appendix

The mathematical model of SCG [16]:

$$p\psi_f = \omega_o[V_f - i_f R_f] \quad (9)$$

$$p\psi_d = \omega_o[V_d + i_d R_a + \psi_q] + \psi_q \omega \quad (10)$$

$$p\psi_{D1} = -\omega_o i_{D1} R_{D1} \quad (11)$$

$$p\psi_{D2} = -\omega_o i_{D2} R_{D2} \quad (12)$$

$$p\psi_q = \omega_o[V_q + i_q R_a - \psi_d] - \psi_d \omega \quad (13)$$

$$p\psi_{Q1} = -\omega_o i_{Q1} R_{Q1} \quad (14)$$

$$p\psi_{Q2} = -\omega_o i_{Q2} R_{Q2} \quad (15)$$

$$p\delta = \omega \quad (16)$$

$$p\omega = \frac{\omega_o}{2H}[T_m - T_e] \quad (17)$$

$$T_e = \psi_d i_q - \psi_q i_d \quad (18)$$

P : derivative operator
ψ : flux linkage
ω_0 : synchronous speed (rad/s)
ω : rotor speed deviation from synchronous speed (rad/s)
δ : rotor angle with respect to infinite bus
H : inertia constant
T_m : mechanical torque

The mathematical model of the turbine and governor system [16, 26]:

$$pY_{HP} = (G_M P_o - Y_{HP}) / \tau_{HP} \quad (19)$$

$$pY_{RH} = (Y_{HP} - Y_{RH}) / \tau_{RH} \quad (20)$$

$$pY_{IP} = (G_I Y_{RH} - Y_{IP}) / \tau_{IP} \quad (21)$$

$$pY_{LP} = (Y_{IP} - Y_{LP}) / \tau_{LP} \quad (22)$$

$$T_m = F_{HP} Y_{HP} + F_{IP} Y_{IP} + F_{LP} Y_{LP} \quad (23)$$

$$pG_M = (U_g - G_M) / \tau_{GM} \quad (24)$$

$$pG_I = (U_g - G_I) / \tau_{GI} \quad (25)$$

P_o : boiler steam pressure
Y : output of a turbine or reheat stage
τ : time constant of stage

G_M , G_I : main and interceptor valve positions
F : fractional contribution of the turbine stage into T_m
U_g : governor actuating signal
The definitions of variables and parameters not defined in the paper can be found in references [8, 25].
Parameters of SCG (M/C #3), turbine and governor systems (inductance and resistance values in p.u; time constants in seconds)

L_f= 0.541, L_d=L_q= 0.5435, L_{D1}=L_{Q1}= 0.2567, L_{D2}=L_{Q2}= 0.4225, L_{fd}=L_{fD1}=L_{dD1}=L_{dD2}=L_{D1D2}= 0.237, L_{fD2}= 0.3898, L_{qQ1}=L_{qQ2}=L_{Q1Q2}=0.237, τ_f=750, R_d=R_q= 0.003, R_{D1}=R_{Q1}=0.01008, R_{D2}=R_{Q2}=0.00134, H=3 s , τ_{GM} =τ_{GI} =0.1, τ_{HP} =0.1, τ_{RH} =10, τ_{IP} =τ_{LP} =0.3, P_o = 1.2 p.u. , F_{HP} = 0.26, F_{IP} = 0.42, F_{LP} = 0.32

Table (2). Parameters of conventional generators

Parameter symbol	M/C #1	M/C #2	M/C #4
L_d (p.u)	2.11	2.13	0.898
L_q (p.u)	2.02	2.07	0.646
M_{dF}=M_{dD}=			
M_{FD} (p.u)	1.955	1.88	0.658
M_{qQ} (p.u)	1.865	1.82	0.406
L_F (p.u)	2.089	2.12	0.724
L_D (p.u)	2.07	1.97	0.668
L_Q (p.u)	1.93	1.88	0.457
R_a (p.u)	0.0046	0.0029	0.0014
R_F (p.u)	0.00013	0.00092	0.00026
R_D (p.u)	0.02	0.018	0.012
R_Q (p.u)	0.024	0.0212	0.02
H (s)	2.32	2.52	5.15

Table (3). Parameters of excitation systems and PSS

Parameter Symbol	M/C 1	M/C 2	M/C 4
K_A	200	4	200
T_A (s)	0.3575	0.02	0.02
T_f (s)	1.0	0.05	1.0
K_f	0.0529	0.05	.01
$E_{f\,min}$ (p.u)	-5.73	0.0	0.0
$E_{f\,max}$ (p.u)	5.73	4.46	7.32
G_s	0.03	0.03	0.04

Table (4). Parameters of transmission lines in p.u

Bus #	***R***	**j*X***	**j*Y***
1-7	0.0	0.12	0.0
7-8	0.009	0.152	0.0688
8-9	0.088	0.1055	0.0982
9-2	0.0	0.12	0.0
9-6	0.009	0.152	0.0688
6-10	0.009	0.152	0.0688
10-3	0.0	0.12	0.0
10-5	0.0088	0.1055	0.0982
7-5	0.009	0.152	0.0688
5-11	0.009	0.152	0.0688
11-4	0.0	0.12	0.0
11-12	0.018	0.304	0.0344

Table (5). Loads and operating points

	***P* + j*Q* (p.u)**	
	Case #1	**Case # 2**
Load 1	-0.5 -j0.309	-0.8-j0.48
Load 2	-0.3 -j0.155	-0.3-j0.18
Load 3	-0.25-j0.155	-0.3-j0.18
Load 4	-0.25-j0.155	-0.3-j0.18
M/C 1	0.12 +j 0.058	0.2237+j0.14
M/C 2	0.2 +j0.04	0.5 +j0.111
M/C 4	0.235+j 0.154	0.235 +j0.2587
SCG	0.75 +j0.11	0.75 +j0.2037

تصميم أمثل لموازن غيمي المنطق لمولد فائق التوصيل في نظام متعدد الآلات باستخدام طريقة السرب

رجائي عبد الفتاح صالح

قسم الهندسة الكهربائية – كلية الهندسة – جامعة القصيم

القصيم – المملكة العربية السعودية

ragaeys@yahoo.com

(قدم للنشر في ٢٠٠٩/٧/١٤م؛ وقبل للنشر في ٢٠١٠/٧/١٠م)

ملخص البحث. يقدم هذا البحث طريقة حديثة و فعالة لتصميم موازن غيمى ، وذلك لإخماد الذبذبات الميكانيكية و تحسين الاستقرار لمولد فائق التوصيل متصل بنظام متعدد الآلات. في هذه الدراسة تم استخدام دوال عضوية غير خطية و غير متماثلة الاتساع لكل من الانحراف في سرعة المولد و معدل التغير في السرعة. واللذان يمثلان المتغيرات الداخلة للموازن الغيمى. تضم مجموعة ثوابت الموازن ١٥عنصرا يجب اختيارها بعناية. تم استخدام طريقة بحث حديثة (تحاكى أسلوب أسراب الطيور فى الوصول إلى أهدافها) لتحديد أفضل قيم لثوابت الموازن الغيمى. توضح نتائج المحاكاة أن الموازن الغيمى المقترح و المصمم بواسطة طريقة السرب يؤدى إلى تحسن واضح في أداء و استقرار النظام المدروس.

Journal of Engineering and Computer Sciences
Qassim University, Vol. 4, No. 1, pp. 41-61 (January 2011/Moharram 1432H)

Analysis of the Electro-Mechanical Performance of Network-Connected Induction Generators Governed by Different AC Voltage Controllers

M. A. Abdel-halim,[*] A. F. Almarshoud[**] and M. Munawer Shees[***]
College of Engineering, Qassim University, Saudi Arabia
[*]masamie@qec.edu.sa, [**]dr_almarshoud@qec.edu.sa, [***]munawwarshees@qec.edu.sa

(Received 15/7/2010; accepted for publication 10/11/2010)

Abstract. This paper presents a complete analysis of an induction generator linked to the power network through an ac voltage controller aiming to control the generated active and reactive power at different speeds. The ac voltage controller uses three different control strategies, namely; the firing angle-, the extinction angle- and the symmetrical angle- control strategies to control the generator terminal voltage. The generator electrical and mechanical performance characteristics regarding the harmonic distortion factors, active power, reactive power, power factor, steady torque, pulsating torques and efficiency have been computed at different speeds. These characteristics have been determined with the help of novel equivalent circuits in the frequency domain. These equivalent circuits enable accurate calculation of the generator performance characteristics as the numerical techniques are omitted. Also, unlike the dqo and the abc models, the present model takes into account the generator iron losses effects.
Keyword**:** *induction generator, ac voltage controller, grid-connected*

1. Introduction

Wind is a promising source of renewable energy in the world. This power may be utilized to generate electrical power using the induction generators [1-2].

The performance of a grid-connected induction generator using a solid state ac voltage controller as an interface between the grid and the stator terminals of the generator is studied in this paper. In this regard a forced-commutated ac voltage controller which utilizes a set of IGBT devices has been used.

Many authors have analyzed the self excited induction generators [3-8] which are utilized in far and isolated sites. The performance of controlled generators using ac voltage controllers has been analyzed in previous publications for naturally commutated voltage controllers, and forced commutated voltage controllers [9-11]. The analysis has been determined using numerical techniques based upon abc-dq reference frame models. In the present paper the steady-state electrical and mechanical performance of the generator has been analyzed through modeling the induction generator and the static converter by novel equivalent circuits in the frequency domain. This is expected to give more accurate results, and enables the iron losses to be taken into consideration which leads to accurate estimation of the generator efficiency.

Computer programs have been developed to determine the performance characteristics of the controlled generator for a wide range of operating conditions and specified switching strategies of the ac voltage controller. In this regard, the firing angle, the extinction angle and the symmetrical angle control strategies have been used. The computed performance characteristics included the generator current and its distortion factors, the generator active and reactive powers and the generator efficiency. Also, the bus current, its distortion factors, reflected harmonics on the supply, the displacement angle, the bus active and reactive powers, and the power factor has been computed. On the other side the mechanical performance characteristics regarding the unidirectional-developed torque and the pulsating components appearing as a result of the use of the ac voltage controller have been determined.

2. Solid State Control of the Induction Generator

Forced commutated AC voltage controller is suggested to be used as an interface between the grid and the induction generator. The proposed circuit is shown in Fig.(1). Each stator phase has control circuit that contains series and shunt IGBT devices in bridges of diodes to allow the current to pass in the two directions [9]. The two IGBT's are operated alternatively, when the series transistor is turned on, the shunt IGBT is turned off and vice versa. This control circuit links the induction generator with the network. The terminal voltage as well as the active and reactive power of the generator can be controlled by variation of the on and off periods of the series transistors. The shunt transistor bridge allows the clamped current in the stator phase during the off state of the series bridge to continue flowing as freewheeling path.

The transistorized AC voltage controller may be controlled using three different control strategies as follows [9]:

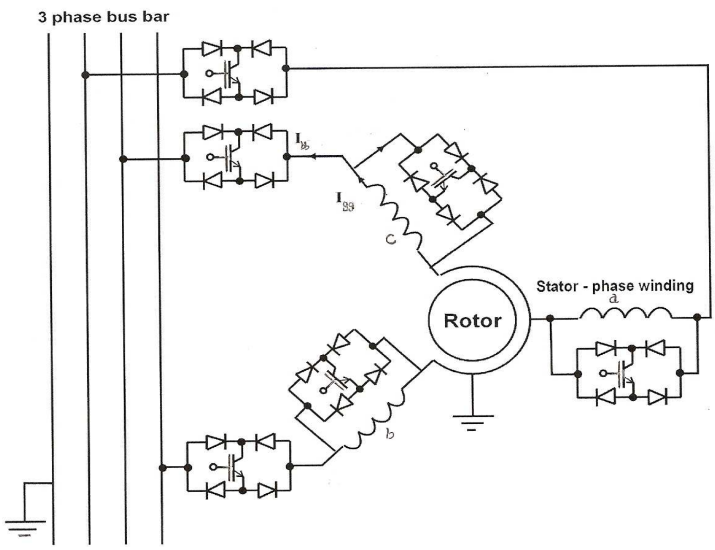

Fig. (1). Induction generator connected to grid via ac voltage controller

a) Firing angle control:

The control of the generator terminal voltage is done by varying the firing angle (α), while the extinction angle (β) is kept at 180 degree as shown in Fig. (2-a).

b) Extinction angle control:

The control is carried out by the variation of the extinction angle (β), while the firing angle (α) is kept constant and equal to zero as shown in Fig. (2-b).

c) Symmetrical angle control:

The control is done by varying both the firing angle and the extinction angle simultaneously (Fig. 2-c). The conduction angle (γ) is given by; $\gamma = \beta - \alpha$, and $\beta = \pi - \alpha$.

The terminal voltages of the induction generator are as follows:

$v_a = V_m \sin \omega t \qquad n\pi + \alpha \leq \omega t \leq n\pi + \beta \;,\; n = 0,1,2,..$ (1)

v_b and v_c lag behind v_a by $2\pi/3$ and $4\pi/3$ respectively.

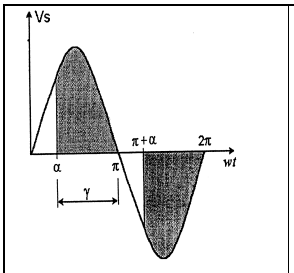

Fig. (2-a). Firing angle control strategy

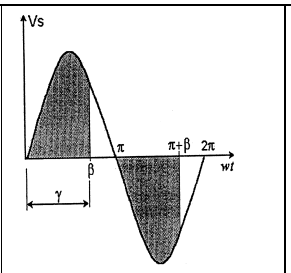

Fig. (2-b). Extinction angle control strategy

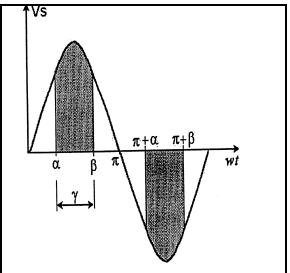

Fig. (2-c). Symmetrical angle control strategy

3. Steady State Modeling

3.1 Frequency Domain Equivalent Circuits

The stator terminal voltage of the induction Generator when using an ac voltage controller is no more a pure sinusoidal voltage. Using Fourier series this voltage can be analyzed into a summation of a series of fundamental voltage and higher order voltage harmonics. Let, the bus voltage; v_b, be :

$$v_b b(\theta) = V_m \sin\theta \quad ; \theta = \omega t \tag{2}$$

Then, the generator terminal voltage; v_g, is given by

$$v_g(\theta) = SF(\theta).v_{bb} \tag{3}$$

Where $SF(\theta)$ is a switching function that is fully determined according to the control technique such that, in the case of firing angle control technique

$$SF(\theta) = 1 \qquad n\pi + \alpha \le \theta \le (n+1)\pi;\ n = 0, 1, 2, \tag{4}$$

Otherwise it is zero.
In the case of extinction angle control,

$$SF(\theta) = 1 \qquad n\pi \le \theta \le n\pi + \beta;\ n = 0, 1, 2, .. \tag{5}$$

Otherwise it is zero.
In the case of symmetrical angle control

$$SF(\theta) = 1 \qquad (n+0.5)\pi - 0.5\gamma \le \theta \le (n+0.5)\pi + 0.5\gamma;\ n = 0, 1, 2, . \tag{6}$$

To get the Fourier series of the voltage, $SF(\theta)$ is analyzed using Fourier series rules. Thus,

$$SF(\theta) = a_o + \sum_n c_n \sin(n\omega t + \varphi_n) \tag{7}$$

where n is an even number. Then,

$$v_g(\theta) = V_m \sin\theta \ \{ a_o + \sum_n c_n \sin(n\omega t + \varphi_n) \} \tag{8}$$

which yields the following equation:

$$v_g(t) = \sum_h V_h \sin(h\omega t + \varphi_h) \tag{9}$$

where h is an odd number. V_h and φ_h are given for the three control techniques in Appendix A.The generator applied voltage components, obtained by Fourier series, are classified as follows:

a) Positive Sequence Voltage Components:

Components of order nf = 1 + 6k; where k = 0, 1, 2, 3,…., are called positive sequence voltages. These voltages generate rotating fluxes in the same direction of rotation of the flux produced by the fundamental voltage. The slip w.r.t the flux of any positive sequence voltage is:

$$S_P = \frac{nf \times N_s - N_r}{nf \times N_s} \tag{10}$$

where N_s is the nominal synchronous speed, and N_r is the rotor speed.

b) Negative Sequence Voltage Components:

Components of order nb = 5 + 6k; where k = 0, 1, 2,…., are called negative sequence voltages. These voltages generate rotating fluxes in the opposite direction of rotation of the flux produced by the fundamental voltage. The slip w.r.t the flux of any negative sequence voltage is:

$$S_N = \frac{nb \times N_s + N_r}{nb \times N_s} \tag{11}$$

c) Zero Sequence Voltage Components:

Components of order no = 3 + 6k; where k = 0, 1, 2, 3,…., are called zero sequence or triplex voltages. The net flux of these harmonic components in the air gap is zero. Therefore, they neither contribute to the torque output nor induce currents in the rotor.

The positive and negative sequence equivalent circuits of the slip ring and plain cage induction machines are as shown in Fig. (3a). In the case of delta connected generator or four wire star generator system, the zero sequence voltage drives zero sequence currents in the stator. Fig. (3b) shows the zero sequence equivalent circuit which applies in this case for all construction types of induction generators.

3.2 Generator Current, Power and Torque Calculations

For each voltage component (of order h) the appropriate equivalent circuit is used to calculate the corresponding stator, magnetizing and rotor currents. Also, the power factor is obtained. Then, the terminal active- and reactive- electrical power, rotor air gap power and the induced torque are calculated as follows:

$$P_{eh} = V_h I_h \cos(\varphi_h - \psi_{gh}) \quad \text{p.u} \tag{12}$$

$$Q_{eh} = V_h I_h \sin(\varphi_h - \psi_{gh}) \quad \text{p.u} \tag{13}$$

$$P_{gh} = I_h^2 R_2/S_h \quad \text{p.u} \tag{14}$$

$$T_{eh} = P_{gh}/h \quad \text{p.u, for +ve voltage} \tag{15-a}$$

$$T_{eh} = P_{gh}/h \quad \text{p.u, for -ve voltage} \tag{15-b}$$

Where φ_h is the phase angle of the h^{th} voltage component; V_h, ψ_h is the phase angle of the h^{th} current component; I_h, and S_h is the slip w.r.t the flux of the h^{th} voltage component.

$$THD = \frac{\sqrt{I^2 - I_1^2}}{I_1} \tag{16}$$

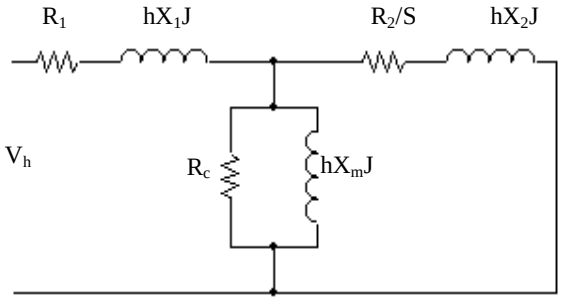

(a) Positive and negative sequence equivalent circuits

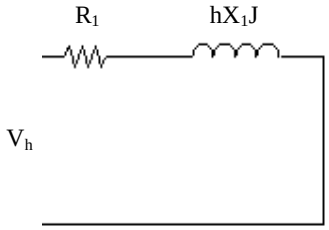

(b) Zero sequence equivalent circuit of the induction machine

Fig. (3). The generator equivalent circuits ($S = S_P$ in the case of +ve sequence harmonics and $S = S_N$ in the case of -ve sequence harmonics).

THD defines the total harmonic content [12], but it does not indicate the level of each harmonic component. If a filter is used at the output of the converters, the higher-order harmonics would be attenuated more effectively. Therefore, knowledge of both the frequency and the magnitude of each harmonic is important. The distortion factor (D.F) indicates the amount of the harmonics distortion that remains in a particular waveform after the harmonics of that waveform have been subjected to a second order attenuation (i.e. divided by n^2). Thus, D.F [12] is a measure of effectiveness in reducing unwanted harmonics without having to specify the values of the second order load filter and is defined as [12]

$$D.F = \frac{1}{I_1}\left[\sum_{h=2,3}\left(\frac{I_h}{h^2}\right)^2\right]^{1/2} \qquad (17)$$

$$D.F_h = \frac{I_h}{I_1.h^2}$$

The total terminal active- and reactive- electrical power are calculated by

$$P_e = \sum_k P_{ek} \qquad (18)$$

$$Q_e = \sum_k Q_{ek} \qquad (19)$$

Interaction between the fluxes that rotate at different speeds results in pulsating torques. The steady and pulsating torque components are calculated in p.u using the following formulas [13]:

$$T_{e1} = X_m \sum_{ks}\sum_{kr}(I_{s(ksf)} I_{r(krf)} \sin((ksf - krf)\omega_s t + \psi_{s(ksf)} - \psi_{r(krf)}) \quad (20\text{-a})$$

$$T_{e2} = X_m \sum_{ks}\sum_{kr}(I_{s(ksb)} I_{r(krb)} \sin((ksb - krb)\omega_s t + \psi_{s(ksb)} - \psi_{r(krb)}) \quad (20\text{-b})$$

$$T_{e3} = X_m \sum_{ks}\sum_{kr}(I_{s(ksb)} I_{r(krf)} \sin((ksb + krf)\omega_s t + \psi_{s(ksb)} + \psi_{r(krf)}) \quad (20\text{-c})$$

$$T_{e4} = X_m \sum_{ks}\sum_{kr}(I_{s(ksf)} I_{r(krb)} \sin((ksf + krb)\omega_s t + \psi_{s(ksf)} + \psi_{r(krb)}) \quad (20\text{-d})$$

$$T_e = T_{e1} - T_{e2} + T_{e3} - T_{e4} \qquad (21)$$

Where ksf, krf are the stator and rotor harmonic orders which induce forward rotating magnetic fields and ksb, krb are the stator and rotor harmonic orders which induce backward rotating magnetic fields. The steady state torques result when ksf = krf in T_{e1} and when ksb = krb in T_{e2}.

3.3 Bus Current and Power Calculations

At any instant the instantaneous bus power; p_{bb}, equals the instantaneous generator power; p_g,thus,

$$p_g = p_{bb} \qquad (22)$$

$$v_g\, i_g = v_{bb}\, i_{bb} \qquad (23)$$

Using Eqs. 3 and 23, leads to

$$i_{bb} = i_g\, SF(\theta) \qquad (24)$$

i_g has components calculated from the equivalent circuits corresponding to the voltage components and SF(θ) has its Fourier Series form. Thus, the bus current; i_{bb}, could be expressed as a summation of current components as given in Appendix A. The active- and reactive- electrical powers are calculated, keeping in mind that the bus voltage is pure sinusoidal, as follows:

$$P_e = V_b\, I_{bb1} \cos(-\psi_{bb1}) \qquad (25)$$

$$Q_e = V_{bb}\, I_{bb1} \sin(-\psi_{bb1}) \quad (26)$$

The angle between the fundamental bus current; I_{bb1}, measured in the output sense and the bus voltage, called the displacement angle (Dangle), is calculated as follows:

$$DAngle = \psi_{bb1} + \pi, \quad (27)$$

The bus power factor is calculated from [12]

$$PF = PuF \,.\, DF \quad (28)$$

Where PuF is the purity factor and is given by; $PuF = I_1/I$
The bus current total distortion factor and the individual distortion factors are calculated using the formula applied to the generator current (Eqs. 16, 17).

4. Performance Characteristics of the Controlled Generator

A simulation program based upon the steady state (frequency domain) equivalent circuits, with the terminal voltage represented as a series of a fundamental voltage and higher harmonic voltages has been developed. The terminal voltage is determined using Fourier series analysis (Appendix A.1) which gives the voltage components for the three control strategies. The program has been used to compute the performance characteristics of the generator having the data given in Appendix B. Various performance characteristics of the generator such as the fundamental current, total current, various distortion factors, the active power, the reactive power, the efficiency and the generator average torque and pulsating torque components of the generator have been computed versus the generator speed at different firing, extinction and conduction angles. Fig. (4) compares the generator current third harmonic distortion factor for the three control strategies. The results show that these components are very similar for the different control cases. This is also the case of the total harmonic distortion of the generator current (Fig.5). Consequently, the efficiency of the generator (Fig.6) is more or less the same for the three control strategies. The bus current distortion factors for the three control strategies are shown in Figs. (6 and 7). These figures indicate that the extinction angle control strategy gives the least harmonic distortion factor compared with the other strategies. The extinction angle control strategy has a much less bus distortion factor compared with the generator harmonic factor, while the bus distortion factors are higher than the generator factors for the other two strategies.

The displacement angle is clearly affected by the speed and the control angle of the control strategies. This angle has a high leading value when the speed is very close to the synchronous speed, then as the speed increases it goes down before it begins to increase again. In the case of firing angle control strategy, the displacement angle goes in the lagging direction as the firing angle increases (Fig. 9-a)

The induced steady torques for the three control strategies is shown in Fig. (10). The 6^{th} and 12^{th} order pulsating torques are shown in Figs (11 and 12). These are given as a ratio of the induced steady torque. The pulsating torques ratio seem to be high at the speeds which are very close to the synchronous speed, then decreases rapidly as the speed increases. As expected, this ratio behaves in a fluctuating manner as the control angle (α, β or γ) increases.

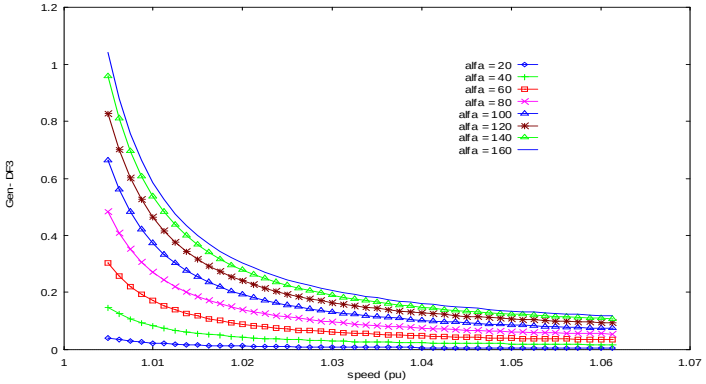

(a) Firing angle control

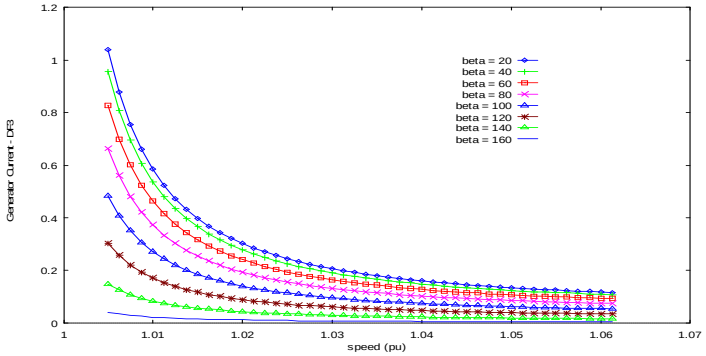

(b) Extinction angle control

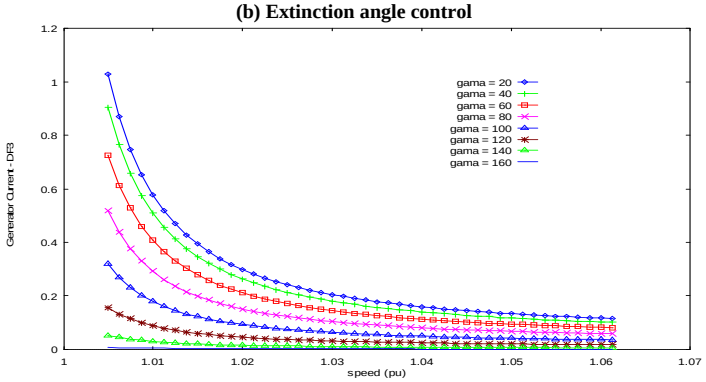

(c) Symmetrical angle control

Fig. (4). Distortion factor of the third order generator harmonic current

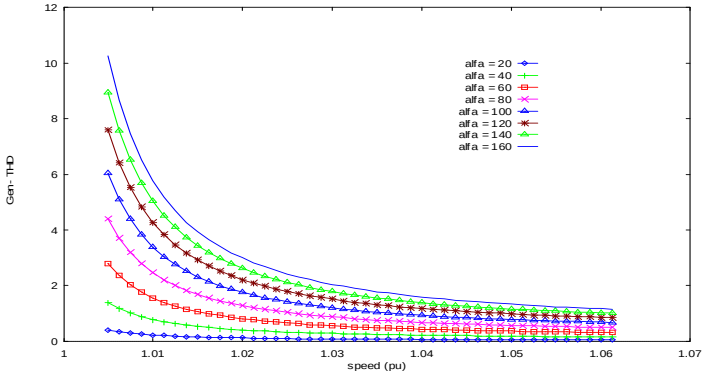

(a)

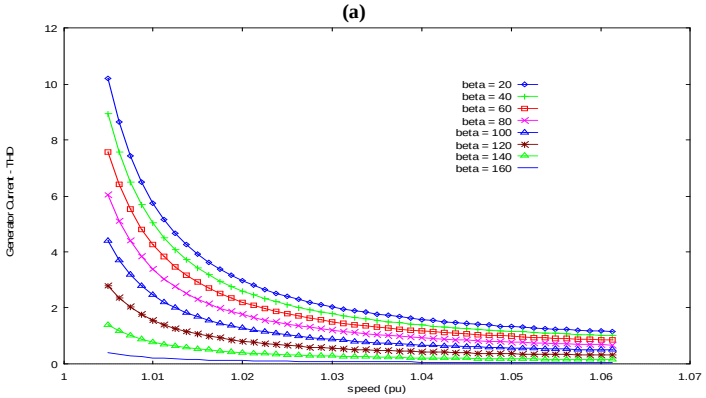

(b)

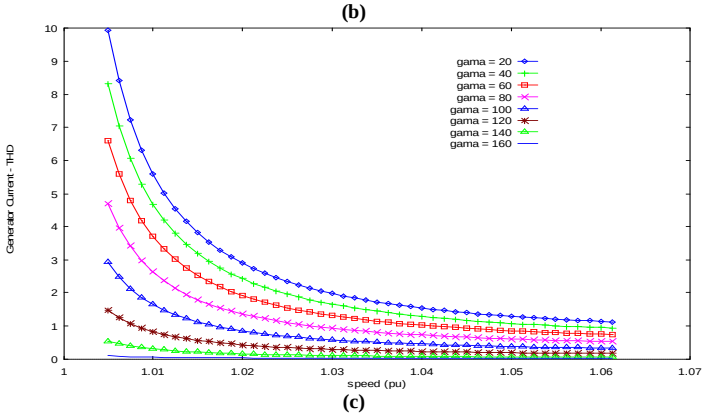

(c)

Fig. (5). Total harmonic distortion factor of the generator current

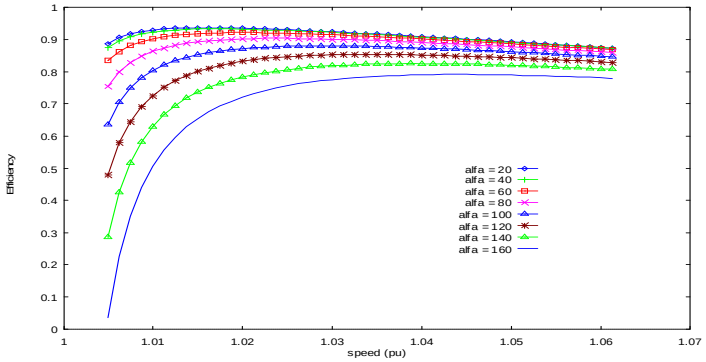

(a)

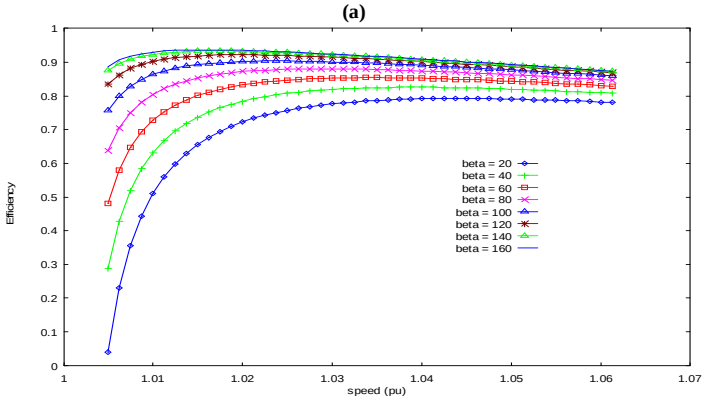

(b)

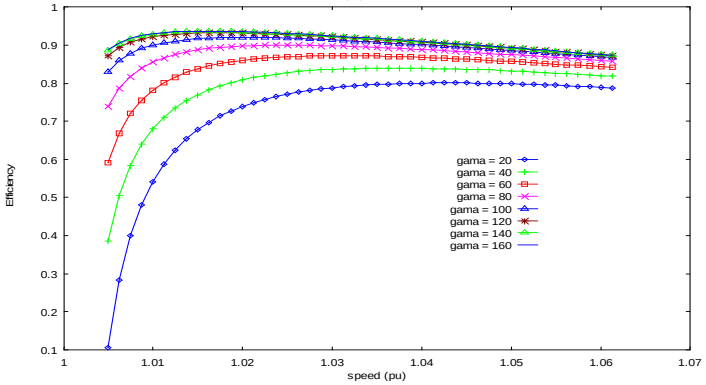

(c)

Fig. (6). Efficiency of the generator

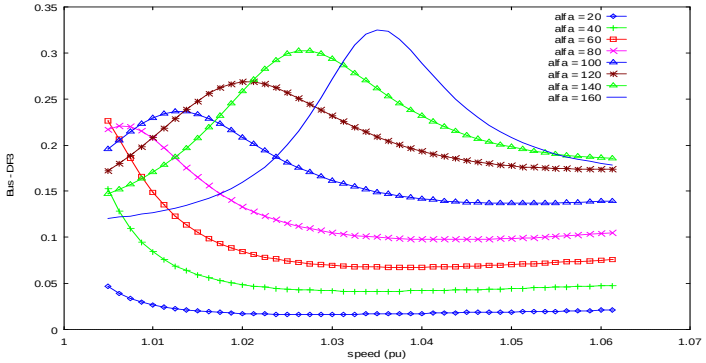

(a)

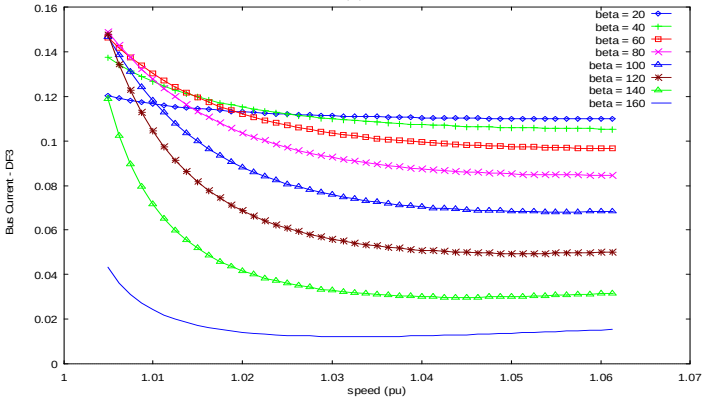

(b)

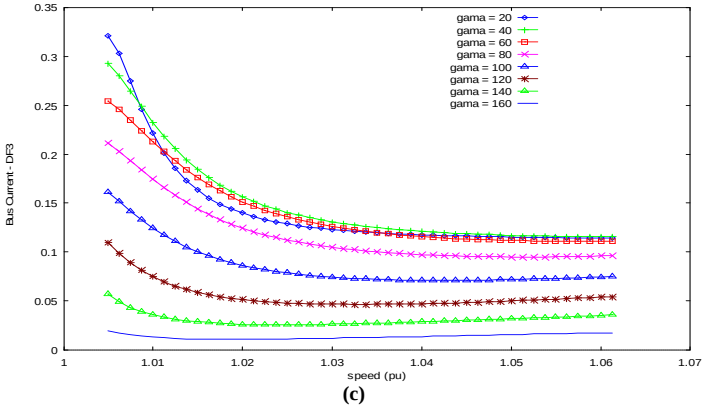

(c)

Fig. (7). Distortion factor of the third order bus harmonic current

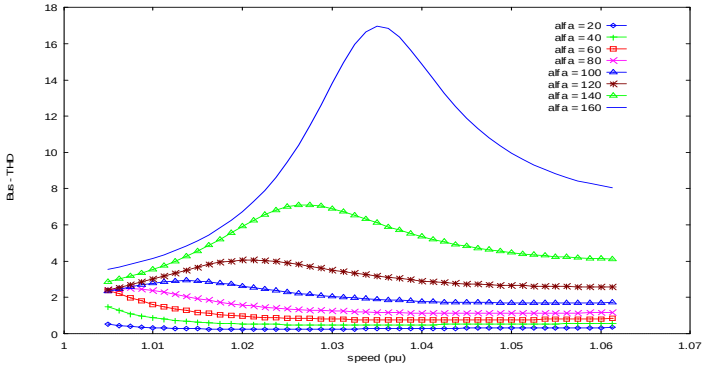

(a)

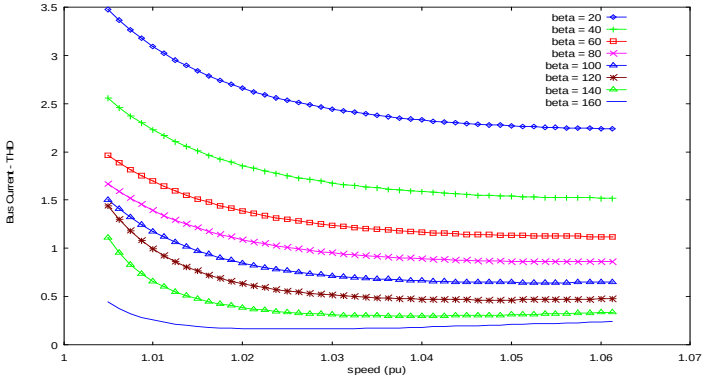

(b)

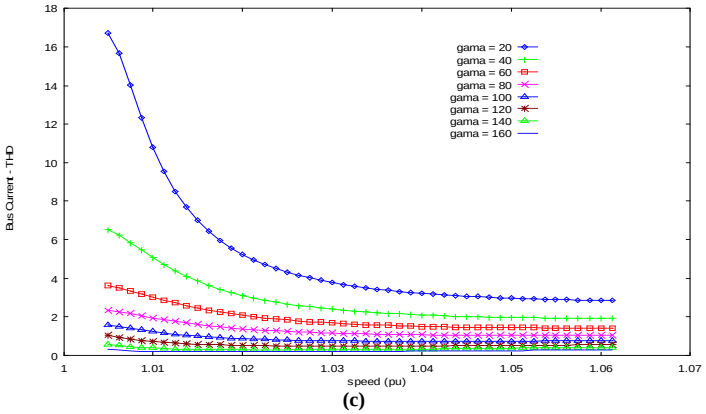

(c)

Fig. (8). Total harmonic distortion factor of the bus current

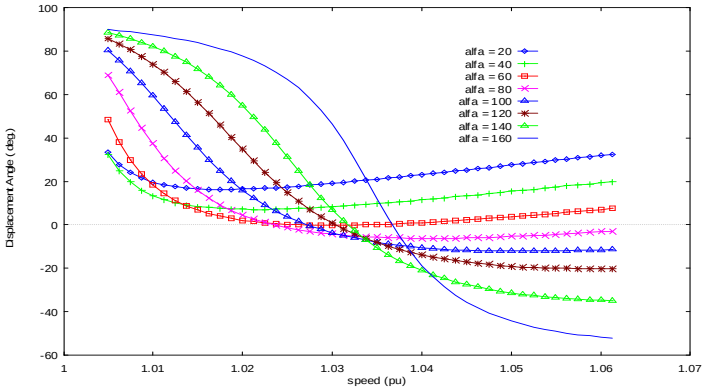

(a)

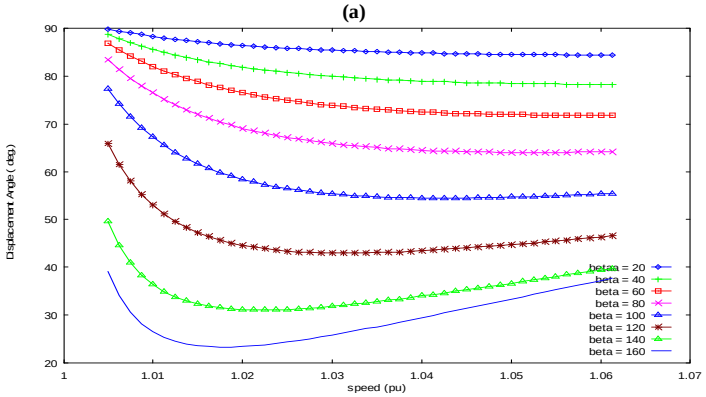

(b)

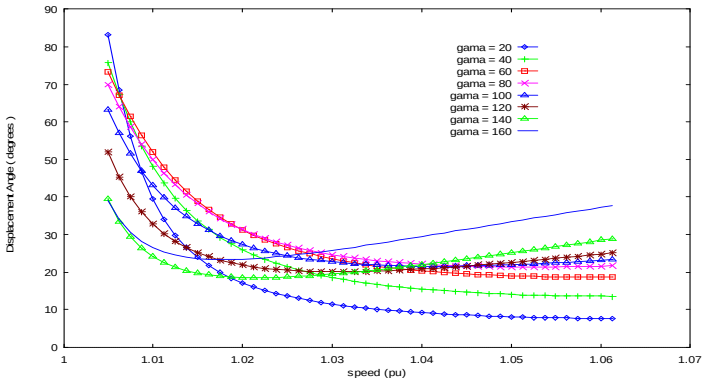

(c)

Fig. (9). Displacement angle of the bus current

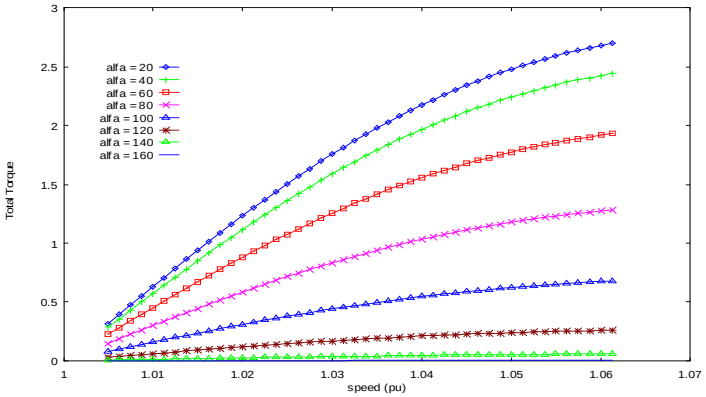

(a)

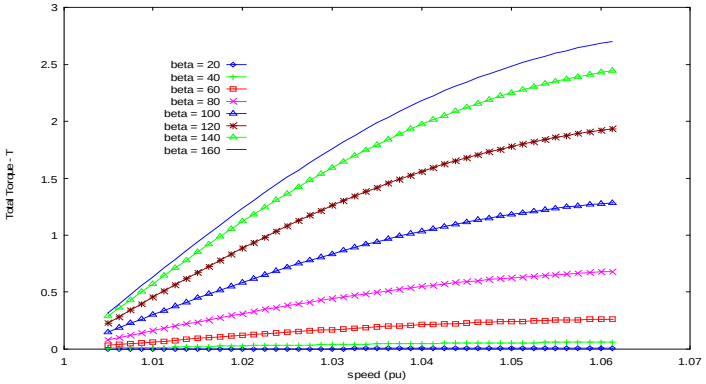

(b)

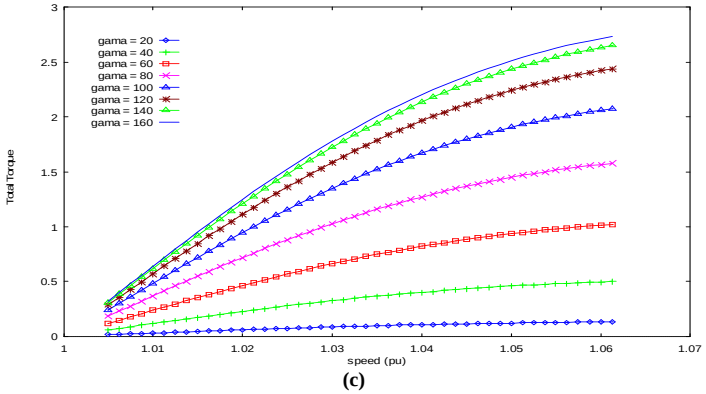

(c)

Fig.(10). Total average induced torque

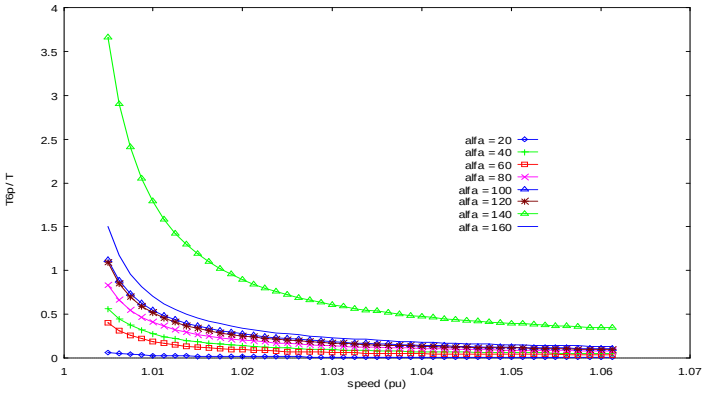

(a)

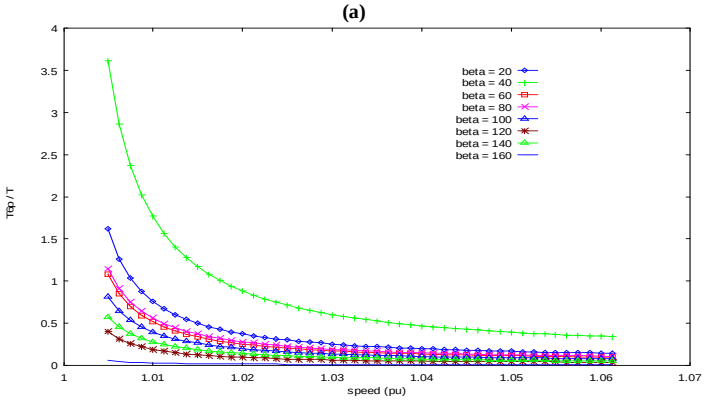

(b)

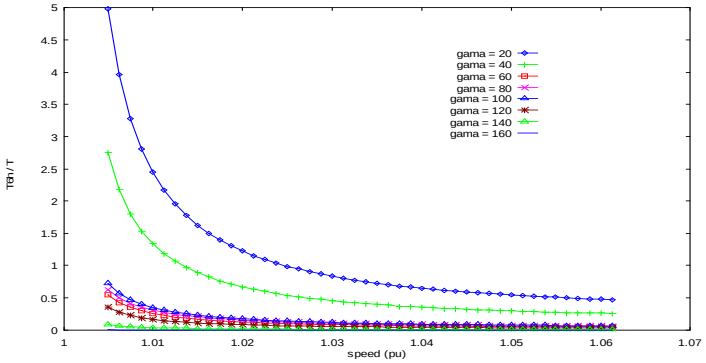

(c)

Fig. (11). The 6th order pulsating torque

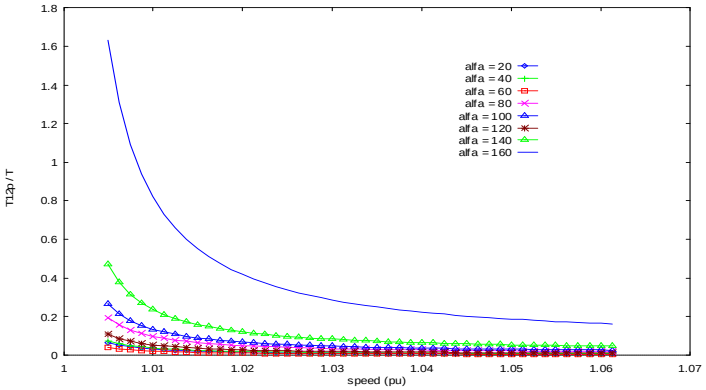

(a)

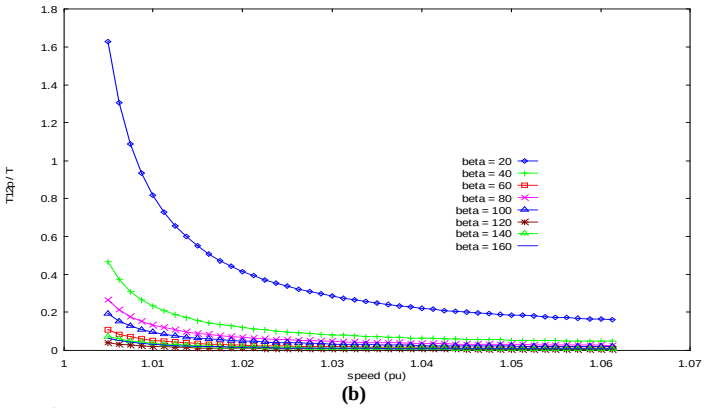

(b)

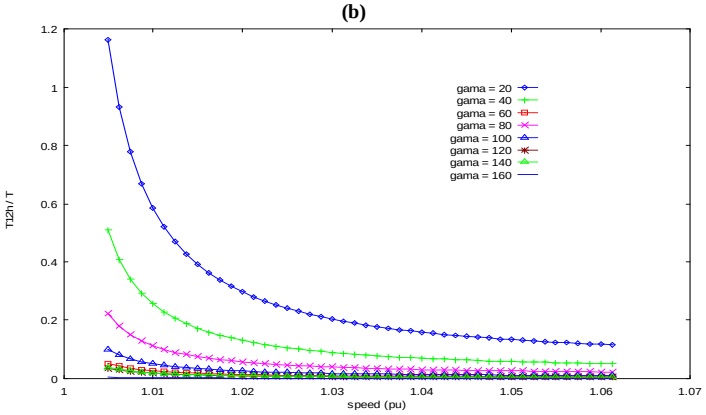

(c)

Fig. (12). The 12th order pulsating torque

5. Conclusions

The steady-state electrical and mechanical performance of a forced-controlled induction generator has been analyzed through modeling the induction generator and the static converter by novel equivalent circuits in the frequency domain. Simulating programs have been developed to determine the performance characteristics of the controlled generator for a wide range of operating conditions and different switching strategies. In this regard, three control strategies of the ac voltage controller have been used, namely; the firing angle control strategy, the extinction angle control strategy and the symmetrical angle control strategy.

When using the ac voltage controllers, the active and reactive powers of the grid connected induction generator can be controlled. The bus reactive power is clearly controlled when using the firing angle control strategy to the extent that it becomes positive over certain ranges of firing angle. This means that the output current lags the voltage. Consequently, the reactive power will be delivered to the network by the induction generator.

Using the solid state electronic switches to control the active and reactive power of the induction generator is associated with the existence of current harmonic contents in the generator and harmonic currents reflected on the supply. Only the odd harmonics especially the third harmonics exist extensively. If our concern is to have reduced generator harmonic contents the symmetrical control is recommended. But, if low bus harmonics and consequently better power quality are required the symmetrical control should be avoided. The symmetrical angle control strategy results in the highest distorted bus current.

6. Acknowledgment

The authors are grateful to the Deanship of Scientific Research for their financial support of this research.

7. References

[1] Fernando D. Bianchi, Herna'n De Battista and Ricardo J. Mantz, "*Wind Turbine Control Systems- Principles, Modelling and Gain Scheduling Design*," Springer, London, 2007.

[2] Singh, B., "Induction generators- A prospective", *Electric Machines and Power Systems*, Vol.23 (1993), 163-177.

[3] Raina, G., and Malik, O. P., "Wind Energy Conversion using a Self-Excited Induction Generator", *IEEE Transactions on Power Apparatus and Systems*, Vol. PAS-102, No. 12 (December 1983), 3933-3936.

[4] Shaltout, A.A., and Abdel-halim, M.A. ,"Solid State Control of a Wind Driven Self-Excited Induction Generator", *Electric Machines and Power Systems*, Vol. 23 (1995) , 571-582.

[5] Shaltout, A. A., and El-Ramahi , A.F. ,"Maximum power tracking for a wind driven induction generator connected to a utility network", *Applied Energy*, Vol.52 (1995), 243-253.

[6] Singh, B., Shridhar, L., and Jha, C.S., "Improvements in the Performance of Self-Excited Induction Generator through Series Compensation", *IEE Proceedings Generation, Transmission and Distribution*, Vol. 146, No. 6 (November 1999), 602-608.

[7] Shaltout, A., Abdel-Halim, M., and Al-Ramahi, A., "Optimised Solid-State Exciter for Wind Powered Pumping Applications", *Proceedings of the Fourth Arab International Solar Energy Conference*, Amman, Jordan, 20-25 November 1993, 233-242.

[8] Brennen, M. B., and Abbondanti, A., "Static Exciters for Induction Generator", *IEEE Transactions on Industry Applications*, Vol. IA-13, No. 5 (September/October 1976), 422-428.

[9] Almarshoud, A. F., Abdel-halim, M. A., Alolah, A. I., "Performance of Grid Connected Induction Generator under Naturally Commutated AC Voltage Controller", *Electric Power Components and Systems*, Vol. 32 (2004), 691-700.

[10] Abdel-halim, M.A., "Solid State Control of a Grid Connected Induction Generator", *Electric Power Components and Systems*, Vol. 29 (2001), 163-178.

[11] Abdel-halim, M.A, M. M. Abdel-aziz, M. M. and Mostafa, H. G., "AC chopper controlled grid-connected induction generator", *Qassim University Scientific Journal- Engineering and Computer Sciences*, Vol.1, No. 1 (2008), 1- 19.

[12] Rashid, M. H., "*Power Electronics: Circuits, Devices, and Applications*", Second Edition, Prentice-hall, USA, 1993.

[13] Abdulrahman, S. M., Kettleborough, J. G. and Smith, I. R., "Fast Calculation of Harmonic Torque Pulsations in a VSI/Induction Motor Drive", *IEEE Trans. On Industrial Electronics*, Vol.40, No.6 (Dec. 1993), 561-569.

8. Appendices

Appendix A: Fourier Series of the Generator Voltage and Bus Current

A.1- Generator Voltage

$$v_g = V_m \sin(\theta).\ F(\theta)$$

where F (θ) is the switching function which is determined according to the control strategy as follows:

$$SF(\theta) = 1 \qquad n\pi + \alpha \le \theta \le n\pi + \beta; \quad n = 0, 1, 2, ..$$

Otherwise it is zero.

Using Fourier series analysis of the switching function, the generator voltage can be expressed as follows:

$$v_g = 0.5V_m [(a_0-a_2) \sin(\theta) + (a_2-a_4) \sin(3\theta) + (a_4-a_6) \sin(5\theta) + (a_6-a_8) \sin(7\theta) + \ldots\ldots$$
$$+ b_2 \cos(\theta) + (b_4-b_2) \cos(3\theta) + (b_6-b_4) \cos(5\theta) + (b_8-b_6) \cos(7\theta) + \ldots\ldots.]$$

Thus, the fundamental component; $v_{g1} = 0.5V_m (a_0-a_2) \sin(\theta) + 0.5V_m (b_2) \cos(\theta)$,

3^{rd} harmonic component; $v_{g3} = 0.5V_m (a_2- a_4) \sin(3\theta) + 0.5V_m (b_4-b_2) \cos(3\theta)$,

5^{th} harmonic component; $v_{g5} = 0.5V_m (a_4- a_6) \sin(5\theta) + 0.5V_m (b_6-b_4) \cos(5\theta)$,

and so on.

a_0, a_n and b_n are given, for the three control strategies, as follows:

a_0, a_n and b_n are given, for the three control strategies, as follows:

i) Firing angle control,

$$a_0 = 2(\pi-\alpha)/\pi$$
$$a_n = [(-2/\{(2n-1)\pi\}]\times\sin(2n-1)\alpha\ , \qquad n = 1,2,3,\ldots.$$
$$b_n = \cos(2n\alpha-1)/n\pi\ , \qquad n = 1,2,3,\ldots$$

ii) Extinction angle control,

$$a_0 = 2\beta/\pi$$
$$a_n = \sin(2n\beta)/(n\pi), \qquad n = 1,2,3,\ldots.$$
$$b_n = [1-\cos(2n\beta)]/(n\pi)\ , \qquad n = 1,2,3,\ldots$$

iii) Symmetrical angle control,

$$a_0 = 2\gamma/\pi$$
$$a_n = [\{-2(-1)^n-2\}\sin(n(\pi-\gamma)/2)]/n\pi\ , \quad n = 1,2,3,\ldots$$
$$b_n = 0\ , \quad n = 1,2,3,\ldots$$

A.2- Bus Current

$$i_{bb} = i_g\, SF(\theta)$$

The fundamental bus current is given by

$$i_{bb1} = \{0.5\, I_{g1}\,((a_0-a_2)\cos(\psi_{g1})+b_2\sin(\psi_{g1})) + 0.5\ I_{g3}\,((a_2-a_4)\cos(\psi_{g3}) + (b_4-b_2)\sin(\psi_{g3})) + 0.5\ I_{g5}\,((a_4-a_6)\cos(\psi_{g5})+(b_6-b_4)\sin(\psi_{g5})) + 0.5\ I_{g7}\,((a_6-a_8)\cos(\psi_{g7}) + (b_8-b_6)\sin(\psi_{g7})) + \ldots.\}\times\sin(\theta) + \{0.5\ I_{g1}\,(b_2\cos(\psi_{g1}) + (a_0+a_2)\sin(\psi_{g1})) + 0.5\, I_{g3}\,((b_4+b_2)\cos(\psi_{g3}) + (a_2+a_4)\sin(\psi_{g3})) + 0.5\ I_{g5}\,((b_6+b_4)\cos(\psi_{g5}) + (a_4+a_6)\sin(\psi_{g5}) + 0.5\ I_{g7}\,((b_8+b_6)\cos(\psi_{g7}) + (a_6+a_8)\sin(\psi_{g7})) + \ldots.\}\times\cos(\theta)$$

3rd harmonic bus current is given by

$$i_{bb3} = \{0.5\ I_{g1}\,((a_2-a_4)\cos(\psi_{g1}) + (b_4+b_2)\sin(\psi_{g1})) + 0.5\ I_{g3}\,((a_0-a_6)\cos(\psi_{g3}) + b_6\sin(\psi_{g3})) + 0.5\ I_{g5}\,((a_2-a_8)\cos(\psi_{g5}) + (b_8-b_2)\sin(\psi_{g5})) + \ldots.\}\times\sin(3\theta) + 0.5\ I_{g7}\,((a_4-a_{10})\cos(\psi_{g7}) + (b_{10}-b_4)\sin(\psi_{g7})) + \{0.5\ I_{g1}\,((b_4-b_2)\cos(\psi_{g1}) + (a_2+a_4)\sin(\psi_{g1})) + 0.5\ I_{g3}\,(b_6\cos(\psi_{g3}) + (a_0+a_6)\sin(\psi_{g3})) + 0.5\ I_{g5}\,((b_8+b_2)\cos(\psi_{g5}) + (a_2+a_8)\sin(\psi_{g5}) + 0.5\ I_{g7}\,((b_{10}+b_4)\cos(\psi_{g7}) + (a_4+a_{10})\sin(\psi_{g7})) + \ldots.\}\times\cos(3\theta)$$

5th harmonic bus current is given by

$$i_{bb5} = \{0.5\ I_{g1}\,((a_4-a_6)\cos(\psi_{g1})+(b_6+b_4)\sin(\psi_{g1})) + 0.5\ I_{g3}\,((a_2-a_8)\cos(\psi_{g3}) + (b_9+b_2)\sin(\psi_{g3})) + 0.5\ I_{g5}\,((a_0-a_{10})\cos(\psi_{g5})+b_{10}\sin(\psi_{g5})) + \ldots.\}\times\mathrm{Sin}(5\theta) + 0.5\ I_{g7}\,((a_2-a_{12})\cos(\psi_{g7}) + (b_{12}-b_2)\sin(\psi_{g7})) + \{0.5\ I_{g1}\,((b_6-b_4)\cos(\psi_{g1}) + (a_4+a_6)\sin(\psi_{g1})) + 0.5\ I_{g3}\,((b_8-b_2)\cos(\psi_{g3}) + (a_2+a_8)\sin(\psi_{g3})) + 0.5\ I_{g5}\,(b_{10}\cos(\psi_{g5}) + (a_0+a_{10})\sin(\psi_{g5})) + 0.5\ I_{g7}\,((b_{12}+b_2)\cos(\psi_{g7}) + (a_2+a_{12})\sin(\psi_{g7})) + \ldots.\}\times\cos(5\theta)$$

where I_{g1} ,I_{g3} ,I_{g5} I_{g7} ..... are the generator harmonic currents.

a_0, a_n and b_n are as given before.

Appendix B: Generator Particulars and Parameters

Three phase generator, Δ connected, 600 V, 475 A, 50 Hz, having the following parameters:

$R_1 = R_2 = 0.015$ p.u, $X_1 = X_2 = 0.091$ p.u, $X_m = 4.251$ p.u, $R_c = 30.0$ p.u.

خواص تحليل الأداء الكهروميكانيكي للمولد الحثي المربوط بالشبكة والمحكوم بحواكم جهد مختلفة

محمد عبد السميع عبد الحليم* عبد الرحمن بن فهد المرشود محمد مناور شيس*****

كلية الهندسة، جامعة القصيم، المملكة العربية السعودية

*masamie@qec.edu.sa, **dr_almarshoud@qec.edu.sa, ***munawwarshees@qec.edu.sa*

(قدم للنشر في ١٥/٧/٢٠١٠م؛ وقبل للنشر في ١٠/١١/٢٠١٠م)

ملخص البحث. يقدم البحث دراسة متكاملة لخواص الأداء لمولد حثي مرتبط بالشبكة من خلال حواكم جهد تستخدم طرقاً مختلفة للتحكم في الجهد، وتغطي الدراسة ثلاثة طرق من التحكم وهي التحكم في زاوية الإطفاء والتحكم في زاوية الإخماد والتحكم المتماثل. يقدم البحث دراسة تقارن أداء المولد من حيث منحنيات خصائص عوامل التوافقيات والقدرة الفعالة وغير الفعالة ومعامل القدرة والعزوم المتوسطة والعزوم الاهتزازية وكفاءة المولد، ولقد تمت دراسة هذه الخواص باستخدام دوائر مكافئة مبتكرة في حقل التردد، وتمكن هذه الدوائر من اجراء الحسابات بدقة وبعيداً عن استخدام الحسابات الرقمية، كما تمكن من حساب الفقد في قلب (حديد) المولد، وكان هذا الفقد يهمل في النماذج التقليدية.

Journal of Engineering and Computer Sciences
Qassim University, Vol. 4, No. 1, pp. 63-81 (January 2011/Moharram 1432H)

Pyrolysis and Combustion Rates of Solid Fuel

Bahgat K. Morsy
Mechanical Engineering Department, College of Engineering, Qassim University
bahgat52@yahoo.com

(Received 28/2/2010; accepted for publication 2/6/2010)

Abstract: A knowledge of the product distribution from the pyrolysis of coal when particles are heated is of considerable importance in understanding the process involved in both the production of gaseous and liquid fuels from coal and the combustion of coal. Studies of decomposition of Sinai coal and combustion rates have been undertaken because the rate and extent of volatilization play an important part in the ignition process of coal particles in circulating fluidized bed. There is a little information available in the literature on the rate of decomposition occurring under the very rapid heating characteristics of Sinai coal firing. This is due to incomplete knowledge about the phenomenon of combustion of Sinai coal in circulating fluidized involved in special care operations. That is why this work is continued to bring new technical solutions and sake knowledge in this scope more profound.
Keywords: Pyrolysis, combustion, solid fuel

List of Symbols

A^d	Quantity of ash determine in standard conditions	A_c^d	quantity of ash remaining in char after coal pyrolysis
C_{O2}	local concentration of oxidizer	D	coal particle diameter
E	activation energy	k_O	frequency factor
M	True reaction order	N	apparent reaction order
Q	degree of devolatilization	Q	char reactivity
R_g	universal gas constant	T_g	ignition temperature
T_s	particle temperature	V^{dav}	quantity of volatile matter (V.M.) determine in standard conditions
V_c^{dav}	Quantity of volatile matter (V.M.) remaining in char after coal pyrolysis	ΔV^{dav}	change in quantity of volatile matter (V.M.)
ΔM^{dav}	actual coal mass loss	ρ_{O2}	density of oxygen
β	stoichiometric coefficient	λ	heat transfer coefficient
ε	Porosity	daf	dry ash free

1. Introduction

The combustion of most solid fuels involves two major steps:

(i) The thermal decomposition (pyrolysis, devolatilization) that occurs during the initial heating, accompanied by drastic physical and chemical changes which usually involve the particle become plastic then rehardening, and

(ii) The subsequent combustion of pores solid residue (char) from the first step. The burning rate of the solid depends in part-on the size of char particle and the natural of its pore structure. These physical properties, together with important chemical properties, are affected by changes during the first step. The first step is rapid, the second is slow. In pulverized flames the time for devolatilization to take place is of the order of 0.1s and for char burn.-out the time is 1s; for particles burning in fluidized bed combustors the corresponding orders are 10s and 1000 s. Therefore the burning of the char has a major effect on the volume of the combustion chamber required to attain a given heat release.

Actually, when necessity of burning low grade fuels, has arisen, there is a demand to find adequate technologies to burn them effectively and with as low emission of pollutants as possible. Circulating fluidized bed may provide the solution. The gas/solid mixing and heat transfer properties of fluidized beds have been utilized in combustion systems for burning low grade coal, but it that the advantages have been appreciated of the high heat transfer rates occurring at surfaces immersed within the bed. Sufficient heat is extracted in this way to maintain the temperature of the bed in the average 700-800 ^{o}C. The high heat transfer rates which result in high combustion intensities and a reduction the weight of expensive tube materials-leading to a substantial saving in the capital cost of steam generation.

Prospecting for coal in Egypt, can be considered to data from early in 1844, when a well near Edfu (Southern Egypt) shown some iodination of bituminous carbonaceous material. Further prospecting for call carried out in 1958-1962 resulted in the discovery of the coal deposits of Ayun Musa, Wadi Thorn and Maghara in Sinai Peninsula. The Safa mine was opened in 1964 and was about to start production in 1967, when it was then abandoned due to Israeli invasion. It is planned to resume production in April 1986. A call-for tender is now being issued for studding the possibility of erecting a coal-fired power plant on the Gulf of Suez (initial) capacity 300 MW, to be followed by other coal fired power stations.

2. Pyrolysis of Coal Particles

Prior studies in which finely-ground coal was heated very rapidly have shown that the fraction of the coal that can be volatilized increases with both the rate of heating and the final temperature to which the coal is heated. For example, Eddinger, *et a1* [1], have presented data from an entrained flow reactor which show that volatile products amounting to 49.9 percent of the coal fed may be produced from a finely-ground coal having an AS'IM volatility of only 35.5 percent, even though maximum reactor temperature was less than the 1223 K reached in the standard volatility test.

Mustafa *et al* [2] studied the effect of particle size on coal pyrolysis by thermogravimetry (TG/DTG). All the experiments were conducted at non-isothermal heating conditions with a heating rate of 10°C min^{-1}. in the temperature range of 20–600°C, under nitrogen atmosphere. Different fractions of Çayırhan coal showed differences in TG/DTG curves, peak temperatures and residue values. The Arrhenius model is applied to determine the kinetic parameters from TG/DTG curves.

Kinetic analysis of rapid coal devolatilization in a spot heater apparatus was made for Tatong coal by [3]. A multiple-stage measuring technique was devised to provide the change of total volatiles with time/temperature during the devolatilization. On the basis of the analyses of the total volatiles yield and measured temperature of coal particle, the kinetic parameters of the rapid devolatilization for Tatong coal were estimated by applying Distributed Activation Energy Model (DAEM).

A poly-generation process of simulated circulating fluidized bed (CFB) combustion combined with coal pyrolysis was developed in a laboratory scale by [4]. Pyrolysis characteristics of three bituminous coals with high volatile contents were investigated in a fixed bed with capacity of 10 kg solid samples. The effects of initial temperature of solid heat carrier, pyrolysis holding time, blending (ash/coal) ratio and coal particle size on gas and tar yields were studied experimentally. The results indicate that the initial temperature of the heat carrier is the key factor that affects the gas and tar yield, and the gas composition. Most of the gas and the tar are released during the first few minutes of the pyrolysis holding time. For caking coal, the amount of char agglomerating on the pyrolyzer inner wall is reduced by enhancing the blending ratio. The experimental results may provide basic engineering data or information for the process design of CFB combustion combined with coal pyrolysis in a large scale.

An experimental apparatus was set up for batch simulation of coal pyrolysis with solid heat carrier in a fixed bed. by [5] Quartz sand as heat carrier preheated to about 700–800°C was mixed with Datong bituminous coal by an agitator. The thermal history of the coal particle has been followed by a K-type thermocouple. The effects of particle size, pyrolysis time and temperature on the gas yield during pyrolysis of coal with solid heat carrier were examined for different conditions. The experimental results showed that a dominant percentage of the gas product is produced during the first 1–3 min, although gas evolution would last for as long as 10 min. The total gas yield, insensitive to particle size of the heat carrier, depends on carrier temperature and coal particle size under tested conditions. The contact heat transfer of cold and hot particles was analyzed.

The authors of the works [6, 7, and 8] observed that heating the coal particles at the rate higher than 10000 K/s substantially influences the quantity of evolutes volatile matters. Rapid heating results in greater quantity of volatile products of pyrolysis than slow heating does. Another feature differentiating pyrolysis in high rate of heating from slow heating is qualitatively different composition of evoluted gaseous products [10].

Complex processes occurring during thermal decomposition of coal are not well known or quantitatively described. Model allowing for more than one reaction are presented in work [6, 7, 8, and 9]. References [7 and 8] propose that pyrolysis may be described by two parallel reactions. The review of pyrolysis models [6, 7, 8, and 9] of volatile matters evolution is presented in tables (1).

Table (1). Review of Pyrolysis models

Author	Model	Commentary
Badzioch and Hawksley [6]	$\frac{dV}{dt} = \mathrm{k}(\mathrm{V}^* - V)$	K: constant rate of chemical reaction
Kobayshi *et al*. [7] Ubkayakar *et al*. [8]	Coal $\rightarrow x_1 v_1 + R_1(1-x_1)$ Coal $\rightarrow x_2 v_2 + R_2(1-x_2)$	V : gas R; solid phase
Solomon [9]	$\frac{dV_i}{dt} = \mathrm{k}_i(\mathrm{V}^* - V_i)$	V^*: emitted quantity of volatile matters (% daf)

Pyrolysis converts coal into volatile products and solid residue. The rate of volatile evolution may be controlled by either chemical decomposition of the coal or gaseous flow through the solid matrix Knowledge of the kinetics of pyrolysis is required for under standing the combustion of coal particles. Volatile evolution is known to influence the combustion of solid particle, and the influence of pre-ignition volatile generation on flame speed. [11 to 18]

The report has determined the degree of devolatilization of SINAI coal in the range of temperature from 923 K to 1323 K for particle diameter from 250 μm to 750 μm, ignition temperature, and reactivity.

2.1. Coal size

A high percentage of coal mined today is by mechanical coal cutters; in most countries the days of pick- and shoved mining disappeared, and mechanical conveying, cleaning and screening the coal is now widely adopted. As a result, there is a much smaller amount of large coal available and generally coal is much cleaner with less dirt and ash. In stoker fired boilers coal size is important. Although large coal is usually the most expensive, it is not the most uitable for use in mechanical stokers. Most large coal suppliers grade their coal into a range of sizes in which both the minimum and maximum particle sizes are stipulated. For example, British coal grade their bituminous and anthracite coal into groups as shown in Table (2). Other industrial countries have their own systems for classifying coal by average particle size, and use their own descriptive names for the various grades.

Table (2). British coal grade of bituminous and anthracite coal

Bituminous coal grading Range of screen sizes			**Typical size groups for graded low, volatile coal**			
			Welsh anthracite		**Welsh dry steam coal**	
Description	**Max, mm**	**Min. mm**	**Description**	**Mm**	**Description**	**mm**
Large Cobbles	150	75	Cobbles	125-80	Cobbles	125-80
Cobbles	100-150	50-100	French nuts	80-63	Large nuts	80-56
Trebles/large nuts	63-100	38-63	Stoves nuts	63-36	Small	56-18
			Stoves	36-2--16	Nuts	18-16
Doubles/nuts	38-63	25-38	Beans	20-10	Beans	18-10
Singles	25-38	12.5-18	Peas	16-10	Peas	10-0
			Grains	10.5	Washed duff.	
			Washed duff.	5-0		

2.2. Coal analysis

SINAI coal was the raw material used for pyrolysis research. The analysis was listed in Table (3) and Table (4). The coal was preheated, milled and divided into groups of particles of diameters by sieving in the range from 250 μm to 750 μm. The samples for proximate and ultimate analysis were carried out according to obligatory Polish Standards. The content of carbon was determined in the examined samples by means of Radmacher–Hoverth method.

Table (3). Analysis of SINAI coal

Proximate Analysis (dry ash free % by weight)			
Moisture	Ash	Volatile matter.	Fixed Carbon
2.9	13.7	54.45	8.95

Table (4). Analysis of SINAI coal

Ultimate Analysis (dry ash free % by weight)				
Carbon	Hydrogen	Sulphur	Nitrogen	Oxygen (by difference)
76	6.6	2.96	1.13	13.31

2.3 Test-rig and measurements

Investigations were carried out on the test-rig as shown in Fig. 1 [19and 20]. Basic elements of the test rig are: vertical reaction chamber, coal supplying sampler extinguishing system of pyrolysis products, installation of reaction chamber electric heating and gas heater, water cooling system, gas flow and temperature measuring system, system for carrying away pyrolysis products. During the operation, the reactor walls and gas heater temperature is measured with six thermocouples. The quantity of gas supplied to the reactor and the feeder and that leaving the reactor is measured by rotameters. As well, the power of heating appliances is measured. Solid and fluid pyrolysis is carried away from the reactor through the installation comprising successively: cyclone, bag filter and suction pump. All measurements probes were calibrated at various conditions in the test section.

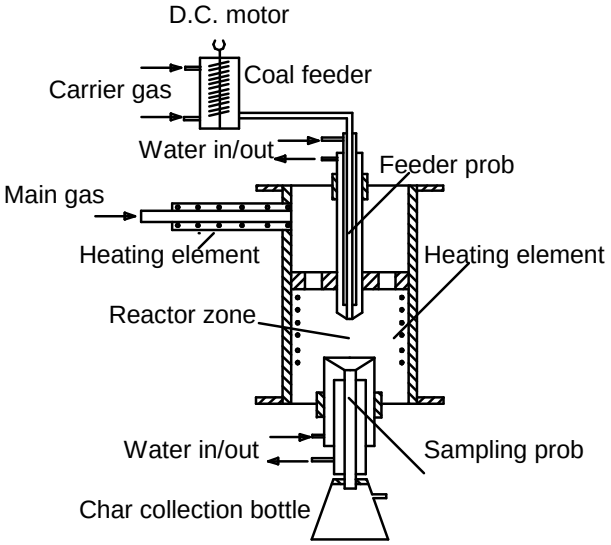

Fig. (1). The reactor system

2.4 Research range

The Experiment was based on continuous transport of pulverized coal particles by a carrier gas (Nitrogen) to the reactor filled with in active atmosphere where they are rapidly heated (10^3 deg/s-10^5 deg/s). The particles flowed through the reactor in 2s-4s. The products were sucked further to the cooling stage. The furnace temperature was controlled from 923 K to 1323 K in 100 deg intervals. The flow of carrier gas was changed from 0.0005 to 0.0023 cubic meters per second in relation to the furnace temperature. The quantity of supplied coal amounted to ca 0.00017 kg/s.

2.5. Degree of devolatilization

The degree of devolatilization of coal can be expressed by the number Q which is the ratio of the actual coal mass losses caused by rapid pyrolysis ΔM^{daf} to the change in quantity of volatile matter determined in standard conditions, i.e. ΔV^{daf} [19 and 20]

$$Q = \frac{\Delta M^{daf}}{\Delta V^{daf}} \quad (1)$$

To obtain the value of "Q" the parameters ΔM^{daf} and ΔV^{daf} have been determined as given below:

The examination of devolatilization in dust-gas stream renders it impossible to measure directly coal; mass loss caused by thermal decomposition. Coal mass loss results from the fact that not all particles reach the collector as some of then get

stuck to the reactor surface. Thus, to determine the actual loss of mass requires the use of ash determined according to chemical analysis, so the actual mass loss is calculated from the equations;

$$M^{daf} = 100 - \left(\frac{100\,A^{d}}{100\,A^{d}}\right)\left(\frac{100 - A_c^{d}}{A_c^{d}}\right) \tag{2}$$

The quantity of volatile matter when left in char after coal devolatilization (V_c^{daf}) can be estimated from the formula;

$$V_c^{daf} = \frac{100\ A^{d}}{100\ - A^{d}}\ \frac{V^{daf}}{A_c^{d}} \tag{3}$$

The change of quantity of volatile matter which was released from coal can be determined by the following equation;

$$\Delta V^{daf} = V^{daf} - V_c^{daf} \tag{4}$$

The values of ΔM^{daf} and ΔV^{daf} obtained through experiments have been presented in Figs. 2 and 3. From these figures it can be said that;

- with the rise in pyrolysis temperature there is an increase in the quantity of emitted matter and the mass loss,
- for fraction of diameters 600 μm -750 μm there is a sudden increase in the values of ΔM^{daf} and ΔV^{daf} up to pyrolysis temperature of 1323 K. Beyond this temperature the increase is very slow.

The calculated values of degree of devolatilization of coal obtained are given in Table (5). From this table Q is found to vary between 1.2-1.5. Considering the small range of variation and the trend of curves in Figs. (2 and 3) it can be inferred that the particle size practically does not affect the degree of devolatilization. Devolatilization rate is reduced since a larger coal particle results in a higher inherent temperature gradient. In addition, a large coal particle size results in a higher mass transfer resistance for volatile gas. A longer path of the volatile inside a larger particle delays the time for volatile release. Smaller coal particles favor the gas and the tar yields.

Table (5). The degree of devolatilization (Q)

Temp., K	**Particle diameters, μm**				
	250-350 μ m	**350-450 μ m**	**450-550 μ m**	**550-650 μ m**	**650-750 μ m**
	Q	**Q**	**Q**	**Q**	**Q**
923 K	1.4	1.23	1.3	1.4	1.3
1023 K	1.4	1.25	1.2	1.43	1.5
1123 K	1.31	1.24	1.26	1.3	0.8
1223 K	1.3	1.20	1.3	2.2	1.3
1323 K	1.4	1.20	1.2	1.3	1.5

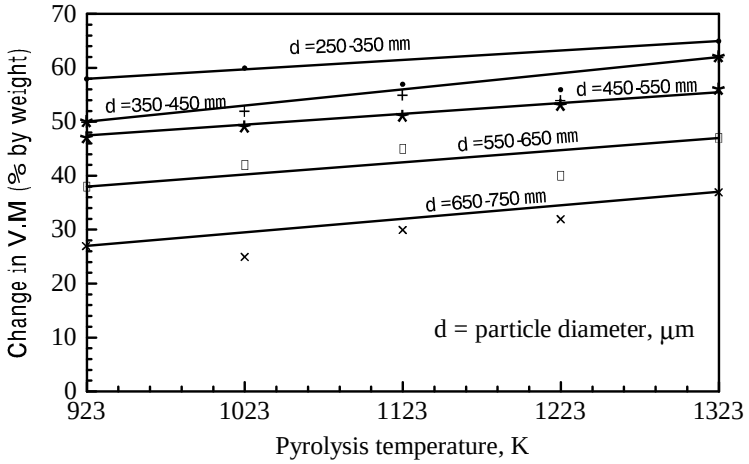

Fig. (2). Measured variation in change of volatile matter various with pyrolysis temperature.

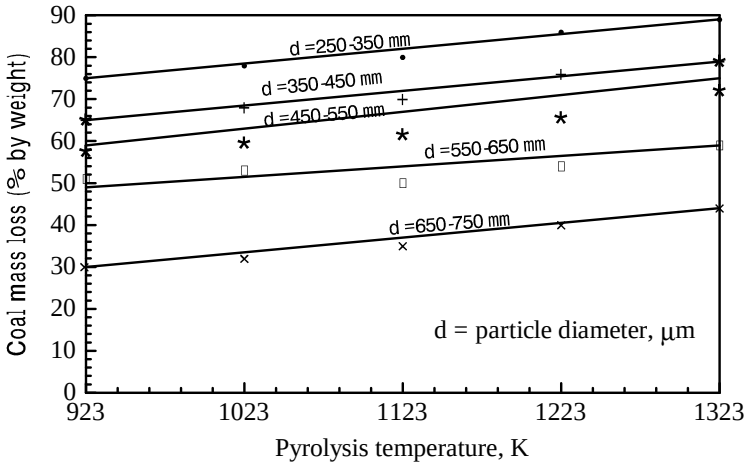

Fig. (3). Measured variation in change of coal mass loss various with pyrolysis temperature.

3. Ignition Temperature of Coal Particles

The test rig where ignition temperature and characteristic burning times were determined is illustrated in Fig. (4) [21]. A single coal particle was put on the top of a fine quartz needle and introduced into a cylindrical furnace of 0.5 m length and a diameter of 0.04 m, the air inside being static. The ignition of particle was watched through an observation port. In the absence of ignition the particle was taken out and

a fresh sample was introduced after raising the furnace temperature. The experimental was repeated until the ignition occurred. (T_s) The lowest temperature, at which the ignition took place, was regarded as ignition temperature. The furnace temperature was changed by five degree centigrade at each step. At one temperature, on the average, 200 particles were tested

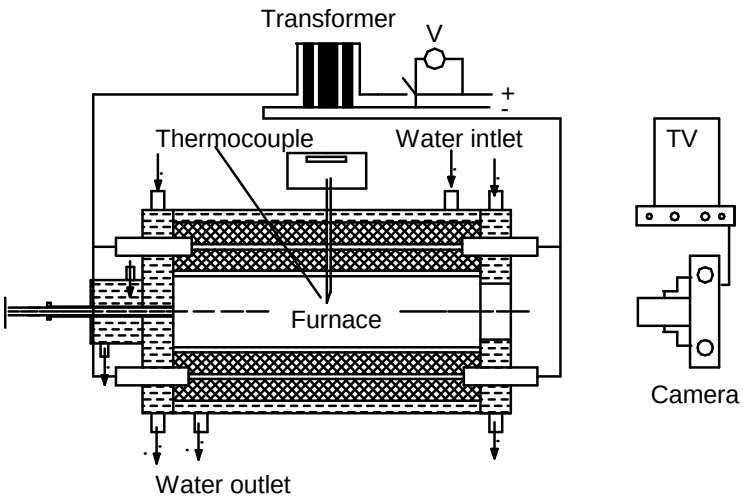

Fig. (4). View of experimental test - rig.

Figure (5) presents experimentally determined changes in ignition temperature with particle diameter for tested chars. The results are presented only for the particle diameters below 490 μm. The figure shows that the ignition temperature with particle diameter for tested chars. The results are presented only for the particle diameters below 490 μm. The figure shows that the ignition temperature increases as the particle diameter decreases. Also the ignition temperature increases with the increase in pyrolysis temperature. Thus determined ignition temperature is the basis for determining the values of kinetic parameters which, in turn form the basis for determining char reactivity.

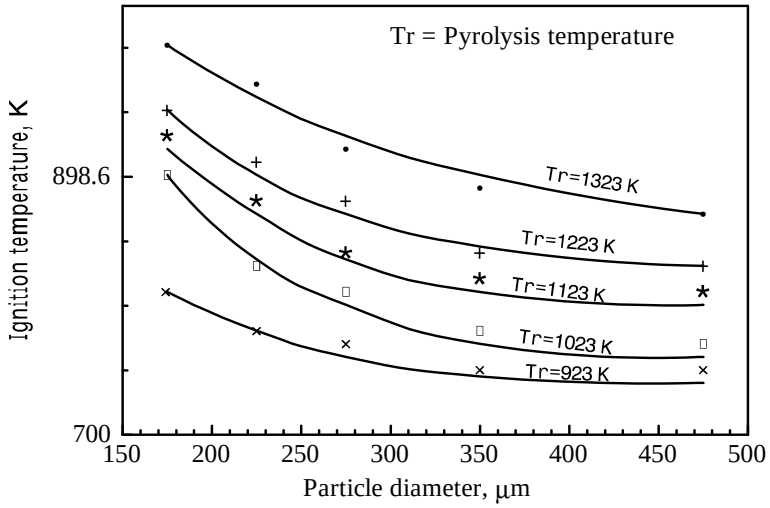

Fig. (5). Ignition temperature as a function of particle diameter for various pyrolysis Temperature.

4. Reactivity of Coal Particles

Reactivity is influenced by many chemical and physical factors characteristic for fuel, e.g.: crystalline structure, presence of mineral substance and trace elements, specific surface of pores, capacity of open pores, porosity etc. Coal reactivity changes together with its devolatilization and depends on the conditions of pyrolysis, such as: rate of heating, temperature and duration of pyrolysis, type of gas and type of coal.

Solid fuel reactivity is mathematically defined by the formula [21]:

$$q = K (C_O)^m \qquad [Kg/m^2 s] \tag{5}$$

Where: K=the intrinsic rate constant [$Kg/m^2 s$]; or [m/s];

C_O=local concentration of oxidizer fraction, and m= the true reaction order.

The rate constant is usually related to temperature by Arrehenius expression:

$$K = k_o \, Exp \left(- \frac{E}{R_g T_s}\right) \tag{6}$$

Where:

k_o **= frequency factor [m/s];**	**E = activation energy [KJ/mol];**
R_g **= gas constant [KJ/mol.K] and**	T_s **= Particle temperature [K].**

The method of determining kinetic parameters on the basis of experimentally measured ignition temperatures was applied in this report. The relation between ignition temperature and kinetic parameters under the conditions of ignition was derived as given below and is presented in the following [21]:

$$\mathrm{Ln}\left(\frac{2T_g\lambda R_g}{273*0.375e*Q*d}\right)=\mathrm{Ln}\left(E*k_o\right)-\left(\frac{E}{R_g}*\frac{1}{T_g}\right) \qquad (7)$$

Where::

T_g **= Ignition temperature K;**	**d = coal particle diameter (m);**
λ **= coal thermal conductivity t (KJ/m.K) and**	**Q = heat of combustion (KJ/Kg.)**

From the above expression it is seen that the independent variable is given by $(\frac{1}{T_g})$ and the dependent variable is given by: $\mathrm{Ln}\left(\frac{2T_g\lambda R_g}{273*0.375e*Q*d}\right)$ so, the above expression can be plotted to determine kinetic parameters (E & k_o).

Figure (6) shows the plot to determine (k_o) and (E). The activation energy (E) is calculated from the slope $(\frac{E}{R_g})$ and the reaction rate constant (k_o) is obtained from the intercept. The results also are shown in Table (6). The Table shows that the pyrolysis temperature increase to 1323K causes insignificant char reactivity decrease as compared to the reactivity of raw coal. Considerable difference in reactivity of chars and raw coal is observed for the char obtained at 923 K. Slight decrease in char reactivity together with the temperature results due to the development of porous structure and short period of particles presence in the reactor.

Table (6). Kinetic parameter values and char reactivity of Sinai coal obtained in various pyrolysis temperatures.

Sample	Pyrolysis Temp. K	Activation Energy ,KJ/mol	Frequency Factor, m/s	Char, Reactivity, $Kg/m^2.s$
Coal	293	55.0	74	0.020
char	923	115.8	$4.4x10^5$	0.101
char	1023	61.41	$1.2x10^2$	0.020
char	1123	72.3	$6.6x10^2$	0.030
char	1223	72.7	$3.5x10^2$	0.014
char	1323	68.5	$1.3x10^2$	0.010

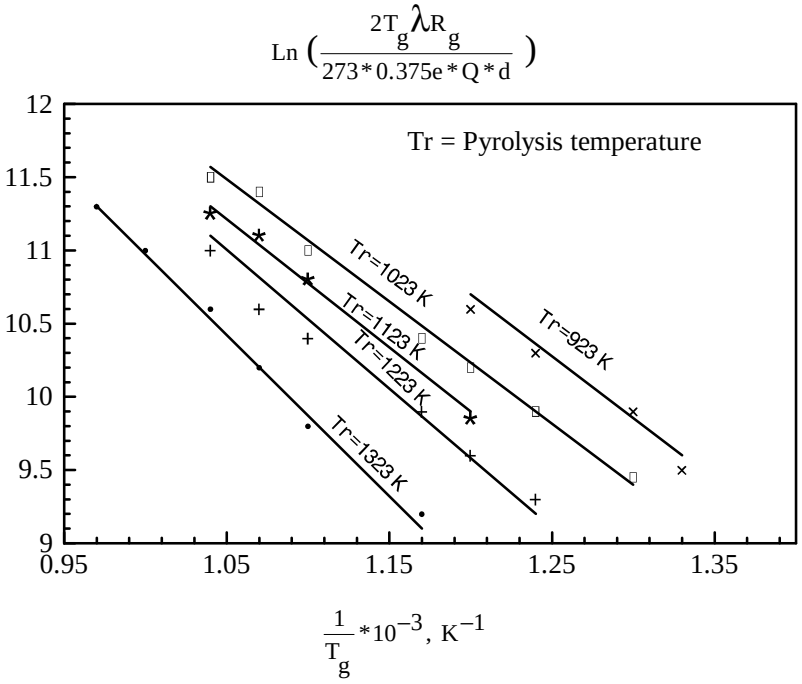

Fig. (6). Determination of kinetics' parameters for various pyrolysis temperatures.

5. Combustion Rates of Sinai Coal at Different Oxygen Concentrations

The Semenov analysis shows that the critical condition for thermal ignition requires that the values of heat generation, (Q_R) and the heat loss, (Q_L), are equal, as are the derivatives of those rates with respect to temperature [22], i.e.

$$Q_R = Q_L \tag{8}$$

$$\frac{dQ_R}{dT} = \frac{dQ_L}{dT} \tag{9}$$

The kinetics is assumed to follow the Arrehenius law, with a reaction of the apparent order, n, in oxygen. For circumstances in which the solid temperature, (T_s) differs little from the gas temperature, (T_g), i.e. (T_s-T_g) << (T_g), the Arrehenius expression can be simplified by the substitution:

$$\text{Exp}\left(-\frac{E}{R_g T_s}\right) \approx \text{Exp}\left(-\frac{E}{R_g T_g}\right).\text{Exp}\left(\frac{E}{R_g T_g^2}(T_s - T_g)\right) \quad (10)$$

The solution of equation (8), (9) and (10) for a spherical fuel particle, considered to be internally isothermal with an irreversible n the order reaction, is given in form:

$$\text{Ln}\left(\frac{2R_g\lambda (T_g)^{2.75+n}}{2.718C^n\beta * Q * d * (273\rho_{O2})^n * (298)^{0.75}}\right) = \text{Ln}\left(E * k_o\right) - \left(\frac{E}{R_g} * \frac{1}{T_g}\right) \quad (11)$$

The intrinsic reactivity, which is defined as the reaction rate per unit surface area of pore surface in the absence of any mass transfer restrictions. The intrinsic kinetic parameters may be obtained directly from the experimentally determined ignition conditions, using the theory of porous particle ignition follows from the theory, is in the form of::

$$\text{Ln}\left(\frac{R_g\lambda(\frac{1+m}{2})^{0.5} (T_g)^{\frac{6+m}{2}}}{C^{\frac{1+m}{2}}\varepsilon * 68.3Q * d * (273\rho_{O2})^{\frac{1+m}{2}} * (298)^{0.75}}\right) = \text{Ln}\left(E * (k_o)^{0.5}\right) - \left(\frac{E}{2R_g} * \frac{1}{T_g}\right) \quad (12)$$

Using experimental data the known left hand side of equations (11) or (12) can be plotted against, $(\frac{1}{T_g})$ and hence (E) and (k_o) determined.

In the report analysis of ignition data it is assumed that (CO_2) is the product of reaction, that carbon consumption prior to ignition is negligible, that heat transfer by radiation can be neglected, that in ignition condition the Arrehenius expression can be simplified by the Frank-Kamenestkii approximation and that ignition of coal particles takes place on a solid surface.

5.1. Ignition Temperature

The influence of the oxygen concentration, (C), on the ignition temperature, (T_g), is shown in Fig. (7). The increasing oxygen concentration raises the oxidation rate and lowers the ignition temperatures of the given material.

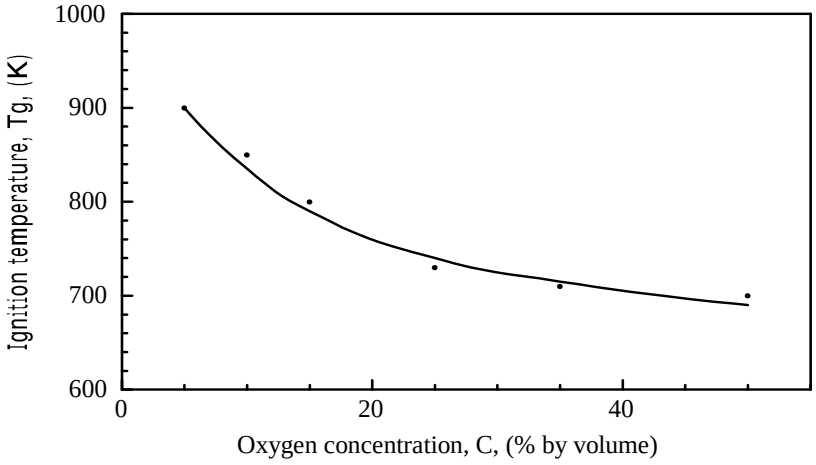

Fig. (7). Ignition temperature of Sinai coal as a function of oxygen concentration.

5.2. Observed (apparent) kinetic

The data in Fig. (7) have been used in equation (12) to give the results shown in Arrehenius form in Fig. (8), assuming n=1. The values of (E) for Sinai coal =87 kJ/mol is at the level found for the reaction of impure carbon with oxygen when pore diffusion and chemical reactions together control the burning rate.

At least squares regression analysis of the ignition data gave the rate of combustion ($\bar{m}$), (kilograms of carbon burnt per second per square meter of the external particle area) related to (T_s) and oxygen concentration (C) by:

$$\bar{m} = 1020.3\left(\frac{273C}{T_s}\right)^{2}\text{Exp}\left(-\frac{78}{R_g T_s}\right) \qquad (13)$$

After conversation to a common oxygen concentration of 100 % volume the computed values of are shown in Arrehenius form in Fig. 9.

$$\text{Ln}\left(\frac{(T_g)^{3.75}}{2.718C * \beta * Q * d * (273\rho_{O2}) * (298)^{0.75}}\right)$$

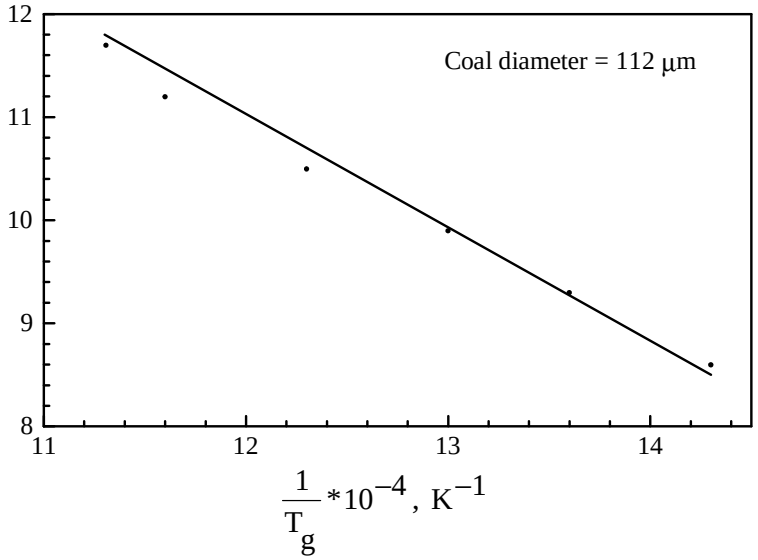

Fig. (8). Plots of observed kinetic versus ignition temperature

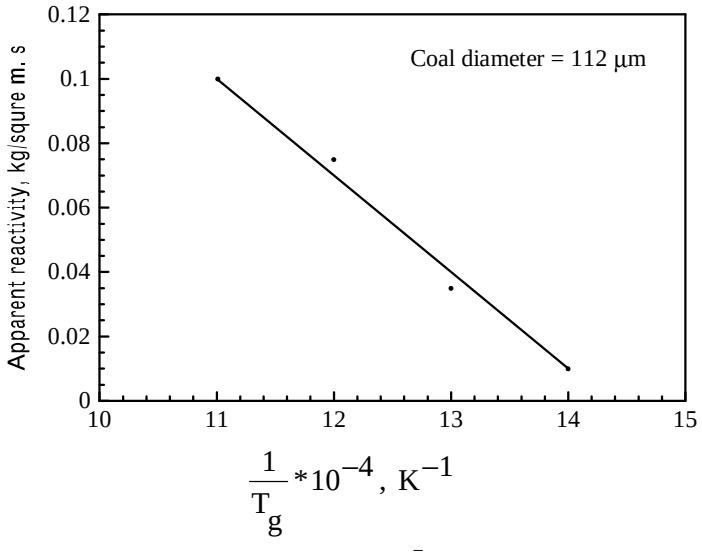

Fig. (9). Dependence of apparent reaction rate ($\bar{m}$) on temperature for Sinai coal.

5. 3. Chemical (intrinsic) reactivity

Figure (10) illustrates the Arrehenius plot for the ignition data calculated according to equation (12). The application of a least squares regression analysis to the ignition data corrected for pore diffusion yielded the following expression for the chemical rate, ($\bar{m}_t$), (kilograms of carbon burnt per second per square meter of the total surface area) related to (T_s) and oxygen concentration (C) by :

$$\bar{m}_t = 8125.2\,(\frac{273C}{T_s}^{2})\,Exp(-\frac{153.1}{R_g T_s}) \qquad (13)$$

The true activation energy =153.1 kJ is about twice the energy determined for the zone reaction by global model = 78 kJ/mol.

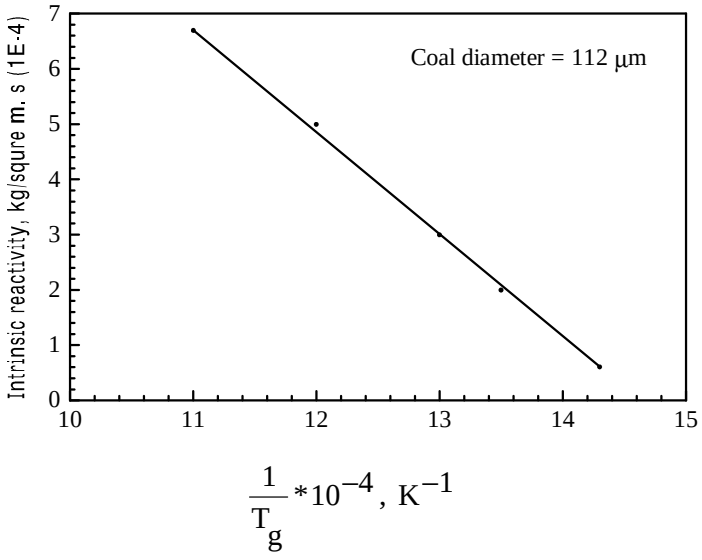

Fig. (10). Dependence of chemical reaction rate ($\bar{m}_t$) on temperature for Sinai coal.

6. Conclusions

The above reported work can be summarized in the following conclusions:

1. The degree of devolatilization of Sinai coal to temperature 1323 K is found virtually not to be affected by change in its particle diameter.
2. In the temperature range 923-1323 K reactivity of obtained chars decreased only 1.2 times in relation to the initial coal reactivity.
3. For particles diameter smaller than 500 μm, the pyrolysis temperature range

1223-1323 K, also proved very useful for char reactivity. Char reactivity in this temperature range does not differ much from the reactivity of raw coal and it is the highest compared with the chars obtained in other pyrolysis temperatures.

4. Chars leave the area of pyrolysis displaying the temperature 1123-1223 K which is much higher than the temperature of ignition.
5. The pre-exponential factor and activation energy in the Arrehenius relation for the rate of reaction of coal with oxygen have been determined using an ignition technique and taking advantage of pore structure properties. Indications are that the apparent activation energy = 78.0 kJ/mol and the true activation energy = 153.1 kJ/mol.

7. References

[1] EDinger, R. T., Friedman, L. D., and Rau, E., "Devolatilization of Coal in a Transport Reactor," *Fue1.45*, (1966), pp.245-252.

[2] Mustafa Versan .Kok., Esber Ozbasb, Ozgen Karacan. and Cahit Hicyilmaz., "Effect of particle size on coal pyrolysis", *J. of analytical and Applied Pyrolysis*, Vol. 45, PP. 103-110, 1998.

[3] Xiaoxun Ma, Hiroshi N., Tadashi Y., Guangwen Xu and Michiaki H., "Kinetics of rapid coal devolatilization measured using a spot heater apparatus", *Fuel processing technology*, Vol. 85, (2003), pp. 43-51.

[4] Peng Liang, Zhifeng Wang and Jicheng Bi, "Process characteristics investigation of simulated circulating fluidized bed combustion combined with coal pyrolysis", *Fuel Processing Technology*, Vol. 88, Issue 1, (2007), pp. 23-28.

[5] Hu G.[1];Fan H.;Liu Y., "Experimental studies on pyrolysis of Datong coal with solid heat carrier in a fixed bed ", *Fuel Processing Technology*, Vol. 69, Issue 3, (2001),pp. 221-228.

[6] Badzioch S.and Hawksley P.G.W.,"Kinetics of thermal decomposition of pulverized coal particles", *Ind. Eng. Chem., Process Des. Develop. 9*, (1970), pp. 521-530.

[7] Kobayashi H, Howard J.B., and Sarofim A.F., "Coal devolatilization at high temperature", *Sixteenth Symposium (International), The Combustion Institute*, Pittsburgh, (1977), pp. 427-436.

[8] Ubbayakar S. K., Stickler D. B. , Von Rosenberg C.W. and Gannon R.E, "Rapid devolatilization of pulverized coal in hot combustion gasses", *Sixteenth Symposium (International), The Combustion Institute*, Pittsburgh, (1977), pp. 411-425.

[9] Solomon P.R., Hamblen D.G., Goetz G. J. and Nskala N.Y., "Coal devolatilization", *Prepr. Div. Fuel Chem, Am. Chem. Soc*., Vol. 26, No. 3, (1981), pp. 6-17.

[10] Mentser M., Donnell H. J., and Ergun S., "*Devolatilization of coal by rapid heating*", Advan. Chem. Series 131, 1974.

[11] Smoot L.D. and Pratt D.T., "*Pulverized coal combustion and gasification – theory and applications for continuous flow processes*", Plenum Press, New York, 1979

[12] Anthony D. B., Howard J. B. and Hottel H. C., "Rapid devolatilization of pulverized coal", *15-th Symposium (International) on Combustion*, 1975.

[13] Anthony D. B. and Howard J. B., "Coal devolatilization and hydro gasification", *AICHE J*. No. 22, (1976), pp. 625-633.

[14] Anthony D. B., "Rapid devolatilization and hydro gasification of bituminous coal", *Fuel No. 55*, (1976), pp.121-133.

[15] Nsakala N. Y., Essenhigh R. H. and Walker P. L., "Studies on coal reactivity: Kinetics of lignite pyrolysis in nitrogen a t 808^{o}C", *Combustion Sci. Tech.*, No. 16, 1977, pp. 153-165.

[16] Nsakala N. Y., Essenhigh R. H. and Walker P. L., "Characteristics of chars produced by pyrolysis following rapid heating of pulverized coal", *Prep. Am. Chem,*. Vol. 22, (1977), pp. 102-120.

[17] Suuberg E. M., Peters W. A. and Howard J. B., "Product composition and kinetics of lignite pyrolysis", *Ind. Eng. Chem., Process Des. Develop. No. 17*, (1978), pp. 37-44.

[18] Suuberg E. M., Peters W. A. and Howard J. B., "Product composition and formation kinetics in rapid pyrolysis of pulverized coal - Implications of combustion", *17-th Symposium (International) on Combustion*, (1979).

[19] Wahhab M. A. and Morsy B. K., "Physical properties of Sinai coal and degree of devolatilization ", *Bulletin of the Faculty of Eng. and Tech.*, Minia university, Egypt, Vol. 9, part I, (1990), pp. 156-172,

[20] Morsy B.K., "Devolatilization of Sinai coal - derived chars ", *Bulletin of the Faculty of Eng. and Tech.*, Minia University, Egypt, vol. 9, part I, (1990), pp. 110 – 125.

[21] Morsy B.K., "*The small scale pyrolysis applied in a coal fired ignition burning"*, Ph. D. Thesis, Technical University of Wroclaw, (1987), Poland.

[22] Morsy B. K., and Rybak W., "The combustion rates of Sinai coal", *Third Minia Conference on Energy and its applications*, (1989).

التحلل الحراري ومعدل احتراق الوقود الصلب (مقالة مرجعية)

بهجت خميس مرسى

قسم الهندسة الميكانيكية – كلية الهندسة – جامعة القصيم

bahgat52@yahoo.com

(قدم للنشر في ٢٠١٠/٢/٢٨؛ وقبل للنشر في ٢٠١٠/٦/٢)

ملخص البحث. معرفة الغازان المتطايرة نوعا وكما ونسبتها بالإضافة إلى الفحم الناتج بعد التحلل الحراري السريع للفحم الخام من العوامل الأساسية والهامة عند دراسة احتراق الوقود الصلب وتصميم غرفة الاحتراق والتحكم في نواتج الاحتراق .هذه الدراسة تمت على الرقود الصلب للفحم المستخرج من سيناء كنموذج للوقود الصلب والنتائج التي تم التوصل إليها مفيدة وضرورية عند تصميم غرف الاحتراق الحلزونية وغرف الاحتراق ذات الطبقات المتميعة وكذلك عندما يكون الهدف هو إنتاج غازلت قابلية للاحتراق من التحليل الحراري السريع.

Journal of Engineering and Computer Sciences
Qassim University, Vol. 4, No. 1, pp. 83-101 (January 2011/Moharram 1432H)

A Developed Softwae For an Improved Mesqa Hydraulic Design

Mohamed A. Nassar[*] and Abdelmoez. M. Hesham[**]
[*]*Assistant Professor, Water & Water Structures Engineering Dept., Faculty of Engineering, Zagazig University, Zagazig 44519, Egypt*
nasserzagazig@yahoo.com
[**] *Physics and Eng. Mathematics Dept., Mataria Faculty of Engineering, Helwan University, Cairo, Egypt, habdelmoez@yahoo.com*

(Received 29/7/2010; accepted for publication 8/1/2011)

Abstract. The proposed software is an advanced computational hydraulic software tool specially adapted for the design, and management of pressurized irrigation networks. The hydraulic solver uses specific strategies and incorporates several new features that improve the algorithms for pipe networks computation. These networks consist of a pumping station, main and secondary flow paths, valves, hydrants, and ancillary equipments. The software simulates hydraulically the flow in the pipe lines by computing the different nodes' pressure. It executes this throughout converting gis maps digitally into pipe lines, valves, and main pumping station. It is applied on the iip (i.e., irrigation improved project) which is one of the national irrigation development projects in egypt. There is no commercial program produces all these targets because iip has its own specific design criteria such as discharge, water duty, and different sets of pumping units. Total economic aspects including pump station and the network parts together with their constituents are computed too. Construction contracts according to the requirements of the egyptian irrigation ministry's specification are accomplished. It has been tested, calibrated and approved on some developed mesqas comparing manual and implemented results. The efficiency of some algorithms has been estimated using computational geometry rules.

Keyword: *hydraulics, gis, mesqa design criteria, vbasic, algorithm efficiency.*

1. Introduction

Reviewing the literature over the past five to ten years, there is indeed a substantial increase in the number of computer programs water-flow models. A number of packages are available that allow simulation models to be constructed for water criteria specific requirements. Popular packages include EPANET (US Environmental Protection Agency) [1], Infoworks (Wallingford software [2], and SynerGEE (Advantica) [3]. The design of distribution networks using these software packages has developed from trial and error to, more recently, the use of various forms of optimization, including genetic algorithms (e.g. Dandy et al., [4]). Bhattacharya et al. [5] proposed an ANN (Artificial Neural Network) with reinforcement learning which could learn to replicate the optimal control strategy (based on capturing operator experience). Rao and Salomons [6] developed a GA (Genetic Algorithm) and an ANN model for capturing the knowledge base of an EPANET model and consequently producing a near optimal solution.

This paper presents a software to simulate the pressurized pipe system. The software may be as simple pipe carrying water from one reservoir through network to one valve, or it may be very complex with many interconnected pipes that distribute the flow throughout a large pipe networks. Our software can model pipe networks and calculate the flow and pressure throughout a system with different pipe sizes and pipe materials, supply and discharge tank, pumps, valves, flow controls, system demands and other component. The pipeline system is modeled by drawing the join points and the connecting pipes on a drawing pane. Horizontal, vertical or sloping lines can be used to connect one node to another node. The optimum design is fulfilled throughout dividing the design process into its main categories and precisely defining each category. Section 3 provides criteria for design of water distribution systems, while section 4 gives the proposed program calibration utilities including a handout solved example on these criteria. Section 5 gives more sophisticated pictures of the proposed software results, while section 6 concludes and suggests the future work of this paper.

2. Software Overview

The program will allow user to draw a complex pipeline system and analyze the features of the system when flow is occurring. It calculates the balanced steady flow and pressure conditions of the system. In addition, it will allow user to perform analysis of alternate systems under various operating conditions. The physical data describing the system is entered by the user and typically includes:

- The internal size, internal roughness and length of each pipe.
- The elevation of each pipe join point (node) and the In-flow and the Out-flow at each join point.
- The elevation, liquid level and surface pressure data for the main tank.

The reported results include: flow rates for each pipe; pressures at each node; HGL (hydraulic grade line) values; pump operating points and NPSH (i.e., Net Positive Suction Head) at pump inlet. Total economic aspects including pump station and the network parts together with their constituents are computed too.

Construction contracts according to the requirements of the Egyptian irrigation ministry's specification are accomplished.

In the other hand, under IIP (i.e., Irrigation Improved Project), hydraulic design of improved branch canals has been carried out using a version of Mott MacDonald's in-house simulation model, which was specially customized at the start of the project in 1996/97 to meet the specific requirements of IIP. This version of the model runs under DOS, which is not now available on most computers. In 1993, Delft Hydraulics introduced a new unsteady-flow simulation software package, SOBEK [7]. It includes a link to MATLAB so that control decisions can be made within that framework. Water levels are passed to MATLAB and gate position changes are passed back to SOBEK. The control routines are written as MATLAB files. Recently, canal control studies have been conducted with the SOBEK–MATLAB combination by Delft Hydraulics.

Actually, the design staff of IIP (i.e., Irrigation Improved Project) was suffering from a big problem, which is the difficulty to abstract the maximum water levels at the different studied point in the same reach. We present here a simple program to abstract these values in easy way. The main purpose is simplifying the way in which the design staff defines the maximum water levels. We added a subroutine to the present software, which helps the user to abstract the water levels and save them as an excel file.

3. Criteria of the Design of Water Distribution Systems

For the IIP-area, the design criteria, which are respected during the development of the software are as the followings:

- Rice (maximum crop water requirement) could be grown in 100% of the mesqa command area.
- Maximum number of pumping units to be 3-units per pump house.
- Mesqas will be designed using PVC pipes 4 bar pressure rating.
- The minimum pipe diameter used for mesqa pipelines will be 200 mm.
- In case of using a stand, the pipeline will be provided with an open air vent at the end of each branch.
- In case of using direct connection, the pipeline will be provided with an air/vacuum valve on the pump delivery manifold and a pressure relief valve at the end of the pipeline.
- The maximum water velocity in the pipeline should not exceed 1.50 m/sec,
- The head loss through the mesqa pipeline network is to be determined according to the following empirical formula:

$$H_L = (c_{in} + n_T K + n_B c_B)\frac{V_P^{\,2}}{2g} + 3.29\frac{V_R^{\,2}}{2g} + H_f + H_{marwa} + \text{Min Valve Head} \quad (1)$$

where: c_{in} is the head loss coefficient at mesqa pipeline inlet, c_{in} = 0.50, K is the head loss coefficient at Tee connection, see table No. (1), n_T is the number of the Tee along mesqa pipeline, c_B is the head loss coefficient in bends, c_B = 0.90; n_B is the number of the bends along mesqa pipeline, V_p is the average water velocity in the mesqa pipeline; V_R is the average velocity in the riser (m/sec); H_f is the friction head loss, it is computed using William-Hazen's equation,

$$H_f = (3.59/C_H)^{1.852} (Q_m{}^{1.852} / D_P{}^{4.87}) L \quad (2)$$

where: Q_m is the discharge (m^3/sec), D_P is the pipe diameter (m), L is the pipeline length (m), and C_H is Hazen friction Coef., 150 and 140 for PVC and PE, respectively, H_{marwa} is the operating head at the marwa off take ranges from 1.5 to 2.0 m [used for case of neglecting the marwa during design stage].

Table (1). Head loss coefficient due to the Tee connection with valves

Diameter of the pipeline (mm)	*K*
200 to 250	0.28
300 to 400	0.26
450 to 600	*0.24*

4. Calibration of the Proposed Software

4.1. Practical calibration:

The developed software is calibrated using a simple type of networks. It simulates the pressurized flow in a simple network. It includes a single path only, see Fig. (1). It is necessary to mention that it is an imaginary network.

4.1.1. Design example:

4.1.1.1. Given:

A parcel of land of about 43F has a main canal, a pump station, and 5 valves. All needed data for design are presented as tabulated in table (2).

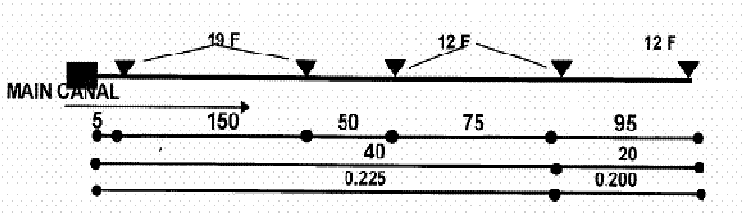

Fig. (1). The pressurized flow in a simple network.

Table (2). Designed data for the simple network

Km	0	0.005	0.155	0.205	0.28	0.375
Land level	2.54	2.41	2.41	2.43	2.37	2.61
land level for marwa		2.33	2.33	2.31	2.35	2.42

4.1.1.2. Required:

The main targets of the design are including both operating head (m), and Stand total height (m).

4.1.1.3. Manual solution:

- Max. Discharge = 0.84*43 = 36.12 1/s ≅ 40 l/s.
- Max no of valves working in certain time = 2 valves.
- $H_L = (c_{in} + n_T K + n_B c_B)\frac{V_P^{\,2}}{2g} + 3.29\frac{V_R^{\,2}}{2g} + H_f + H_{marwa}$ +0.6+(if tank >6.0 take 0.2 into account)
- $H_{L(0)}$ = (0.5 + n x0.28 +0.9 x1) $Vp^2/2g$ +3.29(V_R^2)/2g +(3.59/150) $^{1.852}$ x ($Q^{1.852}/D^{4.87}$) x L + 0.6 +(if tank >6.0 take 0.2 into account)
- $H_{L(0)}$ = (0.5+ 2 x 0.28 + 0.9 x 1) $(1.09)^2/2g$ +3.29(1.0^2)/2g +(3.59/ 150) $^{1.852}$ x($0.04^{1.852}$/(0.216)$^{4.87}$)x 280 +(3.59/150) $^{1.852}$ x ($(0.02)^{1.852}/(0.192)^{4.87}$)x 95+1.5 + 0.6 +(if tank >6.0 take 0.2 into account)
- $H_{L(0)}$ = 0.1186 +0.1676 +1.2511+0.2086+1.5+0.6= 3.84616m
- $H_{L(0.005)}$ = (0.5+ 2 x 0.28 + 0.9 x 1) $(1.09)^2/2g$ +3.29(1.0^2)/2g +(3.59/ 150) $^{1.852}$ x($0.04^{1.852}$/(0.216)$^{4.87}$)x 275 + (3.59/150) $^{1.852}$ x ($(0.02)^{1.852}/(0.192)^{4.87}$)x 95+1.5 + 0.6 +(if tank >6.0 take 0.2 into account)
- $H_{L(0.005)}$ = 0.1186 +0.1676 +1.228+0.2086+1.5+0.6= 3.826m
- $H_{L(0.155)}$ = (0.5+ 2 x 0.28 + 0.9 x 1) $(1.09)^2/2g$ +3.29(1.0^2)/2g +(3.59/ 150) $^{1.852}$ x($0.04^{1.852}$/(0.216)$^{4.87}$)x 125 + (3.59/150) $^{1.852}$ x ($(0.02)^{1.852}/(0.192)^{4.87}$)x 95+1.5 + 0.6 +(if tank >6.0 take 0.2 into account)
- $H_{L(0.155)}$ = 0.1186 +0.1676 +0.558+0.2086+1.5+0.6= 3.15m
- $H_{L(0.205)}$ = (0.5+ 2 x 0.28 + 0.9 x 1) $(1.09)^2/2g$ +3.29(1.0^2)/2g +(3.59/ 150) $^{1.852}$ x($0.04^{1.852}$/(0.216)$^{4.87}$)x 75+ (3.59/150) $^{1.852}$ x ($(0.02)^{1.852}/(0.192)^{4.87}$)x 95+1.5 + 0.6 +(if tank >6.0 take 0.2 into account)
- $H_{L(0.205)}$ = 0.1186 +0.1676 +0.335+0.2086+1.5+0.6= 2.92
- $H_{L(0.280)=}$ (0.5+ 2 x 0.28 + 0.9 x 1) $(1.09)^2/2g$ +3.29(1.0^2)/2g+(3.59/150) $^{1.852}$ x ($(0.02)^{1.852}/(0.192)^{4.87}$)x 95+1.5 + 0.6 +(if tank >6.0 take 0.2 into account)
- $H_{L(0.280)}$ = 0.1186 +0.1676 +0.2086+1.5+0.6= 2.59
- $H_{L(0.375)=}$ (0.5+ 2 x 0.28 + 0.9 x 1) $(1.09)^2/2g$ +3.29(1.0^2)/2g+1.5 + 0.6 +(if tank >6.0 take 0.2 into account)
- $H_{L(0.375)}$ = 0.1186 +0.1676 +1.5+0.6= 2.38

Finally, the hydraulic calculation can be tabulated in the following table (3) and figure (4).

- Stand total height = 3.8461 + 0.75+0.4+.25= 5.2461 m
- Stand Top level = 5.2461 + 1.09= 6.336 m.

Table (3). Manual design operating head for the different nodes in the simple network

Km	**0**	**0.005**	**0.155**	**0.205**	**0.280**	**0.375**
Land level	**2.54**	**2.41**	**2.41**	**2.43**	**2.37**	**2.61**
Op. head (m)	**3.84**	**3.82**	**3.15**	**2.92**	**2.59**	**2.38**

4.1.2. Solution of the simple network using the proposed software:

The simple network is modeled using the proposed software in three steps as following:

1- Input the data of the design including area served by the pump station; the land level the pump station; and the necessary definition of the network.

2- Digitizing the network path as shown in Fig. (2A), and checking the input date for the path itself, see Fig. (2B), and.

3- Presenting the output data including the design for the path and pump sets and both operating head (m), and Stand total height (m), see Fig. (3).

It can be noticed that, the out screen of the software including the all design data for the flow paths and network see, Fig. (3) at the left hand side. In addition, the hydraulic gradient line and all graphs for the designed path are presented in the same figure. The output of the software can be listed as following:

- Stand height (m)= 5.270;
- Q (l/s)=40 ;
- Mesqa Length (m)= 364.3;
- Length per fed.(m)= 15.839;
- Pump Cat. = Categ. 2 cover (5.0 to 8.5 m); and
- Pump sets (i.e., the formulation of the pumps): two pumps of 20(lit/s)

4.1.3. Analysis of practical calibration:

Figure (4) shows a comparison between the hydraulic gradient line calculated with the developed software and that calculated manually for the studied network. It can be seen that the hydraulic gradient line calculated from the software is higher than that calculated manually by about 18cm, see Fig.(4). The calculated stand height using the proposed software is nearly identical with that calculated by the manual procedure. The difference was about 13.1 cm. The statistics' measures, which are R2 and correlation factor, are used to measure the ability of the developed software as a tool to calculate the hydraulic gradient line through the studied network. R^2 and correlation factor are 0.978 and 0.989, respectively. Using statistical analysis principles, and based on both modeled and calculated values of the hydraulic gradient line, it was found that the developed software is well verified and an accurate tool to the hydraulic gradient line along the studied network. The accuracy was more than 97%.

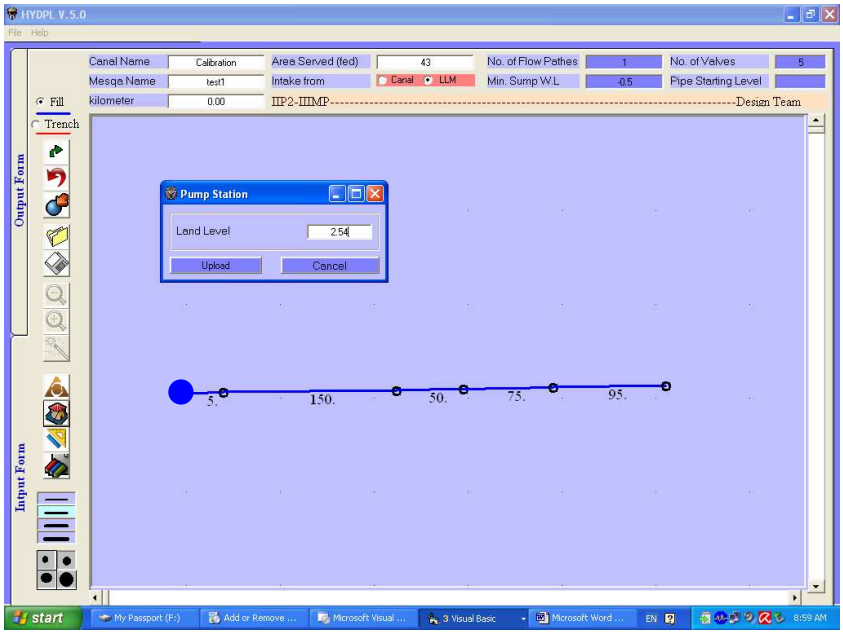

(a)

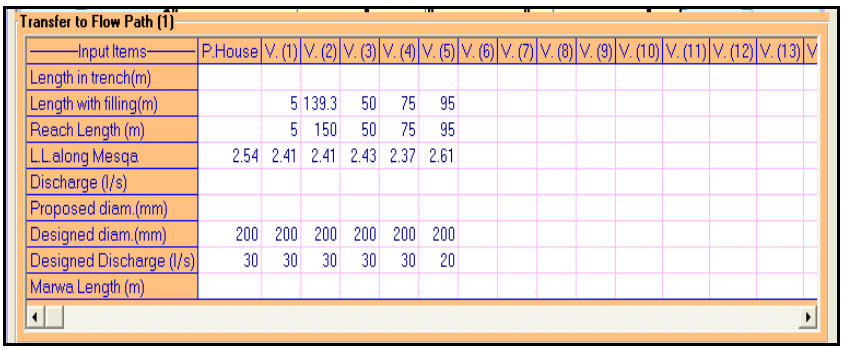

Transfer to Flow Path (1)

Input Items	P.House	V. (1)	V. (2)	V. (3)	V. (4)	V. (5)	V. (6)	V. (7)	V. (8)	V. (9)	V. (10)	V. (11)	V. (12)	V. (13)	V
Length in trench(m)															
Length with filling(m)		5	139.3	50	75	95									
Reach Length (m)		5	150	50	75	95									
L.L along Mesqa	2.54	2.41	2.41	2.43	2.37	2.61									
Discharge (l/s)															
Proposed diam.(mm)															
Designed diam.(mm)	200	200	200	200	200	200									
Designed Discharge (l/s)	30	30	30	30	30	20									
Marwa Length (m)															

(b)

Fig. (2). The inputs screen shots of the software; (a) the digitizing form (b) digitized data.

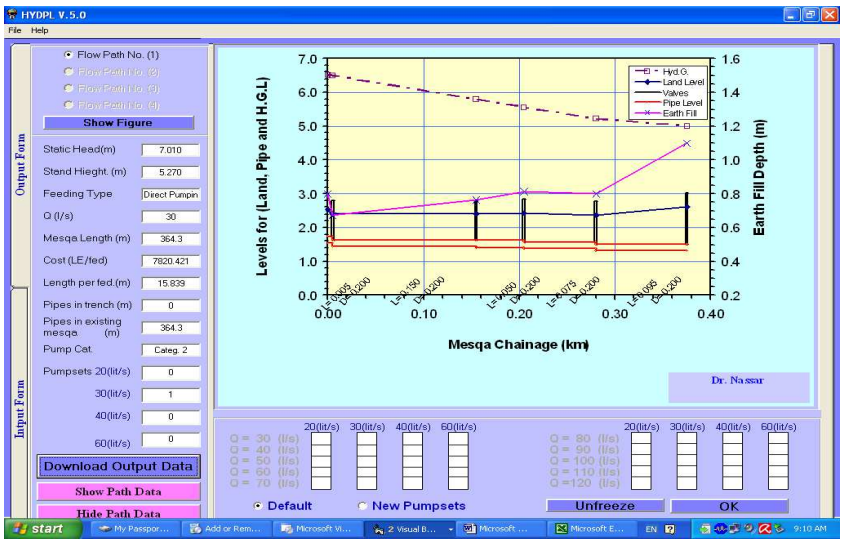

Fig. (3). The outputs screen shot of the software for the simple network.

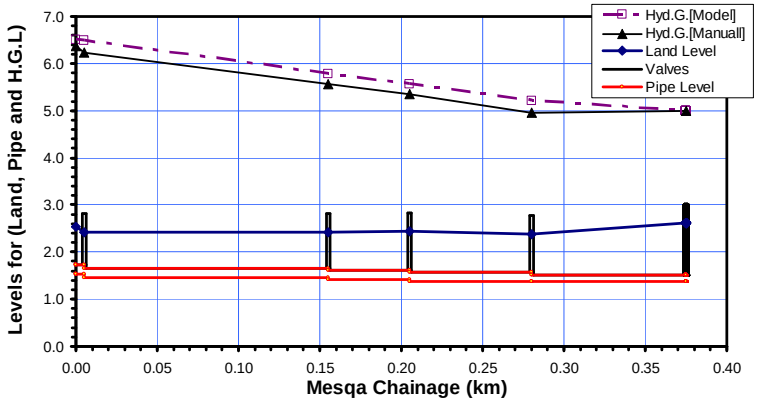

Fig. (4). Calculated and modelled hydraulic gradient line through the studied network.

4.2. Theoretical Calibration

4.2.1. The Efficiency of some algorithms included:

The algorithm efficiency can be measured either by the time it takes to run a program or by the space the program takes up in memory [8]. We will focus on an algorithm's efficiency with respect to time. How do we compare the time efficiency of two algorithms that solve the same problem? One approach: implement the two

algorithms in Visual Basic (VB) and run the programs … this presents some difficulties:

i) How are the algorithms coded?

If algorithm A runs faster than algorithm B, it will obviously give one algorithm an advantage. Hence, we would be comparing the algorithms' implementations, rather than the algorithms themselves. We should not compare implementations, because they are sensitive to factors, such as programming style, that tend to cloud the issue of which algorithm is inherently more efficient.

ii) What computer speed should we use?

If one computer is faster than the other, it will obviously give one algorithm an advantage. Hence, both algorithms should be run on the same computer.

iii) What computer type should we use?

The type of computer is also more important. The particular operations that the algorithms require can cause A to run faster than B on one computer while the opposite is true on another computer. Hence, we must be able to compare efficiencies independent of a particular computer.

iv) What data should the program use?

There is always the danger of selecting data sets for which one of the algorithms runs uncharacteristically fast (or slow). Example: sequential search vs. binary search when search item is the first element in the array. Hence, we must be able to compare efficiencies independent of a particular data set. To overcome these difficulties, computer scientists employ mathematical techniques that analyze algorithms independent of specific implementations, computers, and data [9, 10]. An algorithm's efficiency is related to the number of operations it requires. If a function contains no loops, its efficiency is simply a function of the number of instructions it contains. In other words, the more instructions the function contains, the longer it will take to execute. That being said, with current computer speeds on the order of 3 GHz, it doesn't make much of a difference if our program has 10 instructions or 1000 instructions … we really won't notice a difference. However, when we are dealing with functions that loop, the problem becomes non-trivial. The study of algorithm efficiency therefore focuses on loops.

We typically discuss an algorithm's efficiency as a function of the number of elements to be processed. For example, if we want to determine the efficiency of an array-sorting algorithm, we express the efficiency of the algorithm as a function of the number of elements of the array, *n*. The general format is: f (n) = efficiency.

Let us start with a simple loop. We want to know how many times the body of the loop is executed

In the following code:

```
i=1
  loop (i<=1000)
            (loop body)
             i = i + 1
  end loop
```

The answer is 1000 times. The number of iterations is directly proportional to the loop factor, 1000.

Hence, the larger the loop factor, the more loop iterations we will complete. Because the efficiency is directly proportional to the number of iterations, its efficiency can be represented as: f(n) = n. However, the answer is not always as straightforward as it was in the previous example. For example, consider the following loop:

```
i = 1
loop (i <= 1000)
        (loop body)
        i = i + 2
end loop
```

In this case, the body of the loop is executed 500 times – half the value of the loop factor. Once again, however, the larger the loop factor, the more loops we execute. The efficiency of this loop is therefore:

f(n) = n/2. If you were to plot either of these loop efficiencies, you would get a straight line. Hence, they all called *linear loops.*

In our previous examples, our control variable was incremented by either 1 or 2 each time through the loop. Now consider a loop in which the controlling variable is multiplied or divided in each loop.

```
Multiply Loops
i = 1
loop (i < 1000)
        (loop body)
        i = i * 2
end loop
Divide Loops
i = 1000
        loop (i >= 1)       (loop body)
        i = i / 2
end loop
```

How many times are the loop bodies executed in the above code sections? See table (4).

As we can see, the number of loop iterations is 10 in both cases. Note that in each iteration the value of i doubles for the multiply loop and is cut in half for the divide loop. Thus, the number of iterations of the loop is a function of the multiplier or divisor, in this case, 2. That is, the loop continues while the Condition shown below is true:

multiply: $2^{iterations} < 1000$, divide: $1000 / 2^{iterations} >= 1$

Generalizing the analysis, we can say that the efficiency of loops that multiply or divide by 2 is determined by the following formula: $f(n) = \log_2 n$.

For linear logarithmic loops, the following code will be considered:

```
i = 1
loop (i <= 10)
```

```
        j = 1
        loop (j <= 10 )
                (loop body)
                j = j * 2
        end loop
        i = i + 1
end loop
```

Table (4). Logarithmic loops.

Multiply Loop		Divide Loop	
Iteration	Value of i	Iteration	Value of i
1	1	1	1000
2	2	2	500
3	4	3	250
4	8	4	125
5	16	5	62
6	32	6	31
7	64	7	15
8	128	8	7
9	256	9	3
10	512	10	1
(exit)	1024	(exit)	0

The inner loop is a multiply loop. The number of iterations in the inner loop is therefore $\log_2 10$. We must then multiply this by the number of times the outer loop executes. This gives us $10*\log_2 10$ which is generalized as $f(n) = n\log_2 n$.

With the speed of computers today, we are not concerned with an exact measurement of an algorithm's efficiency as much as we are with its general order of magnitude [11, 12]. For example, if the analysis of 2 algorithms shows that one finishes after 15 iterations while the other takes 25 iterations; then they are both so fast that we can't see the difference. However, if one algorithm finishes after 15 iterations and the other takes 15,000 iterations, this is a more significant difference.

We have shown that the number of iterations an algorithm executes, f(n), can be expressed as a function of the number of elements associated with the algorithm. Although the efficiency equation derived for a function can be complex, we can examine the dominant factor in the equation to determine the relative magnitude of the efficiency.

Hence, we don't need to determine the complete measure of efficiency, only the factor that determines the magnitude. This factor is the *big-O*, as in "on the order of," and is expressed as O (n). This simplification of efficiency is known as *big-O notation*. The big-O notation can be derived from
f (n) using the following steps:

1- We set the coefficient of each term to 1.

2- We keep the largest (least efficient) term in the function and discard the others.

Terms are ranked from most efficient (leftmost terms) to least efficient (rightmost terms) as shown below:

constants $\log_2 n$ n $n\log_2 n$ n^2 $n^3 \ldots n^k$ 2^n n!
For example, let's calculate the big-O notation of the following efficiency:

$$f(n) = \frac{n(n+1)}{2} = \frac{1}{2}n^2 + \frac{1}{2}n$$

First, we set all coefficients to 1. This gives us: $\boldsymbol{n^2 + n}$

Next, we keep the largest term in the function and discard all others. This leaves: n^2. Therefore, we can write the big-O notation as: $O(n^2)$.

As another example, let's look at the polynomial expression:

$$f(n) = 6n^4 \log n + 12n^3 + 2n^2 + n + 128$$

First, we eliminate all of the coefficients: $f(n) = n^4 \log n + n^3 + n^2 + n + 1$

We then select the largest term and discard the rest. This gives us: $O(n^4 \log n)$

Note that constants are the MOST efficient. We think about it like this: If we have an efficiency of 100,000,000 vs. n, which is more efficient? Answer: since n can equal 100,000,001, the constant is the most efficient. See the following criteria:

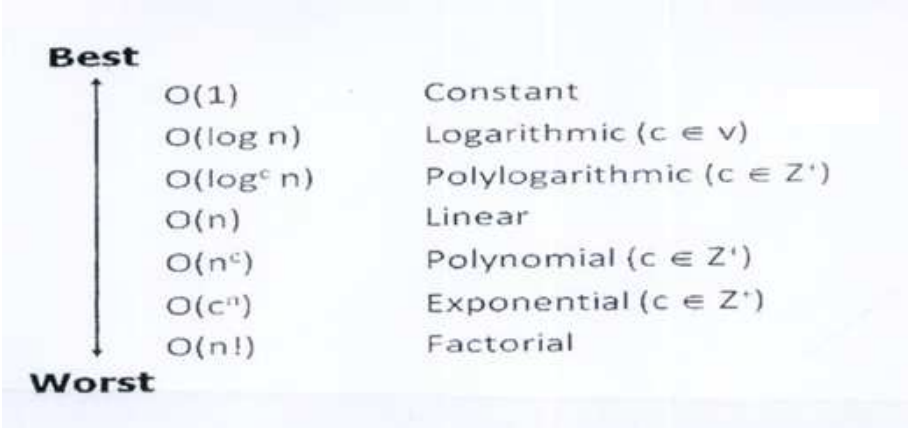

When comparing two algorithmic efficiencies, the "most efficient" one grows the slowest. Easy test: After computing the efficiencies (e.g., $n^{0.5}$ and n^2) plug in a huge value for n; then whichever efficiency results in the smallest value is the most efficient. Here $n^{0.5}$ is more efficient than n^2.

To get a feel for how much of a difference an algorithm's efficiency makes, check out the table (5) together with figure (5). The table assumes an instruction speed of 1 microsecond, 10 instructions per loop, and n=10,000.

Note: performing an order-of-magnitude analysis implicitly assumes that the algorithm will be used to solve large problems.

Table (5). Standard measure of algorithm efficiency.

Efficiency	Big-O	Iterations	Estimated Time
Logarithmic	$O(\log_2 n)$	14	Microseconds
Linear	$O(n)$	10,000	0.1 seconds
Linear Logarithmic	$O(n\log_2 n)$	140,000	2 seconds
Quadratic	$O(n^2)$	$10,000^2$	~17 minutes
Polynomial	$O(n^k)$	$10,000^k$	Hours
Exponential	$O(c^n)$	$2^{10,000}$	Intractable
Factorial	$O(n!)$	10,000!	Intractable

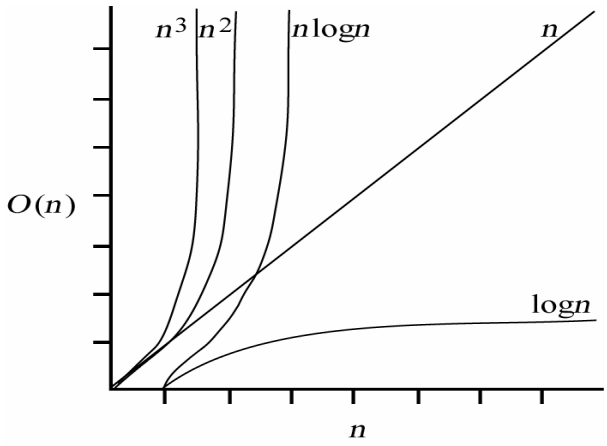

Fig. (5). Standard measure of algorithm efficiency.

4.2.2. Analysis of theoretical calibration:

Algorithm analysis is the area of computer science that provides tools for comparing the efficiency of different methods of solution. This analysis concerns itself primarily with *significant* differences in efficiency. Usually, significant differences only arise through superior solutions and rarely through clever coding tricks. Reductions in computing costs due to clever coding tricks are often more than offset by reduced program readability, which increases human costs.

An algorithm analysis should focus on gross differences in the efficiency of algorithms that are likely to dominate the overall cost of a solution. Otherwise, we could select an algorithm that runs a fraction of a second faster than another algorithm yet requires many more hours of our time to implement and maintain.

In our proposed software there are many algorithms. One of the very beginning ones are that for transporting design data for every path of the network paths under study from the program design file (since the program carries out the design operations in a hidden Excel file) and showing them to the designer on the screen as a table form to ensure the input data. This algorithm contains the following iterations:

```
For i = 3 To 25
iii = i - 2
If Option1.Value = True Then grdRunData.TextMatrix(7, iii) = C.Cells(18, i).Value
If Option2.Value = True Then grdRunData.TextMatrix(7, iii) = C.Cells(28, i).Value
If Option3.Value = True Then grdRunData.TextMatrix(7, iii) = C.Cells(38, i).Value
If Option4.Value = True Then grdRunData.TextMatrix(7, iii) = C.Cells(48, i).Value

If Option1.Value = True Then grdRunData.TextMatrix(8, iii) = C.Cells(60, i).Value
If Option2.Value = True Then grdRunData.TextMatrix(8, iii) = C.Cells(61, i).Value
If Option3.Value = True Then grdRunData.TextMatrix(8, iii) = C.Cells(62, i).Value
If Option4.Value = True Then grdRunData.TextMatrix(8, iii) = C.Cells(63, i).Value

Next
```

The iterations start from 3 to 25, i.e. 23 points, which is the maximum number of points on the same path. Every iteration contains 4 paths as a maximum allowed number of paths. Each path has two data entries that are final diameters in mm and the discharge in l/s. As we see in that loop, the efficiency of this loop is *O (n)* which is a constant efficiency. It is the best algorithm efficiency.

Another loop is that creates virtual pumps formulations. This means that the total pump station discharge has to be partitioned into smaller pumps formulation components that are available in the execution contracts. As example, if the total pump station discharge is 100 l/s and the contract allows only 40 and 60 l/s pumps, then it is obvious to use these two discharge pumps formulation components. These virtual formulations are come from both experience and user demands.

```
For gf = 0 To 3
If C.Cells(13, 8).Value <= 30 Then Text40(gf).Text =C.Cells(13, 9+ gf).Value Else Text40(gf).Text=
If C.Cells(13, 8).Value <= 40 And C.Cells(13, 8).Value > 30 Then Text40(gf).Text = C.Cells(13, 9 + gf).Value Else Text40(gf + 4).Text=
If C.Cells(13, 8).Value <= 50 And C.Cells(13, 8).Value > 40 Then Text40(gf + 8).Text = C.Cells(13, 9 + gf).Value Else Text40(gf + 8).Text=
If C.Cells(13, 8).Value <= 60 And C.Cells(13, 8).Value > 50 Then Text40(gf + 12).Text = C.Cells(13, 9 + gf).Value Else Text40(gf + 12).Text=
If C.Cells(13, 8).Value <= 70 And C.Cells(13, 8).Value > 60 Then Text40(gf + 16).Text = C.Cells(13, 9 + gf).Value Else Text40(gf + 16).Text=
```

If C.Cells(13, 8).Value <= 80 And C.Cells(13, 8).Value > 70 Then Text40(gf + 20).Text = C.Cells(13, 9 + gf).Value Else Text40(gf + 20).Text"=
If C.Cells(13, 8).Value <= 90 And C.Cells(13, 8).Value > 80 Then Text40(gf + 24).Text = C.Cells(13, 9 + gf).Value Else Text40(gf + 24).Text"=
If C.Cells(13, 8).Value <= 100 And C.Cells(13, 8).Value > 90 Then Text40(gf + 28).Text = C.Cells(13, 9 + gf).Value Else Text40(gf + 28).Text"=
If C.Cells(13, 8).Value <= 110 And C.Cells(13, 8).Value > 100 Then Text40(gf + 32).Text = C.Cells(13, 9 + gf).Value Else Text40(gf + 32).Text"=
If C.Cells(13, 8).Value > 110 Then Text40(gf + 36).Text = C.Cells(13, 9 + gf).Value Else Text40(gf + 36).Text"=

Next

As we see in that loop, the efficiency of this loop is *O (n)* which is a constant efficiency. It is the best algorithm efficiency. The following is a group of loops that are designed efficiently to fulfil the requirements of the excel file. The later contains the design properties such as the internal diameter for every pipe type, the design water duty, pipe class, … etc. It transports them from the design properties file to the designer on the screen in order to accept, modify, or cancel if it is required.

```
iii = 0

For iii = 1 To 9
Text13 (iii - 1).Text = C.Cells(iii + 9, 7).Value
Next

iii = 0
For iii = 9 To 17
Text13 (iii).Text = C.Cells(iii + 1, 11).Value
Next

iii = 0
For iii = 18 To 25
Text13 (iii).Text = C.Cells(iii - 15, 20).Value
Next

iii = 0
For iii = 26 To 29
Text13 (iii).Text = C.Cells(iii + 11, 5).Value
Next
```

After the theoretical calibration has been achieved one can conclude that, all the algorithms of the presented software are efficient more than 50% and have the best quality. This is because the program fulfils time requirement, which is half the way to the complete algorithm efficiency. The rest of the efficiency of the algorithms which is the memory requirement is about 40 % achieved. This is because the reserved memory size for the proposed software constants and variables are so minimized that the available memory size for the user is huge. As a result, the algorithm efficiency is more than 90 %.

5. Snap Shots of Some Sophisticated Field Solved Problems

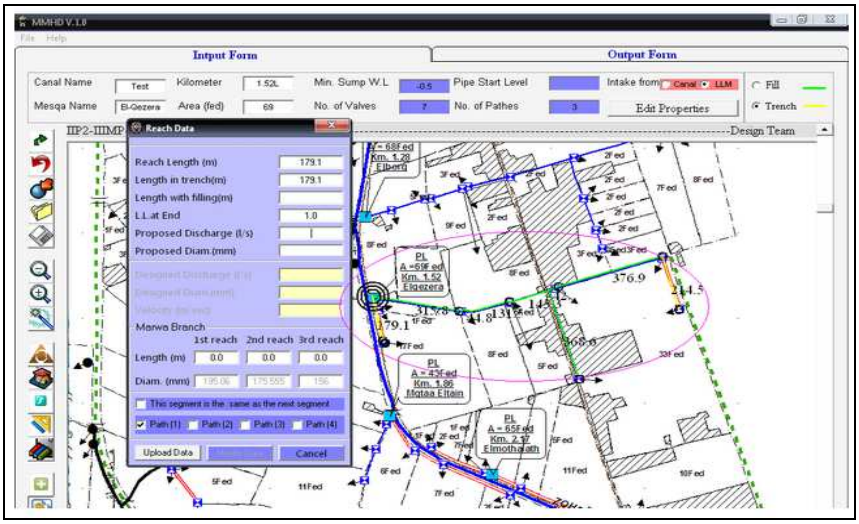

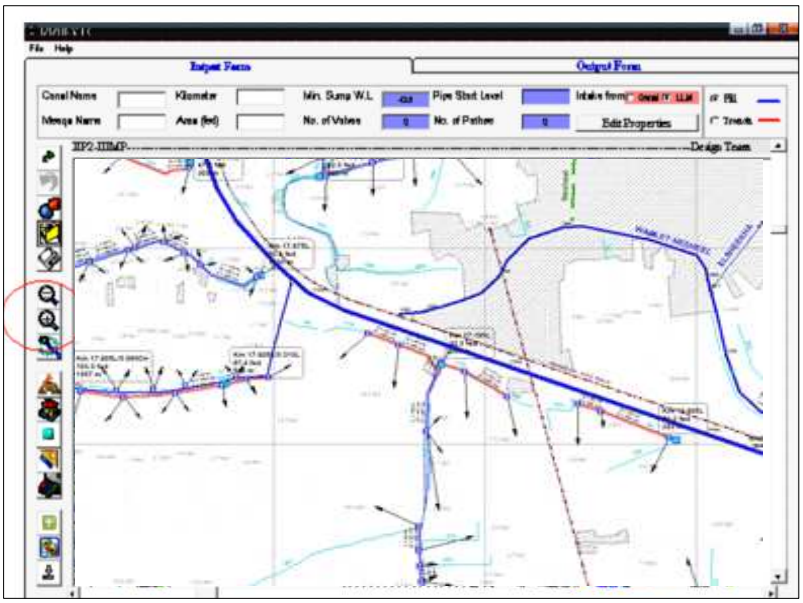

Figure (6). Two selected screen shots of the software for the complicated networks

6. Conclusions

We have proposed software for fully integrated design framework of a multi-disciplinary approach and cost computations for pressurized pipe lines used in IIP projects. It can carry out many tasks such as:

- Simulations of flows through the pipe lines implemented in IIP projects,
- Estimates the cost for the all elements of the pipe lines including the pump stations,
- Prepare the engineering estimates and Arabic version of the contract which is necessary to biding stage,
- It includes new features to assist Sobek software to extract the date about the longitudinal sections,
- It gives the ability to users to detect the maximum and minimum water levels and
- It prepares the necessary files to change all the abstraction points in any Sobek case.

It has been designed for experts and non-experts alike. The framework is composed of several modules, grouped around a mutual interface, while being capable to interact with one another. Some of the used algorithms in the presented software are reviewed against efficiency. The proposed program is calibrated both practically and theoretically.

In the future, it may add a module to the software to prepare the necessary Auto Cad files for layout and longitudinal section of the available paths of the designed mesqa,

7. References

[1] Lewis A. Rossman, "EPANET 2-USERS MANUAL", *National Risk Management Research Laboratory, Office of research and development, U.S. Environmental Protection Agency, Cincinnati, Oh 45268,* (2000).

[2] Wallingford Software, "*InfoWorks CS Technical Review*", (2009).

[3] StonerSofware, "*SynerGEE – ESRI, For City of Leesburg Integration*", (2008).

[4] Dandy, G. A., Simpson, A. R., and Murphy, L. J. "An improved genetic algorithm for pipe network optimization", *Water Res.*, Vol. 32, No. 2, (1996), pp. 449–458.

[5] Bhattacharya, B., Lobbrecht, A. H., and Solomatine, D. P. "Neural networks and reinforcement learning in control of water systems", *J. Water Res. Pl.-ASCE*, Vol. 129, No. 6, (2003), 458–465.

[6] Rao, Z. and Salomons, E. "Development of a real-time, nearoptimal control process for water distribution networks", *J. Hydroinform., IWA Publishing*, Vol. 9, No. 1, 2007), pp. 25–37.

[7] Delft Hydraulics LTD, The Independent Consulting and Research Institute, "*SOBEK210, SOBEK Software and Manuals*", Netherlands, http://www.wldelft.nl and http://www.SOBEK.nl, (2006).

[8] Boissonnat, J.D, Yvinec, M., *Algorithmic Geometry""*, Cambridge, UK, (1988).
[9] Jason. C, Zhiru. Z, "An Efficient and Versatile Scheduling Algorithm Based on SDC Formulation", *Proceedings DAC 2006*, San Francisco, California, USA, June 24-26, (2006).
[10] Elad H., Seshadhri C., "Efficient Learning Algorithms for Changing Environments", *Proceedings of the 26th International Conference on Machine learning*, Montreal, Canada, (2009).
[11] Hendrik B., Jan S., "Efficient Algorithms for Decision Tree Cross-Validation", *Journal of machine Learning Research*, Vol. 3, (2002), pp. 621-650.
[12] Ning Z., Zhixiong C., Guozhen X., "Efficient Elliptic Curve Scalar Multiplication Algorithms Resistant to Power Analysis", *Journal of Information Sciences*, Vol. 177, (2007), pp. 2119-2129.

برمجية مطورة للتصميم الهيدروليكي للمسقى المحسنة

محمد أحمد نصار * وهشام عبد المعز محمد عبد الجواد **

* قسم المياه ومنشآت المياه –كلية الهندسة بالزقازيق– جامعة الزقازيق، nasserzagazig@yahoo.com

** قسم الفيزيقا والرياضيات الهندسية –كلية الهندسة بالمطرية – جامعة حلوان، habdelmoez@yahoo.com

(قدم للنشر في ٢٠١٠/٧/٢٩م ؛ وقبل للنشر في ٢٠١١/١/٨م)

ملخص البحث. تقدم هذه الورقة خوارزميات جديدة فى صورة برنامج تم تطويره بلغة البيسيك المرئى لتصميم شبكات الري ذات الضغوط المنخفضة ، وهذه الشبكات تتكون من محطة ضخ ومسارات تدفق رئيسية وثانوية وصمامات بأنواع مختلفة ، ومعدات مساعدة ضرورية لنقل المياه من المحطة إلى مختلف وجهات الاستعمال. والبرنامج المقترح يحاكى هيدروليكيا التدفق في خطوط الأنابيب من خلال حساب الضغوط الفعلية في جميع نقاط الشبكة حتى صمامات النهاية ، ويقوم أيضاً بتحويل خرائط نظم المعلومات الجغرافية رقميا إلى خطوط الأنابيب والصمامات وكذلك نقطة محطة الضخ الرئيسية ، وقد تم تطبيق هذا البرنامج على (مشروع تطوير الري IIP) والذي يعد واحدا" من المشروعات القومية في مصر. و من المعلوم أنه لايوجد برنامج معروف ينتج كل هذه المعلومات لأن مشروع تطوير الري يلتزم بمعايير محددة ، مثل وجود تصرفات محددة في الأفرع المختلفة لشبكة الري ، ووجود مقنن مائي محدد لمناطق المشروع ، ووجود تراكيب محددة من المضخات والتي يجب استخدامها طبقا لعقود التنفيذ. هذا ويقوم البرنامج بالإضافة إلى ذلك بحساب التكاليف الإجمالية بما في ذلك الجوانب الاقتصادية لمحطة الضخ وأجزاء الشبكة ، وكذلك بناء عقود التنفيذ وفقا لمتطلبات مواصفات وزارة الري المصرية ، وإمكانية التعامل مع برامج هيدروليكية مشهورة مثل سوبك. وقد تم اختبار هذا البرنامج موضوع البحث ، ومعايرته على بعض المساقي المصممة يدوياً مسبقاً وقد لوحظ وجود توافق جيد بين النتائج التي قدمها البرنامج وتلك التي تم حسابها يدوياً ، كما قدرت كفاءة بعض الخوارزميات باستخدام قواعد الجيومترى الحسابية.

قواعد النشر

أهداف المجلة

تهدف المجلة إلى نشر إنتاج الباحثين من داخل الجامعة وخارجها في جميع تخصصات العلوم الهندسية وعلوم الحاسب، والمجالات الرئيسية التي تشملها المجلة هي:

- الهندسة الكهربائية
- الهندسة المدنية
- الهندسة الميكانيكية
- الهندسة الكيميائية
- هندسة التعدين والبترول
- هندسة الحاسب
- علوم الحاسب
- تكنولوجيا المعلومات
- نظم المعلومات
- العلوم الهندسية الأساسية

لغة المجلة:

تقبل المجلة البحوث باللغة الإنجليزية.

أ) المواد التي تقبلها المجلة للنشر:

١- البحث: وهو عمل أصيل للمؤلف (أو المؤلفين) يضيف جديداً للمعرفة في مجال تخصص (فرع المجلة).

٢- المقالة المرجعية: وتتناول العرض النقدي والتحليلي للبحوث والكتب ونحوها التي سبق نشرها في ميدان معين والرسائل العلمية المتميزة.

٣- المقالة القصيرة (تعليق تقني): مقالة قصيرة تحوي تطبيقاً تقنياً.

٤- الابتكارات العلمية المتميزة وبراءات الاختراع.

٥- المراسلات: وتتناول عرض فكرة أو رأي علمي أو اقتراح بحثي.

٦- انتقادات الكتب

ب) شروط النشر:

١- أن يكون البحث متسماً بالأصالة والابتكار والمنهجية العلمية وسلامة الاتجاه وصحة اللغة وجودة الأسلوب.

٢- أن لا يكون البحث قد سبق نشره أو قدم للنشر لجهة أخرى.

٣- جميع البحوث المقدمة للنشر في المجلة خاضعة للتحكيم.

ج) تعليمات النشر:

عند تقديم البحث للنشر يشترط الآتي:

١- أن يقدم الباحث طلباً بنشر بحثه، ويوضح فيه العنوان الالكتروني للمراسلات.

٢- لا يجوز إعادة نشر أبحاث المجلة في أي مطبوعة أخرى إلا بإذن كتابي من رئيس التحرير.

٣- يرسل الباحث بحثه باللغة الانجليزية عن طريق البريد الالكتروني على العنوان الالكتروني المذكور في فقرة المراسلات، وكذلك ملخص باللغتين العربية والإنجليزية بحيث لا تزيد كلماته عن ٢٠٠ كلمة.

٤- يكتب البحث باستخدام برنامج (Microsoft word) ويستخدم font 12 Times New Roman في كتابة المتن، مع ترك مسافة ونصف بين الأسطر.

٥- يجب ألا يزيد عدد صفحات البحث شاملا الرسومات والجداول عن ٢٠ صفحة حجم A4.

٦- أن يكتب عنوان البحث واسم الباحث وعنوانه ولقبه العلمي والجهة التي يعمل بها على الصفحة الأولى مستقلة.

٧- توضع هوامش كل صفحة أسفلها.

٨- يشار إلى المراجع داخل المتن بالأرقام حسب تسلسل ذكرها وتثبت في فهرس يلحق بآخر البحث.

أ) الدوريات: يشار إليها في المتن بأرقام داخل أقواس مربعة على مستوى السطر. أما في قائمة المراجع فيبدأ المرجع بذكر رقمه داخل قوسين مربعين فاسم عائلة المؤلف ثم الأسماء الأولى أو اختصاراتها فعنوان البحث (بين علامتي تنصيص) فاسم الدورية (تحته خط) فرقم المجلد، فرقم العدد فسنة النشر (بين قوسين) ثم أرقام الصفحات.

مثال: الحميدي، إبراهيم عبدالله. "الهجرة الداخلية في المملكة العربية السعودية حجمها واتجاهاتها." مجلة كلية الآداب، جامعة الملك سعود، م١٦، ع١ (٢٠٠٤م)، ١٠١-١٥١.

ب) الكتب: يشار إليها في المتن داخل قوسين مربعين مع ذكر الصفحات، مثال ذلك [٨، ص١٦]. أما في قائمة المراجع فيكتب رقم المرجع داخل قوسين مربعين متبوعاً باسم عائلة المؤلف ثم الأسماء الأولى أو اختصاراتها فعنوان الكتاب (تحته خط) فمكان النشر ثم الناشر فسنة النشر.

مثال: اليوسف، صالح سليمان. المشقة تجلب التيسير: دراسة نظرية وتطبيقية، الرياض: المطابع الأهلية للأوفست، ١٩٨٨م.

٩- ترفق جميع الصور والرسوم المتعلقة بالبحث في ملف مستقل.

١٠- ترقم الجداول والرسومات ترقيماً مستقلاً عن ترقيم البحث ويعنون الجدول بعنوان فوق الجدول والرسم بعنوان تحت الرسم.

١١- لا يعاد البحث إلى صاحبه سواء نشر أو لم ينشر.

١٢- يعطى الباحث نسختين من المجلة وعشرين مستلة من بحثه المنشور.

١٣- يلزم الباحث إجراء التعديلات المنصوص عليها في تقارير المحكمين، مع تعليل ما لم يعدل.

١٤- تعبر المواد المنشورة في المجلة عن آراء ونتائج مؤلفيها فقط.

عناوين المراسلة

E-mail: quecjour@qec.edu.sa


بسم الله الرحمن الرحيم

Qassim University جامعة القصيم
المجلة العلمية لجامعة القصيم
(مجلة محكمة)

المجلد (٤) – العدد (١)

مجلة
علوم الهندسة والحاسب

محرم ١٤٣٢هـ - يناير ٢٠١١م

النشر العلمي والترجمة

هيئة التحرير

رقم الإيداع : ٢٠٢٣ / ١٤٢٩

مجلة علوم الهندسة والحاسب، جامعة القصيم
المجلد (٤)، العدد (١)، ص ص ١-١٠٥ بالإنجليزية (يناير ٢٠١١م / محرم ١٤٣٢هـ)

المحتويات

صفحة